UNIVERSITY OF THE WITWATERSRAND

MASTERS THESIS

Cosmological Simulations of the Effects of Primordial Molecules on the First Generation of Stars

Author:
Matthew UNTERSLAK
566102

Supervisors:
Prof. Andreas FALTENBACHER

Prof. Andrea V. MACCIÓ

A thesis submitted in fulfillment of the requirements for the degree of Master of Science

in the

Astrophysics Group
School of Physics

April 29, 2018

Declaration of Authorship

I, Matthew UNTERSLAK, declare that this thesis titled, "Cosmological Simulations of the Effects of Primordial Molecules on the First Generation of Stars" and the work presented in it are my own. I confirm that:

- This work was done wholly or mainly while in candidature for a research degree at this University.
- Where any part of this thesis has previously been submitted for a degree or any other qualification at this University or any other institution, this has been clearly stated.
- Where I have consulted the published work of others, this is always clearly attributed.
- Where I have quoted from the work of others, the source is always given. With the exception of such quotations, this thesis is entirely my own work.
- I have acknowledged all main sources of help.
- Where the thesis is based on work done by myself jointly with others, I have made clear exactly what was done by others and what I have contributed myself.

Signed:

Date:

UNIVERSITY OF THE WITWATERSRAND

Abstract

Faculty of Science

School of Physics

Master of Science

Cosmological Simulations of the Effects of Primordial Molecules on the First Generation of Stars

by Matthew UNTERSLAK

In this study I present new results based on the implementation of molecular cooling and primordial streaming velocities into the hydro-dynamical simulation code `GASOLINE`. I demonstrate that the inclusion of molecular cooling as a cooling branch in the primordial gas and the addition of a homogeneous streaming velocity in the initial velocity field, are both critical to the study of Pop III stars. Pop III stars have a profound impact on galaxy formation, completely altering the chemical composition and thermal evolution of the gas. Future observations with the SKA telescope are expected to reveal some of the signatures of primordial star formation and thus enable the comparison with the numerical predictions. Numerical simulations employed to model the evolution of the primordial gas are able to capture the dynamics well-enough to predict the formation times of Pop III stars. The present study confirms that H_2 and HD are the most dominant coolants at high redshifts. The implementation of a homogeneous streaming velocity field, generated by the decoupling of gas and DM at the epoch of decoupling ($z \sim 1100$), delays the collapse of the gas at the centre of the DM haloes and thus delays Pop III star formation. The overall result of the implementation of molecular cooling and primordial streaming velocities is that they compensate each other to a certain degree, such that the formation times of the first stars remain roughly unchanged - accelerated by the inclusion of molecules and decelerated as a consequence of the primordial streaming velocities, but it is unclear whether these effects exactly compensate one another.

Acknowledgements

This study could not have been accomplished without the following people and organisations:

- The financial assistance of the National Research Foundation (NRF) towards this research is hereby acknowledged. Opinions expressed and conclusions arrived at, are those of the author and are not necessarily to be attributed to the NRF.
- Prof. Andreas Faltenbacher for his endless patience, and hours of discussions and guidance without which this thesis would never have been possible.
- Prof. Andrea V. Macció for his collaboration on this work and running all the simulations on the New York University Abu Dhabi (NYUAD) cluster at his disposal.
- I wish to thank both Prof. Andreas Faltenbacher and Prof. Andrea V. Macció for organising my trip to visit NYUAD. The experience was invaluable and the discussions and aid were critical in producing the version of the code I created and tested for this thesis.
- Scott Hazelhurst at the University of the Witwatersrand for allocating time and resources on his cluster for running all of the test simulations to check all of the reaction rates.
- My family and fianceé, Raquel Bonegio, were instrumental in supporting me emotionally through a very difficult and challenging period, for which I am very grateful and appreciative.
- My friends were a fantastic support structure. I wish to thank Shaun de Carvalho in particular for his hours of discussions and advice throughout my research, but also for the emotional and intellectual support he gave me. Without his help, this would have been a much tougher experience.

Contents

Declaration of Authorship iii

Abstract v

Acknowledgements vii

1 Introduction 1

2 Theory - First Stars and Primordial Winds 3
- 2.1 Pop III Stars and their Formation . . . 4
- 2.2 Chemistry Models for Star Formation . . . 6
  - 2.2.1 Modelling the Cooling of the Gas . . . 6
  - 2.2.2 Primordial Chemistry . . . 7
  - 2.2.3 Metal Enrichment . . . 12
- 2.3 Streaming Velocities - the Primordial Winds . . . 13

3 Simulations 17
- 3.1 SPH Simulation Codes: GASOLINE AND GADGET . . . 18
- 3.2 Simulating Stars . . . 19
  - 3.2.1 Star Formation Models . . . 20
    - 3.2.1.1 GADGET - Multiphase Star Formation . . . 20
    - 3.2.1.2 GASOLINE - Stochastic Star Formation . . . 21
  - 3.2.2 Stellar Winds and SN Feedback . . . 22
    - 3.2.2.1 GADGET - Superwind Model . . . 23
    - 3.2.2.2 GASOLINE - Cooling Mechanisms . . . 24
  - 3.2.3 Cold Cloud Enlargement . . . 26
- 3.3 Chemistry Cooling Model - GASOLINE Description . . . 28
  - 3.3.1 General Description of Cooling and Heating in the Code . . . 28
  - 3.3.2 Metal Cooling under a UV Radiation Background . . . 29
  - 3.3.3 Turbulent Metal Diffusion . . . 31
- 3.4 Streaming Models . . . 33
  - 3.4.1 Maio et al. 2011 . . . 34
  - 3.4.2 Stacy et al. 2011 . . . 34
  - 3.4.3 Greif et al. 2011 . . . 35
  - 3.4.4 Results . . . 36

4 Numerical Implementation 39
- 4.1 Implementing Molecular Cooling . . . 39
  - 4.1.1 Dust Grain Formation . . . 42
  - 4.1.2 Gas-phase Formation and Dissociation . . . 43
    - 4.1.2.1 H2 Non-equilibrium Formation and Destruction . . . 43
    - 4.1.2.2 HD Non-equilibrium Formation and Destruction . . . 44
  - 4.1.3 Heating and Cooling . . . 45

4.1.3.1 H2 Implementation 45
4.1.3.2 HD Implementation 46
4.2 Streaming Velocities 46
4.3 Simulation Setup and Parameters 46

5 Results **49**
5.1 Effects Resulting from the Inclusion of Molecular Cooling 49
5.1.1 Evolution of the Temperature Distribution of the Gas 49
5.1.2 Star Formation History 51
5.1.3 Evolution of the DM 53
5.1.4 Thermal and Density Evolution of the Gas 55
5.1.4.1 Thermal Evolution 55
5.1.4.2 Gas Density Evolution 57
5.1.5 Evolution of the Gas Metallicity 59
5.1.6 Summary 61
5.2 The Effects of the Streaming Velocity 62
5.2.1 Evolution of the Temperature Distribution of the Gas 62
5.2.2 Star Formation History 63
5.2.3 Evolution of the DM 64
5.2.4 Thermal and Density Evolution of the Gas 65
5.2.4.1 Thermal Evolution 65
5.2.4.2 Gas Density Evolution 66
5.2.4.3 Difference in Gas Density Evolutions 66
5.2.5 Evolution of the Gas Metallicity 68

6 Conclusions **71**

A Cooling in the GASOLINE code **73**
A.1 Makefile Options 73
A.2 Molecular Cooling Files 74
A.2.1 The Header File 74
A.2.2 The .c File 76

B Chemical Network **79**

Bibliography **85**

Chapter 1

Introduction

Understanding how the first stars developed is a key topic in cosmology, as their appearance ended the cosmic dark ages, completely transforming the early Universe. It is generally accepted that they formed within haloes of $\sim 10^6$ $M_\odot$ and that collapse began between $z \sim 20 - 30$ (Yoshida et al., 2003). They produced hydrogen-ionizing photons which caused the epoch of reionization, and their supernova (SN) explosions ejected trace amounts of D and Li and predominantly large amounts of heavier elements (Karlsson, Bromm, and Bland-Hawthorn, 2013). The exact time of their formation is critical to how the Universe evolved, completely altering the evolution of the primordial gas with signatures possibly observable with the future SKA. This formation time depends critically on the chemical composition of the gas.

Early numerical simulations assumed that hydrogen and helium atoms, with their ions, were sufficient to capture the chemistry of the early Universe, as they were the dominant species. However, these prove inefficient coolants, leaving the gas at $\sim 10^4$ K. Since the formation of stars depends on a density threshold (generally between $10^{-1} and 1$), these simulations produced very heavy stars, as large quantities of hot gas were needed to meet this threshold. Theoretically, stars are meant to form at ~ 0 K, so it was clear that additional cooling was required. Molecules provide a physical avenue as they have rotational and vibrational modes, and line cooling, as potential branches for radiating away thermal energy. This makes them ideal candidates for improved cooling models.

The first molecule identified as an excellent addition was H_2. In low-metallicity environments (such as the primordial Universe), H_2 collisions are important coolants between 5000 and 200 K (Glover and Mac Low, 2007 ; Gnedin and Kravtsov, 2010), and have a strong influence on early star formation (Jappsen et al., 2007). In addition, the formation of cold, dense gas clouds enables shielding of the interior gas from UV photons and thus avoids photo dissociation of the molecules (Krumholz, Leroy, and McKee, 2011; Glover and Clark, 2012). H_2 offers both increased cooling rates at low temperatures, and effective gas shielding. The addition of H_2 therefore provides a more accurate modelling of the primordial cooling process.

Although H_2 drastically changes the temperature of the gas at early times, HD is the dominant coolant below 200 K. Its abundance is coupled to the H_2 abundance, which is generally $\frac{[HD]}{[H_2]} \simeq 10^{-2} - 10^{-3}$ (e.g. Puy et al., 1993; Galli and Palla, 1998). Nevertheless, it is an extremely efficient coolant, and is able to allow much smaller characteristic masses to collapse at high redshifts. This is due to its permanent electric dipole moment, releasing radiative energy via collisions with H and He. It also allows dipole rotational transitions which generally have energies about two times smaller than those of the H_2 quadrupole transitions. The combination of H_2 and HD provides an effect molecular network at high redshifts, leading to star formation at smaller virial masses.

The chemical composition of the gas is not the only contributor to accurately modelling the dynamics of the gas which produces the first stars. At the epoch of decoupling ($z \sim 1100$), the baryons lose most of their momentum to the cosmic microwave background (CMB) photons. This sets up a relative streaming velocity between the gas and the dark matter (DM). The work by Tseliakhovich and Hirata, 2010 found that this was homogeneous over a few Mpc (comoving) and had an rms value of 30 kms^{-1}. Numerical simulations done by Maio, Koopmans, and Ciardi, 2011, Stacy, Bromm, and Loeb, 2011 and Greif et al., 2011b found that the inclusion of a streaming velocity delays the formation of the first stars. A streaming velocity should therefore be added to the model.

This study will show that both the addition of H_2 and HD to the chemical network, and the addition of a streaming velocity to the initial conditions, are crucial to providing a more accurate description of the environment in which the first stars form. The addition of molecular cooling will be shown to hasten the formation of the first stars and completely alter the thermal evolution of the gas in comparison to a chemical network without them. Finally, this study will confirm that star formation is indeed delayed by the inclusion of a streaming velocity, which effectively suppresses the formation of stars in small-mass DM haloes at early times. The net effect is to have star formation times which roughly agree with simulations which neglect molecular cooling and streaming velocities all together.

This dissertation is laid out in the following way. The theory behind the first stars: how they form and die, the chemical composition of the primordial gas and how it is modelled, and the theoretical origins of the streaming velocity are discussed in chapter 2. The numerical implementation of the star formation cycle, atomic and metallic gas cooling and streaming velocities are detailed in chapter 3. The method for introducing molecules into the already existing version of the cosmological code `GASOLINE`, the method to including a streaming velocity into the initial conditions of a cosmological simulation, and the exact parameters and setups used for the simulations conducted in this study are outlined in chapter 4. The analysis and discussion of the results of these simulations are in chapter 5. The conclusions drawn from these results, and a discussion of future endeavours are contained in chapter 6. Finally, Appendix A gives a brief outline of the way in which `GASOLINE`'s cooling implemented and details all the changes made to add molecular cooling into the code and Appendix B tabulates the entire chemistry reaction network implemented in our version of `GASOLINE`.

Chapter 2

Theory - First Stars and Primordial Winds

In this chapter, we will discuss how the first stars formed and why they are so critical in the study of the evolution of the cosmos, as well as in the study of large scale structures (such as galaxies). Since we are interested in how stars form, this chapter is mainly focussed on the theory behind their formation (section 2.1) and the conditions necessary for them to form. The chemical and thermal composition and evolution of the gas are critical to this formation, and are discussed in detail in section 2.2. Having a full understanding of the chemical environment in which stars form, and the effects both after they form and once they die, is crucial to modelling star formation as accurately as possible. The final section in this chapter, section 2.3, discusses the effects on star formation from streaming velocities generated during the epoch of decoupling. With all this information, we aim to construct the theoretical foundation from which an accurate and detailed star formation model can be constructed.

The current understanding of star and galaxy formation is that DM and gas begin by collapsing into small haloes, through gravitational collapse and subsequent virialisation. The haloes progressively merge into larger haloes, a process which is referred to as hierarchical structure formation. In contrast to the DM, the gas can radiate off energy. Thus it cools and sinks to the centres of the DM haloes where some fraction of it forms stars.(White and Rees, 1978; Mo, van den Bosch, and White, 2010). The gas settles into a rotating disc due to the conservation of angular momentum, leading to star formation within the disc.

The infall of the gas on the disc is governed by radiative cooling, thermal pressure (Binney, 1997; Rees and Ostriker, 1977) and the incident radiation field (Rees, 1986; Efstathiou, 1992; Cantalupo, 2010; Gnedin and Hollon, 2012). It is therefore clear that for accurate numerical modelling a complete description of the cooling rate is required in order to determine the amount of fuel available for star formation.

The mass of a star dictates how long it lives for and how it dies. A discussion of these will follow in this chapter, but the first stars, Population III (Pop III) stars, have masses of ~ 100 solar masses. These die very quickly as massive SN explosions which eject hot gas (and metals within it) into the inter-stellar and inter-galactic mediums, which contain cold gas. This creates heating and ionization of the gas in these regions. Gas cooling is therefore incredibly important for allowing the hot gas to become cold again and allow the next generation of stars to be formed. This will theoretically happen at ~ 0 K, and so the purpose of section 2.2 is to model how to do this. The combination of these processes: star formation, stellar winds and supernovae (SNe) re-heating the gas and then gas cooling again to form stars, is referred to as the star formation cycle. The numerical implementation of the star formation cycle follows in the next chapter.

2.1 Pop III Stars and their Formation

Pop III stars have a significant impact on cosmic evolution due to their radiative, mechanical and chemical feedback mechanisms (Ciardi and Ferrara, 2005). In order to discuss stellar evolution, we make the distinction that any elements heavier than He will be referred to as metals. There are three main populations of stars: Pop III, II and I stars. Pop III stars form in regions of metal-free gas (comprised of H and He atoms and molecules) and are formed first, followed by Pop II and Pop I stars. Pop II stars have $\sim 0.5\%$ metals and Pop I stars have $\sim 1\%$ metals. The effects of primordial chemistry on star formation are discussed in section 2.2. Two different sub-populations of Pop III stars exist, and we adopt nomenclature used by O'Shea et al., 2008. Pop III.1 stars are those with an electron fraction $\sim 10^{-4}$ eV. Pop III.2 stars are those whose formation was affected by the radiative or kinematic feedback produced by pre-existing stars. Note that Pop III.2 stars are named differently depending on the author (e.g. Pop II.5 Mackey, Bromm, and Hernquist, 2003). The distinction between Pop III.1 and Pop III.2 stars is important because they form differently due to the molecular composition of the gas.. The differences and their correspondingly different stellar evolutions are discussed in section 2.2.

The Pop III stars emit far-ultraviolet (FUV) photons, which have energies in the Lyman-Werner (LW) bands between 11.2 and 13.6 eV, that initiate the reionization of the intergalactic medium (IGM) by ionizing the circumstellar gas to form H^+ regions. These FUV photons have the ability to suppress star formation in their haloes (Omukai and Nishi, 1999; Glover and Brand, 2001). Another impact is from SNe. The mass of a star corresponds to the way in which it dies. In particular, Pop III stars with masses $\geqslant 150\ M_\odot$ will completely evacuate the gas from the halo in which they form (Bromm, Yoshida, and Hernquist, 2003; Wada and Venkatesan, 2003). Even smaller stars with masses $20 - 40\ M_\odot$ have SN explosions which blow out a considerable amount of material, in this case some of the gas eventually may fall back into the halo (Ritter et al., 2012) and contribute to further star formation. The material ejected into the IGM, via galactic winds from both SNe and star formation, enriches it with metals, and providing the chemical environment necessary for the formation of Pop II-I stars. The extent to which these feedback mechanisms influence the cosmic environment depends critically on the particular initial mass function (IMF) chosen and the star formation rate (SFR). This interplay between the birth and death of the first stars and the IGM, in conjunction with metal cooling in the presence of a UV background, regulates star formation at later stages. The model for star formation is discussed in detail in section 3.2.

The formation of stars, in any regime, is governed by the Jean's mass. This separates all gaseous objects into either those which will, or will not, collapse under a gravitational instability. Any object with a mass above the Jean's mass, will collapse. Those objects with lower mass do not collapse because pressure can build up sufficiently fast to counteract gravity. For a perfect, isothermal gas, the Jean's mass is defined as:

$$M_J = \frac{\pi}{6} \left(\frac{k_B\, T}{\mu\, m_H\, G} \right)^{\frac{3}{2}} \rho^{-\frac{1}{2}} \tag{2.1.1}$$

From this, it is clear that total density and temperature are the major driving forces for star formation. These are both related to the thermal evolution and chemical composition of the gas, which are studied in more detail in section 2.2, where we discuss, in particular, the role of the cooling function.

Pop III stars are more massive than Pop II-I stars, affecting the feedback effects and stellar winds. The subsequent discussion follows the work of Maio et al., 2010. Within their simulations, the first star bursts occur for stars with masses between 100 and 500 $M_\odot$. All these stellar populations were distributed via a Salpeter IMF (Salpeter, 1955). The stellar lifetimes of $\sim 100 M_\odot$ stars is $\sim 3 \times 10^6$ years, while stars which are $> 100 M_\odot$ have very short lifetimes. The stellar lifetimes of these stars are important as they dictate the change of regime from Pop III to Pop II-I star formation. This occurs because of metal pollution provided by the PISN of Pop III stars, typically having a mass in the range 140 $M_\odot$ and 260 $M_\odot$. The metallicity of the environment therefore dictates the change in regime.

Once the particle metallicity, Z, reaches (or passes) the critical density, Z_{crit}, the regime change occurs. Pop II-I stars have masses in the range $0,1 M_\odot$ to $100 M_\odot$. These can be assumed to also follow a Salpeter IMF. The substantial difference in mass leads to stars which live longer. Still, the $\sim 100 M_\odot$ stars still live for $\sim 3 \times 10^6$ years, as before, but the $\sim 0,1 M_\odot$ stars have lifetimes of $\sim 2 \times 10^{10}$ years.

The winds and feedback which distribute metals within the interstellar medium (ISM) and IGM are therefore critical to determining the generation of stars produced in a particular region of the Universe. They are also crucial for the regulation of star formation. The details pertaining to winds are deferred to the next chapter as the complexity means that our understanding of them is based on the results from simulations, but a brief outline of their importance is included here.

The typically assumed scenario is that star formation is the driving force in creating galactic winds, which dominate IGM enrichment (Aguirre and Schaye, 2007).These winds can be the result of a combination of: ejecta of a large number of co-existing SN explosions (Heckman, Armus, and Miley, 1990), or SN and stellar winds, both mechanisms inject momentum in the ISM which drive the winds, or starbursts and AGNs which drive winds via radiation pressure (Murray, Quataert, and Thompson, 2005).

Galactic winds and outflows have a crucial role in a number of different areas, which include chemical enrichment, and possible heating, of the IGM (Nath and Trentham, 1997; Aguirre et al., 2001a; Aguirre et al., 2001b; Aguirre et al., 2001c; Madau, Ferrara, and Rees, 2001); dust pollution of the IGM (Aguirre, 1999b; Aguirre, 1999a); and, on somewhat larger scales, enrichment of the intracluster medium and the intragroup medium. Galactic winds have been observed (e.g. Heckman, 2001; Pettini et al., 2001) to have velocities $\sim 10^2 - 10^3$ kms^{-1} and lose mass at rates which are comparable to the rates at which stars form. Wind material exhibits a structure which is both multi-phase and complex, the hot phase is believed to contain the bulk of the metal population (Veilleux, Cecil, and Bland-Hawthorn, 2005, and the references within it).

2.2 Chemistry Models for Star Formation

This section outlines how chemical cooling is modelled theoretically. Subsection 2.2.1 shows where the cooling function comes from and why it is only temperature dependent. The cooling function is used to find the amount of energy lost (or gained) by atoms and molecules due to their reactions with one another, or with an external UV field. Atomic and molecular cooling of the primordial elements are treated in a separate manner from metals, which is the subject of subsection 2.2.2. The final subsection, 2.2.3, discusses the cooling of metals and their effects on the cooling function. They also interact differently to the presence of an external UV field. The complexity of the effects of chemical cooling is highlighted in this section and is used within the discussion of how chemical elements and their effects are added to numerical codes, which appears in the next chapter.

2.2.1 Modelling the Cooling of the Gas

Two important time-scales exist for chemical cooling of the primordial gas: the free-fall time (t_{ff}) and the cooling time (t_{cool}). In the case where $t_{cool} < t_{ff}$ the gas will condense. The free-fall time for a sphere of density ρ is defined as:

$$t_{ff} = \sqrt{\frac{3\pi}{32\, G\, \rho}} \quad , \tag{2.2.1}$$

where G is the gravitational constant. The cooling time can be expressed in terms of the number density of the gas n, the temperature of the gas T, and the cooling function $\mathscr{L}(T, n_i)$. Indicating the number densities of various species within the gas as n_i the cooling time is given by:

$$t_{cool} = \frac{3}{2} \frac{n\, k_B\, T}{\mathscr{L}(T, n_i)} \quad . \tag{2.2.2}$$

$\mathscr{L}$ represents the amount of energy which is emitted per unit time and unit volume. This is far too complex to solve in cosmological simulations, and so a low-density limit is opposed for two-body interactions. can re-express the cooling function $\mathscr{L}$ in terms of the quantum mechanical function Λ in the form $\mathscr{L}(T, n_x, n_y) = \Lambda(T) n_x n_y$. This is the same Λ as is used in the star formation recipes, where it represents the cooling function of the gas.

Λ represents the cooling function for the gas and has greatest dependence on the density ($\Lambda \sim n_g^2$), ionization state and metallicity. The gas densities are determined by the local gas hydrodynamics, while the metallicity is determined by chemical enrichment via stellar evolution. The ionization state of the gas is dependent on the incident radiation field and gas temperature, with active galactic nuclei (AGNs) and stars being the major contributors. Most galaxy formation models represent this radiation field as a uniform background which uses the histories of cosmic star formation and quasar luminosity to determine how it evolves with redshift (Haardt and Madau, 2012). A detailed discussion of these various effects and the way they are modelled follows in the next few subsections.

2.2.2 Primordial Chemistry

From Big Bang Nucleosynthesis (BBNS), we know that the primordial gas was ~ 75 % H , 25 % He, 10^{-5} % D, and trace amounts of heavier elements and molecules. What follows is the discussion of the formation of Pop III stars and the chemical composition and evolution of the environment in which they form. What is essential is the fact that the gas is meant to be ~ 0 K so that stars can form. Our goal is therefore to find the best model for getting the gas to such low temperatures We begin this discussion by highlighting the differences in the formations of Pop III.1 and Pop III.2 stars.

Pop III stars are expected to form in small protogalactic DM haloes $\sim 10^6 M_\odot$ in size. The gas, theoretically, should reach ~ 0 K in order to form stars. The goal of the chemistry models created are therefore to get the temperature of the gas as close to 0 K as possible.

Pop III.1 stars, in a Λ cold dark matter (CDM) universe, are predicted to form within haloes of $\sim 10^6 M_\odot$ (Couchman and Rees, 1986; Haiman, Thoul, and Loeb, 1996; Tegmark et al., 1997). During the protostellar collapse of these stars, when the gas temperature $T \geq 10^4$ K, cooling is dominated by the collisions of hydrogen atoms (H-atoms) which make up ~ 93 % of all atoms. Λ will also have a relationship substantially depending on hydrogen, scaling as $\Lambda \sim n_H^2$, with n_H representing the number density for H. Once the temperature drops below the virialization temperature so that $T \lesssim 10^4$ K, He becomes a more effective and efficient coolant of the gas, allowing cooling to $\sim 10^3$ K.

However, during the protostellar collapse, H_2 is the only coolant below 10^3 K, and is produced via an electron-catalysed reaction called the H^- channel (Peebles and Dicke, 1968; Hirasawa, Aizu, and Taketani, 1969):

$$\mathrm{H} + \mathrm{e}^- \longrightarrow \mathrm{H}^- + \gamma \tag{2.2.3}$$

$$\mathrm{H}^- + \mathrm{H} \longrightarrow \mathrm{H}_2 + \mathrm{e}^- \quad . \tag{2.2.4}$$

Once the gas has a temperature $T \sim 200$ K, and a number density $\sim 10^4$ cm^{-3}, the Jeans mass sets the characteristic fragmentation masses at $\sim 10^3 M_\odot$ (Abel, Bryan, and Norman, 2002; Bromm, Coppi, and Larson, 1999; Bromm, Coppi, and Larson, 2002; Yoshida et al., 2006; and reviews by Bromm and Larson, 2004; Glover, 2005). The final masses of stars formed in this regime are set by the growing protostar's radiative feedback, and are $\sim 10 - 10^2 M_\odot$. This is much higher than present-day stars (Omukai and Palla, 2001; Omukai and Palla, 2003; O'Shea and Norman, 2007; McKee and Tan, 2008; Yoshida, Omukai, and Hernquist, 2008; Hosokawa et al., 2011; Stacy, Greif, and Bromm, 2012; Susa, 2013; Hirano et al., 2014). Such large Pop III masses are seen in simulations with only H_2, due to little subfragmentation during later stages of the collapse, and because high gas temperatures lead to high protostellar accretion rates.

In contrast, Pop III.2 form in regions, which are still metal-free, but have been affected by the formation of earlier generations of stars which have produced kinematic or radiative feedback. Pop III.2 stars have been generally found to form in haloes dominated by atomic-cooling which have virial temperatures $\gtrsim 10^4$ K (Greif et al. 2008; O'Shea and Norman, 2008). For example, defunct Pop III stars produce relic H^+ regions in which Pop III.2 stars have been found to form (Kitayama et al., 2004; Whalen, Abel, and Norman, 2004; Abel, Wise, and Bryan, 2007; Yoshida et al., 2007). Within scenarios such as this, the H^- channels produced an amount of H_2 equal to $\sim 10^{-3}$ which is more than is produced within scenarios for Pop III.1 which produce about $\sim 10^{-4}$ in comparison (e.g O'Shea et al., 2005).

These Pop III.2 stars allow us to introduce the molecule hydrogen deuteride (HD) into our calculations, as the temperature of the gas will plummet to lower temperatures where HD could become effective. To determine the impact of introducing HD, and whether or not it is a good choice, we need to investigate whether enough HD actually forms to make a difference. We begin by considering the main reactions involved in its creation and destruction (thereby regulating the amount of HD). These are:

$$\mathrm{H}_2 + \mathrm{D}^+ \longrightarrow \mathrm{HD} + \mathrm{H}^+ \tag{2.2.5}$$

$$\mathrm{HD} + \mathrm{H}^+ \longrightarrow \mathrm{H}_2 + \mathrm{D}^+ \tag{2.2.6}$$

These reaction equations highlight that the fraction of HD to H_2 is an important determinant of the efficiency of HD as a coolant. Reaction 2.2.5 is exothermic and reaction 2.2.6 is endothermic by 462 K. Therefore, chemical fractionation occurs at low temperatures, leading to the fraction of HD to H_2 being enhanced above that of

D to H by a large numerical factor. As the temperature decreases, the HD cooling rate per molecule also decreases, but the the HD cooling rate per volume can in fact increase. Thus, HD has the potential to be the most effective coolant below 200 K.

A problem which has been debated is that, in some calculations, HD seems to be unimportant. This is because the fractional ionization in conventional calculations for Pop III star formation (e.g. Abel, Bryan, and Norman, 2002) is generally small, and due to PdV heating, the gas never reaches a temperature which is low enough for chemical fractionation to become an efficient process. This would suggest that HD cooling is completely negligible. However, if the gas is initially in an ionized state and is then cooled, more H_2 forms because of non-equilibrium fractional ionization present in the cooling of the gas (Shapiro and Kang, 1987). The presence of more H_2 cools the gas further than in conventional calculations and so chemical fractionation now becomes very important since is it is now much more efficient. This results in HD now becoming dominant.

Combining these results, HD is the dominant coolant once the gas is below 200 K, particularly around 150 K where HD production is very rapid. It also remains effective up to high gas number densities of $\sim 10^6$ cm^{-3} . As a result, HD cools the gas to ~ 30 K (e.g. Nagakura and Omukai, 2005) leading to stars with characteristic masses of $\sim 10 M_\odot$ (Uehara and Inutsuka, 2000; Nakamura and Umemura, 2002; Mackey, Bromm, and Hernquist, 2003; Machida et al., 2005; Nagakura and Omukai, 2005; Johnson and Bromm, 2006; Yoshida et al., 2007; Yoshida, Omukai, and Hernquist, 2007; Wolcott-Green and Haiman, 2011; Hosokawa et al., 2012), although the most massive stars that can form under these conditions reach $\sim 40 M_\odot$. It must be noted here that in relic primordial H^+ regions, the characteristic masses of objects collapsing from the gas have already been demonstrated to be smaller O'Shea et al., 2005. What is evident, however, is that Pop III.2 stars are more massive than ordinary present-day stars, but less massive than their predecessor Pop III.1 stars. As a consequence, Pop III.2 stars have longer lifetimes and can delay the transition between Pop III and Pop II-I stars.

The introduction of HD cooling relies heavily on the accuracy of the H_2 calculations. It turns out that, when introducing H_2 calculations, several issues need to be considered (Glover and Abel, 2008). We will briefly discuss each of these.

There are two quantum mechanical spin-states for molecular hydrogen. Ortho-hydrogen has spin quantum number $I = 1$ and para-hydrogen has spin quantum number $I = 0$. The first problem is that most calculations of the H_2 abundance assume that the ratio of ortho-hydrogen to para- hydrogen is

$$\frac{(2I_{ortho} + 1)}{(2I_{para} + 1)} = 3.$$

This relationship suggests a ratio of 3:1 for ortho-hydrogen to para-hydrogen (ortho-para), i.e. 75 % of all molecular hydrogen is in the ortho-hydrogen state. This only holds so long as the H_2 population is in local thermodynamic equilibrium (LTE) and is warm, since many of the rotational and vibrational levels will be populated. Once H_2 is at low temperatures and low densities, the ortho-para ratio may differ drastically from 3:1. The significance lies in the differences between the rotational and vibrational level transitions of ortho-hydrogen and para-hydrogen. To illustrate this, the energy of the rotational transition of para-hydrogen from $v = 0, J = 2 \rightarrow 0$ is $E_{20} = 509.85$ K, while the energy of the rotational transition of ortho-hydrogen from $v = 0, J = 3 \rightarrow 1$ is $E_{31} = 844.65$ K. Therefore, para-hydrogen can continue to cool the gas at lower temperatures where ortho-hydrogen cannot. It has also been demonstrated that at lower temperatures, the fraction of para-hydrogen exceeds that of ortho-hydrogen and that at ~ 20 K, pure para-hydrogen exists since it is more stable. The increase of para-hydrogen drives the temperature of the gas down to the low temperatures required for HD dominance. Therefore the model we implement must be sensitive to the ortho-para ratio, or HD will not dominate.

A second problem lies in uncertainty surrounding the low-temperature behaviour of H_2. An interaction potential is used to calculate the $H - H_2$ excitation cross-sections, and how sensitive the low-energy cross-sections are to this potential is still unknown. Most calculations apply a fitting function to the low-density cooling rate for H_2 so that studying HD is possible. The most widely used fit was made by Galli and Palla, 1998. For temperatures $T < 600$ K, their fitting function used the Forrey et al., 1997 excitation rates, whose equations were determined utilising the BKMP2 potential energy surface proposed by Boothroyd et al., 1996. A new set of excitation rates for H_2 was published by Wrathmall and Flower, 2007, which was based on calculations which utilised the Mielke, Garrett, and Peterson, 2002 potential energy surface. A fit of the Wrathmall and Flower, 2007 coefficients produces a very different H_2 cooling function from that of Galli and Palla, 1998 when $T < 1000$ K. The impact of this difference has not yet been explored in much detail. Our model is based on the work by Galli and Palla, 1998.

Thirdly, most calculations only consider collisional excitations between H_2 and atomic hydrogen. However, H_2 can also be collisionally excited by H_2 , He , H^+ and e^-. The implementation of these extra collisional species is dealt with in section 4.1. We include some of the neglected processes as outlined in Glover and Abel, 2008.

The fourth point is related to the above. Several uncertainties exist in relation to several key rate coefficients for reactions involved in the creation and destruction of H_2. It is noted, however, that the rate coefficient uncertainties were studied previously by Savin et al., 2004 and Glover, Savin, and Jappsen, 2006.

As was mentioned in section 2.1, Pop III stars emit large amounts of FUV photons. These photons prevent the gas from cooling efficiently by photodissociating H_2. Gas in haloes is also vulnerable to external FUV photon irradiation, which severely regulate Pop III.1 star formation (e.g. Haiman, Rees, and Loeb, 1997). In larger haloes, Pop III.2 star formation is relatively unaffected since atomic cooling remains relatively undisturbed, even when subjected to a FUV background (Haiman, Rees, and Loeb, 1997; O'Shea and Norman, 2008). Pop III.2 could in all likelihood make up the major portion of the Pop III stellar population, and contributing large amounts of radiative and chemical feedback which alter subsequent stellar populations (Trenti and Stiavelli, 2009; de Souza, Yoshida, and Ioka, 2011). As has been mentioned earlier, the longer lifetimes of Pop III.2 stars mean that they could have survived until as recently as $z \sim 6$ (Tornatore, Ferrara, and Schneider, 2007; de Souza, Yoshida, and Ioka, 2011; Johnson, Dalla Vecchia, and Khochfar, 2013). It is possible, with the assumption that this holds true, that future facilities could detect SNe and gamma-ray bursts (GRBs) produced by Pop III.2 stars and provide data which will allow us to probe the nature of primordial stars in more detail (Nakauchi et al., 2012; Tanaka, Moriya, and Yoshida, 2013; Whalen et al., 2013).

Some studies consider scenarios (such as in large-mass haloes) where the density of the gas is lower, thereby exposing more molecules to the FUV photons (Yoshida, Omukai, and Hernquist, 2007; Wolcott-Green and Haiman, 2011). They find that this slightly suppresses the abundance of H_2 by photodissociation, leading to significant suppression HD formation . In such a case as this, Pop III.2 stars would evolve identically to Pop III.1 stars, and share the same characteristic masses. A study by Nakauchi, Inayoshi, and Omukai, 2014 concludes that there are several important effects which favour HD cooling and make Pop III.2 stars fairly common. These effects are outlined below.

Shocks occur ubiquitously during the galaxy formation epoch, for instance during the virialization of haloes or SN explosions. HD and H_2 formation and cooling are more efficient due to the elevated ionization degree present within a shocked gas (Uehara and Inutsuka, 2000; Mackey, Bromm, and Hernquist, 2003; Vasiliev and Shchekinov, 2005; Johnson and Bromm, 2006; Shchekinov and Vasiliev, 2006; Greif et al., 2008; Bovino et al., 2014). When a strong shock occurs, the post-shock gas cools as a function of density, with its temperature dropping as the density increases (e.g. Shapiro and Kang, 1987). Free-falling clouds existing within relic H^+ regions experience very swift cooling which is also a function of density, but the temperature drops with constant density rather than increasing density (as before; Johnson and Bromm, 2006; Yoshida, Omukai, and Hernquist, 2007; Wolcott-Green and Haiman, 2011). Higher column densities provide more effective shielding from the FUV radiation field. Thus, the post-shock flows have a lower FUV flux than the relic H^+ regions. Despite this, previous studies (e.g. Wolcott-Green and Haiman, 2011) did not fully account for the isobaric nature of the evolution.

An additional radiation field, the cosmic ray (CR) background, is also associated with star formation and is generated by the CR acceleration in SN remnants. Once more, the ionization degree is enhanced by CR irradiation, increasing HD and H_2 production and cooling (Jasche, Ciardi, and Enßlin, 2007; Stacy and Bromm, 2007; Inayoshi and Omukai, 2011). It is therefore possible that the negative feedback associated with FUV radiation could be counteracted by irradiation produced by the CR background. Previous to the Nakauchi, Inayoshi, and Omukai, 2014 study, the effects of combining both fields into one study had not been done (Jasche, Ciardi, and Enßlin, 2007; Stacy and Bromm, 2007; Wolcott-Green and Haiman, 2011), leaving the effects of these joined fields not well understood. Nakauchi, Inayoshi, and Omukai, 2014 show that, within free-falling clouds which exist within relic H^+ regions, the intensity of the FUV photons tends to be an order of magnitude lower than the intensity which exists within a cloud compressed by plane-parallel steady shocks. The most important conclusion they find is that Pop III.2 stars forming where HD is the dominant coolant of the gas is fairly common during the epoch of galaxy formation.

According to the above discussion it is extremely important to include HD in the modelling cosmological star formation. The numerical implementation of the primordial chemistry models constitutes the main focus of the present study and will be described exhaustively in section 4.1.

2.2.3 Metal Enrichment

So far, we have discussed the primordial chemistry and how HD affects the formation of Pop III stars. However, metals play the crucial role of differentiating Pop III stars from later stellar populations. Without the tracking of metals, the numerical star formation models cannot determine if Pop III stars are still in existence, nor when the Pop III regime has ended.

Through observations of metal absorption lines (e.g. C_{III} , C_{IV} , Si_{III} , S_{IV} , and O_{IV}) in quasar spectra, it has been found that the IGM far outside galaxies ($\frac{\rho}{\rho_{mean}} < 10$) is metal enriched (e.g. Songaila and Cowie, 1996; Davé et al., 1998; Ellison et al., 2000; Schaye et al., 2000; Pettini et al., 2003; Schaye et al., 2003; Aguirre et al., 2004; Simcoe, Sargent, and Rauch, 2004). Evidence exists that enrichment extends back to $z > 5$ (Pettini et al., 2003; Simcoe, 2006), although metallicities are very low between $z = 4$ and $z = 2$ (Schaye et al., 2003). Due to the fact that metals are created within stars which reside within galaxies, the only way for the IGM to become enriched is by metals escaping from galaxies as already discussed in section 2.1.

The mixing of metals between the wind and the surrounding gas also plays an important role. SN explosions have been identified as a major driver of the large amount of turbulence within the ISM (Mac Low and Klessen, 2004). Large velocity shears (which exist between winds and gaseous haloes) also produce turbulence and mixing. Metals and thermal energy are redistributed (changing the metallicity and temperature) between the winds and ambient gas via turbulent mixing, altering the future evolution of the gas. The impact of metal mixing on the IGM is unclear. For example, Schaye, Carswell, and Kim, 2007 observed $\sim$ 100pc compact, highly enriched, transient C_{IV} absorbers, indicative of poor small-scale chemical mixing. To explain these absorbers, it was suggested that they were enriched clumpy medium immersed in hot galactic winds. Supposing that the major mechanism generating turbulent mixing between winds and the surroundings is velocity shear, then the clouds being carried by hot winds at the same speed would account for this poor small-scale mixing. Investigating this would require resolving wind structures, which is impossible in cosmological simulations at present.

2.3 Streaming Velocities - the Primordial Winds

This section introduces the work by Tseliakhovich and Hirata, 2010, which showed that the relative velocities existing between DM and gas from the epoch of decoupling were an order of magnitude or two larger than previous studies suggested. The fact that, due to the relative streaming velocities the gas might take longer to fall into DM haloes and therefore has the potential to delay star formation, is critical to the overall model for star formation. This section outlines the theory behind how these winds are generated, and gives a rough value for the velocity of such a wind. We begin by explaining where these winds originated.

The epoch of recombination is of particular interest because it directly impacts the initial conditions for cosmological simulations. Before recombination, Thomson scattering tightly coupled baryons and photons to one another, forming a plasma which is radiation-dominated and has a sound speed $c_s \sim \frac{1}{\sqrt{3}}c$. Due to the fact that the CDM components and radiation do not have a significant electromagnetic interaction, they do not create a significant drag on one another. This means that perturbations in the CDM components are allowed to grow. The expansion and subsequent cooling of the Universe gives rise to kinematic decoupling, which happens at $z \approx 1020$, of the baryons from the radiation, allowing the baryons to be able to fall into CDM potential wells. This event, occurring slightly after the surface of last scattering, happens because the baryons have a lower inertia than the microwave background photons during this epoch. The Universe then becomes transparent because the protons and electrons now recombine to form atoms, of which $\sim 75\%$ is Hydrogen and $\sim 25\%$ is Helium.

Post-recombination, the baryonic sound speed in the gas is

$$c_s = \sqrt{\frac{\gamma\, k_B\, T_b}{\mu\, m_H}} \tag{2.3.1}$$

where $\gamma = \frac{5}{3}$ for an ideal monatomic gas, the mean molecular weight, $\mu = 1.22$, includes the He mass fraction of 0.24, m_H is the mass of the hydrogen atom, and T_b is the kinetic temperature of the baryons. This temperature represents the competition between the adiabatic cooling and Compton heating (due to the CMB photons). The `RECFAST` code was used to find T_b (Seager, Sasselov, and Scott, 1999, Seager, Sasselov, and Scott, 2000] and parametrize it as:

$$T_b(a) = \frac{T_{CMB,0}}{a}\left[1 + \frac{\frac{a}{a_1}}{1 + \left(\frac{a_2}{a}\right)^{\frac{3}{2}}}\right]^{-1} \quad , \quad a_1 = \frac{1}{119}\,,\; a_2 = \frac{1}{115}\,,\; T_{CMB,0} = 2.726\text{ K} \tag{2.3.2}$$

Before decoupling, the relativistic sound speed of the plasma created pressure which prevented the baryons from being trapped in any of the CDM potential wells.

Thus, the gas forms a static plasma below which the CDM is accelerating due to the underlying gravitational field. After decoupling, the photons decouple from the baryons, taking most of the momentum with them, while the baryons recombined into atoms. The velocities of the baryons dropped rapidly to thermal velocities. The CDM, having an insignificant electromagnetic component, evolved following gravitational interactions and formed proto-haloes. The result of this is that the velocity of the CDM was unaffected, and so the relative velocity between the CDM and the gas is now significant. It is expressed as

$$\mathbf{v}_{bc}(\mathbf{k}) = \frac{\hat{\mathbf{k}}}{ik}\left[\theta_b(\mathbf{k}) - \theta_c(\mathbf{k})\right] \quad . \tag{2.3.3}$$

Here, $\hat{\mathbf{k}}$ is the unit vector in the direction of $\mathbf{k}$, and the velocity divergence is represented by $\theta \equiv a^{-1}\nabla \cdot \mathbf{v}$. The variance is given by

$$\begin{aligned} \left\langle v_{bc}^2(\mathbf{x}) \right\rangle &= \int \frac{dk}{k}\, \Delta_\zeta^2(k) \left[\frac{\theta_b(k) - \theta_c(k)}{k}\right]^2 \\ &= \int \frac{dk}{k}\, \Delta_{v_{bc}}^2(k) \end{aligned} \tag{2.3.4}$$

where, $\Delta_\zeta^2(k) = 2.42 \times 10^{-9}$ is the initial curvature perturbation per $\ln k$ Dunkley et al., 2009. By integrating (2.3.4) at the time of recombination ($z_{rec} = 1020$), it is shown that there is a relative velocity between the dark matter and the gas of $\sim$ 30 km s^{-1}. This corresponds to a Mach number of $\mathscr{M}\ equiv \frac{v_{bc}}{c_s} \sim 5$.This motion is supersonic, resulting in baryons being advected out of DM potential wells. This results in significant suppression of structural growth at wave numbers above

$$\begin{aligned} k_{v_{bc}} &\equiv \left.\frac{aH}{\left\langle v_{bc}^2 \right\rangle^{\frac{1}{2}}}\right|_{dec} \\ &= \frac{k_J}{\mathscr{M}} \sim 40\ \mathrm{Mpc}^{-1} \end{aligned} \tag{2.3.5}$$

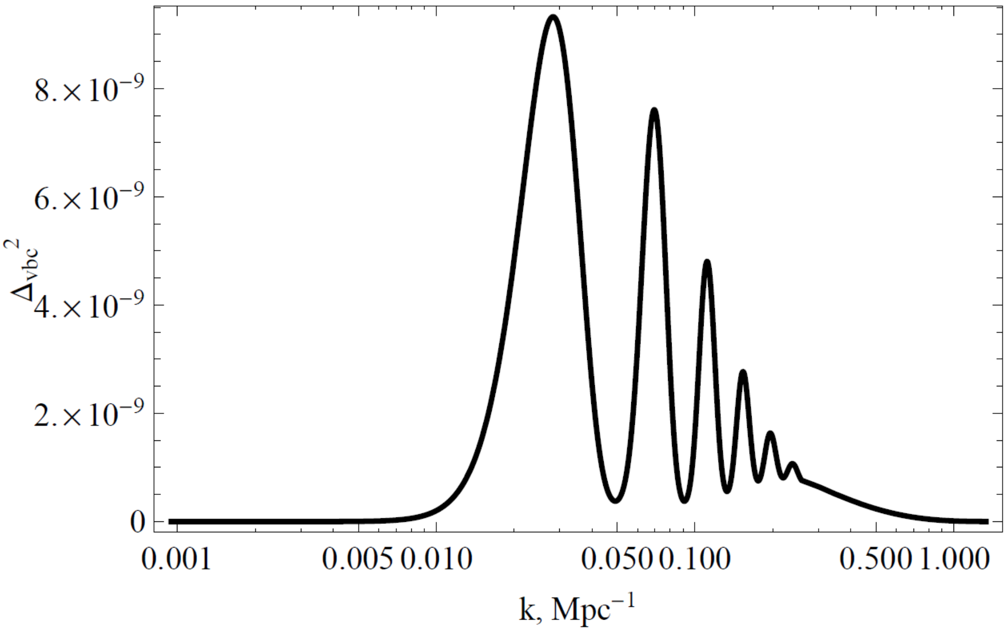

FIGURE 2.1: This plot shows the variance of the relative velocity perturbation per $\ln k$ as a function of k, $\Delta^2_{v_{bc}}(k)$, showing where $\Delta^2_{v_{bc}}(k)$ is non-zero. From this, the coherence length of v_{bc} can be determined. As can be seen from the plot, once $k > 0.5\,\mathrm{Mpc}^{-1}$, the power spectrum decays rapidly, showing that the relative velocity, v_{bc}, is only coherent over scales smaller than a few Mpc comoving.

Figure 2.1 shows the relative contributions to the relative velocity v_{bc} from the varying scales. From this plot, it is clear that the largest scales provide no contribution to v_{bc}, since at the decoupling time these are the regions which were outside the sound horizon. The dominant contributions are provided by the region of the plot where it looks Gaussian, due to the fact that this corresponds to the areas of the plasma where acoustic oscillations were present. These had velocities which were generally a few times c and were unaffected by Hubble damping at early epochs when $\rho \gg \rho_b$ (Hu and Sugiyama, 1995). The smallest scales are those regions where photon diffusion damped the baryonic acoustic oscillations, and the Hubble drag during the radiation era suppressed the CDM velocities. We therefore conclude that v_{bc} is most affected by scales ranging from the sound horizon down to the Silk dampening length. The conclusion drawn from this information, and the explanation thereof, is that the system has a separation of scales: the first baryonic objects form at scales of ~ 10 kpc, which is much smaller than the coherence length at which the relative velocity field setup by these oscillations is generated (this is usually $\sim$ a few Mpc). This is clearly crucial to the study of the early Universe when considering structure formation.

We will use this information to modify the initial conditions of simulations to see how these changes will affect the formation time of stars and the dynamics of the gas in surrounding regions. In section 3.4, we will discuss several simulations implementing coherent homogeneous velocity fields in their initial conditions and discuss their results and conclusions.

Before concluding this chapter, the work of Ahn, 2016 needs to mentioned briefly. The fact that the streaming velocity is only coherent within a few Mpc comoving means it is only homogeneous within small regions. The boundaries of these regions could have different gas streams colliding, producing regions where matter builds-up. The effect of these build-ups could differ from the description of Tseliakhovich and Hirata, 2010. Ahn, 2016 claims to have constructed a mathematical model that naturally generates these matter build-ups by coupling the density and velocity fields on both small and large scales, as opposed to the Tseliakhovich and Hirata, 2010 model which only couples these fields on large scales. This model has not been studied in enough detail to verify this result. The model has never been implemented into the initial conditions of cosmological simulations.

In this chapter, how stars form - particularly focussing on Pop III star formation - has been explained theoretically. What becomes important for simulations is that the DM haloes will trap cooling gas, thereby forming sites for star formation. We then covered in detail the chemical composition of the gas in the early Universe, and included a discussion of the effects produced by stars once they die. These details allowed us the full picture of star formation, allowing us a clear distinction between when Pop III stars form and when later generations of stars will form. With these two major ideas, the discussion of what the simulations require to form Pop III stars can be discussed in sections 3.2 and 3.3.Finally, we discussed the dynamics of the gas at $z \sim 1100$ and concluded that the early- time baryonic acoustic oscillations play a critical role in the relative velocity field between the gas and DM. Putting all of this information together, it is clear that cosmological simulations of the first stars need to have detailed chemical networks and accurate star formation models, along with all the feedback mechanisms and winds, in place before the addition of the velocity fields can be studied. In the next chapter, we will outline and discuss the way in which star formation and destruction are modelled within cosmological simulations (section 3.2), which chemical networks already exist and how they are implemented (section 3.3), and finally conclude with a discussion of what velocity fields have already been implemented in cosmological simulations and what the impact of these velocity fields were (section 3.4).

Chapter 3

Simulations

This chapter focusses on the numerical models used to regulate star formation in cosmological simulations. Each numerical code differs in its approach producing variation in the final results. This makes comparisons between the results obtained by different groups difficult. However, the broad features seem to match fairly well.

Three different methods are currently employed in modelling gas physics within simulations: Eulerian grid codes, Lagrangian particle codes, and adaptive mesh refinement (AMR) codes incorporating elements from both of these.

Eulerian codes (e.g. Cen and Ostriker, 1993; Kravtsov, 1999; O'Shea et al., 2004) use a fixed grid of cells to track the movement of gas. They use the analytical Riemann solution of the Euler equations coupled with the upwind scheme of Courant, Isaacson, and Rees, 1952 to numerically evolve fluid systems on this discretized mesh. Such schemes deal very well with properties of the gas, such as density and temperature, but have trouble with the motion of the gas, since propagating the gas requires moving it from cell to cell rather than point to point, adding numerical errors to the results.

Lagrangian codes (e.g. Springel, Yoshida, and White, 2001; Wadsley, Stadel, and Quinn, 2004) model the fluid through particles and discretise their masses. Modelling the gas requires a further treatment called smoothed particle hydrodynamics (SPH; Monaghan, 1992), where particle motion is easily modelled and particles concentrate naturally in dense regions of interest, improving resolution. The gas properties are difficult to resolve, and so SPH codes use a spline kernel to interpolate over neighbouring particles to determine these quantities. These are then used to solve the equations of hydrodynamics. This study uses an SPH code, and so the focus of this thesis is on the numerical recipes used in SPH codes.

There are two competing approaches to star formation: "explicit" or "ordinary" star formation, and stochastic star formation. The first tracks the gas explicitly and forms stars using the densities of individual gas particles. This is the model adopted by Springel and Hernquist, 2003a. The second uses the densities and temperatures of the gas particles, together with a criterion relating to whether they are collapsing to ascertain potential star producing particles. A subset of these are chosen to probabilistically form stars. The comparison between these methods and their strengths and weaknesses are discussed in section 3.2.

These two models are implemented in the codes GASOLINE (Wadsley, Stadel, and Quinn, 2004) and GADGET (Springel, Yoshida, and White, 2001). Their different star formation recipes mean that they introduce the cooling function's role in the code in different places, but they both implement and follow the cooling in the same way due to their use of the Lagrangian SPH approach. The description of the cooling and diffusion models used for primordial and metal cooling are the subject of section 3.3.

Forming a more detailed and accurate simulation of Pop III star formation requires the inclusion of a streaming velocity (discussed in section 2.3). Several authors (Maio, Koopmans, and Ciardi, 2011; Stacy, Bromm, and Loeb, 2011; Greif et al., 2011b) have implemented these streaming velocities and the initial setups and final results from each of these have been summarised in section 3.4.

3.1 SPH Simulation Codes: GASOLINE AND GADGET

This work utilises the parallel tree and SPH code GASOLINE (Wadsley, Stadel, and Quinn, 2004), which extends the N-body gravity code PKDGRAV (Stadel, 2001). A spline kernel is used to interpolate between neighbouring particles when solving the hydrodynamical equations, which is 32 nearest-neighbours in GASOLINE. Each particle's gravitational component is calculated by using the tree elements which span, at most, $\theta = 0.7$ of the tree element's distance from the particle in question. .

GASOLINE has been extensively used to study galaxy formation and evolution. It has proven itself to be successful in the reproduction of the Tully–Fisher relation (Governato et al., 2009). Dwarf galaxies and their rotation curves (Governato et al., 2010), and disc galaxies' internal structures (Governato et al., 2007; Roškar et al., 2008; Brooks et al., 2009; Stinson et al., 2009) have been well-produced in GASOLINE simulations. Damped Ly-α systems have been studied through simulations and their column density distributions have matched closely with observations (Pontzen et al., 2008; Pontzen et al., 2010). GASOLINE has also been employed to study the observed stellar mass- metallicity relationship (Brooks et al., 2007).

GASOLINE models gravity and gas dynamics, and also incorporates physical processes which include a UV background, gas cooling rates, ion abundances, star formation and feedback from SNe. These were significantly improved by Shen, Wadsley, and Stinson, 2010 who added detailed metal cooling and turbulent mixing. A semi-implicit integrator is used to calculate the gas cooling rates and non-equilibrium ion abundances using collisional ionization rates (Abel et al., 1997), radiative recombination (Black, 1981; Verner and Ferland, 1996), photoionization, bremsstrahlung, and cooling from H, He (Cen, 1992) and metal lines (Shen, Wadsley, and Stinson, 2010). A redshift-dependent UV background is incorporated into the code based on radiation from external stars and galaxies (Haardt and Madau, 1996), which affects the radiative recombination and ionization rates. The version of GASOLINE used in this work contains all of these components, onto which molecular cooling is added with updated rates from Glover and Abel, 2008.

An alternative star formation model was developed by Springel and Hernquist, 2003a and introduced into their code GADGET (Springel, Yoshida, and White, 2001; Springel and Hernquist, 2002; Springel and Hernquist, 2003a; Springel and Hernquist, 2003b;), and this star formation recipe is compared to alternative recipe used in GASOLINE.

GADGET is a massively parallel TreeSPH code which implements an N-body approach for studying collisionless fluids and SPH to track gas particles. As in the case of GASOLINE, A spline kernel is used to interpolate between neighbouring particles when solving the hydrodynamical equations, with the kernel usually set to 32 nearest neighbours. GADGET has been used in the study of many cosmological problems. The additions of chemical network and atomic cooling were added by Yoshida et al., 2003. Molecular hydrogen cooling was added by Yoshida et al., 2006, with Maio et al., 2007 adding HD and HeH^+ onto this already existing framework. A UV background is implemented in the same way as GASOLINE, following the work of Haardt and Madau, 1996. This work is not a comparison between the two SPH codes, but rather an overview of their differences since they are the major SPH competitors.

3.2 Simulating Stars

Including the modelling of stars in a cosmological simulation requires implementing the complete star formation cycle: cold gas condenses into stars, hot gas is ejected via SNe into the ISM and then hot gas must cool and reform cold clouds from which stars form. The interplay between these processes is far too costly for cosmological simulations to resolve at present. Simulating individual stars within a cosmological simulation is completely impossible. As a result, a large number of simplifying assumptions are made to reduce the complexity of the processes so that a simplified but effective regulated star formation model can be constructed.

Various methods have been employed to convert SPH gas particles into stars. Early simulations converted dense gas into “galaxy particles”, but the improvements in computational power have allowed the development of codes capable of converting dense gas into “star particles” representing “clusters of stars”.

Cosmological simulations are setup for the formation of stars $\gtrsim 100\ M_{\odot}$, and therefore introduce an IMF to study the sub-grid physics. Moving to a resolution where stars of much smaller masses ($\sim 1\ M_{\odot}$) would require disregarding the IMF and finding a recipe for star formation which would handle the physics of individual star formation.

This study does not introduce a new model for star formation, and so discusses the stellar models which utilize an IMF. The two most widely used models are discussed in this section both suffer from this resolution problem, but employ completely different descriptions for forming stars. Springel and Hernquist, 2003a formulated a multiphase model which explicitly calculates “ordinary” star formation, while Stinson et al., 2006 employ a stochastic approach based on a star formation efficiency.

These two approaches are contrasted in this section so that it is clear that no ideal solution exists as yet, as both methods suffer from weaknesses.

3.2.1 Star Formation Models

This subsection provides an overview of the methods of star formation mentioned previously. The multi-phase ISM model of star formation developed by Springel and Hernquist, 2003a is investigated first, followed by the blastwave model developed by Stinson et al., 2006.

3.2.1.1 GADGET - Multiphase Star Formation

The model for quiescent self-regulated star formation outlined here comes from Springel and Hernquist, 2003a which is implemented in `GADGET`. All the the equations derived and presented in this subsection do not contain any terms related to changes in temperature, due to expansion or contraction.

From the previous chapter, it is clear that the total density and star formation are linked. This model assumes a multi- phase medium comprised of hot ambient gas, cold clouds and stars, whose local densities are ρ_h, ρ_c and ρ_*, respectively. These are all averages over the ISM - due to the inability of cosmological codes to resolve individual molecular stars and clouds. From these, the total gas density is defined as

$$\rho = \rho_h + \rho_c \quad . \tag{3.2.1}$$

It is assumed that a coarse-graining procedure has already been carried out implicitly, and that the average densities are calculated over an ISM which has constant volume. An expression for the average thermal energy per unit volume (ε) can then be defined in terms of ρ_h and ρ_c as

$$\varepsilon = \rho_h u_h + \rho_c u_c \quad , \tag{3.2.2}$$

where u_c is the energy per unit mass of the cold clouds and u_h is the energy per unit mass of the hot ambient gas. This expression will be used later to find the full energy equation. In order to do this, it is assumed that a characteristic time-scale (t_*) can be defined for cold clouds to be converted into stars, and that the mass fraction of total stars which are short-lived and instantly die as SNe can be expressed by a parameter β.

These are massive stars with masses $> 8\ \mathrm{M}_\odot$. It is important to note that β depends on the stellar IMF , which is employed to set the initial mass distribution of the stellar population represented by the star particle. In principle, the time taken between the formation of a star and its death by a SN explosion does exist, usually $\sim 10^7$ yrs. For star formation within a quiescent regime, the speed at which self-regulation is established is so fast that the time delay is negligible, and is therefore neglected from the model. Within this context, self-regulating star formation is able form stars from cold clouds, model SN explosions to eject hot gas into the cold clouds and then cool the gas again to form stars. This cycle does not, for example, need cold gas to be pumped into the system. Using these assumptions, the star formation rate is defined as

$$\frac{d\rho_*}{dt} = \frac{\rho_c}{t_*} - \beta\frac{\rho_c}{t_*} = (1-\beta)\frac{\rho_c}{t_*} \quad . \tag{3.2.3}$$

In this equation, $\frac{\rho_c}{t_*}$ represents the rate at which the reservoir of the cold clouds is depleted during star formation. Once these stars explode as SNe, their ejections are assumed to return hot gas which will increase the mass of the ambient hot-phase gas. This process is expressed by $\beta\frac{\rho_c}{t_*}$.

The value of β depends on the IMF due to its dependence on the masses of stars above 8 $M_\odot$, which are affected by the choice of IMF, since β depends on the choice of the masses of the heaviest and lightest stars. These then affect the value of the slope of the IMF. The choice of the IMF is therefore important; for instance if a Salpeter IMF (Salpeter, 1955) is assumed, with a mass range between 0.1 $M_\odot$ and 40 $M_\odot$, and with a power law slope of -1.35, the value of $\beta = 0.106$.

3.2.1.2 GASOLINE - Stochastic Star Formation

In contrast to the prescription in `GADGET`, `GASOLINE` implements the blastwave model Stinson et al., 2006) for its star formation and feedback recipes, which is still a quiescent model for star formation. Stars form from dense ($n_{min} = 0.1$ cm^{-3}) and cold ($T_{min} = 30$ K) gas particles. Of the gas particles which meet these criteria, only a subset are selected stochastically to form stars, using the commonly adopted star formation equation

$$\frac{dM_*}{dt} = c_*\frac{M_{\rm gas}}{t_{\rm dyn}} \quad , \tag{3.2.4}$$

where M_* represents the mass of stars which are created, c_* represents the star formation efficiency and is constant, $M_{\rm gas}$ represents the mass of gas from which the star is formed, dt represents how frequently star formation is calculated, and $t_{\rm dyn}$ represents the dynamical time of the gas. For the simulations in this work, c_* was 0.15, so that the simulations obey a Kennicutt-Schmidt law (Kennicutt, 1998), in agreeance with the work by Stinson et al., 2006. Gas particles which meet these conditions will produce a single star particle which represents a stellar population spanning the entire IMF (Kroupa, Tout, and Gilmore, 1993). Their mass is set to $\frac{1}{3}$ of the gas mass when they form, but they lose mass according to their initial IMF. The mass lost is returned to the mass of the surrounding gas particles. Stellar lifetimes as a function of stellar masses are based on the stellar evolution model by Raiteri, Villata, and Navarro, 1996. This approach allows gas particles to maintain their own, unique character and temperature, hot, cold or warm.

At this point, both models need to prescribe a way for SN feedback to produce effective galactic outflows. Their approaches are very different and it is still widely contested as to which resembles the physical process better. An assessment in that regard requires a discussion of the effects of these galactic outflows.

3.2.2 Stellar Winds and SN Feedback

To date, the ISM in galaxies has been studied by a number of hydrodynamical simulations (e.g. Mac Low and Ferrara, 1999;Strickland and Stevens, 2000;Williams and Dyson, 2002) which have been able to produce galactic outflows and thus facilitated the investigation of various wind properties and different gas phases on the overall gas dynamics.

Winds have the dual ability to reheat material which has collapsed with the centre of a galaxy and transport it from here to the extended DM halo surrounding it (and further in some cases). This leads to a reduction in the overall cosmic SFR so that it is consistent with observation constraints. However, implementing realistic wind models and tracking winds directly in cosmological simulations is a still developing area of research. It has been shown that without any implementation of SN (or black hole) feedback, simulations suffer from the over-cooling problem (Navarro and Steinmetz, 1997) which leads to unrealistically concentrated simulated galaxies.

In order to counter this, a number of 'subgrid' wind and stellar feedback models have been created. These models fulfill two main functions: firstly the regulation of star formation(Scannapieco, Ferrara, and Broadhurst, 2000; Scannapieco and Broadhurst, 2001b ; Scannapieco and Broadhurst, 2001a) and secondly the (re-)distribution of the gas and any newly formed metals both within and into the environment around galaxies. Two main approaches to achieve this have been implemented: energetic feedback and kinematic feedback. The last approach is analogous to increasing the effective pressure. What follows is a discussion of these approaches and their effects.

The simplest way of introducing energetic feedback is to add the stellar feedback as a thermal energy of the ambient gas particles, but this causes over-cooling as demonstrated by Katz, Weinberg, and Hernquist, 1996. Kinematic feedback (e.g. Navarro and White, 1993; Springel and Hernquist, 2003b; Oppenheimer and Davé, 2006; Dalla Vecchia and Schaye, 2008) converts some of the SN energy into kinematic energy and injects it into the gas. The resolution and hydrodynamic method adopted are critical to the effectiveness of kinematic feedback. This feedback model, although generally called SN feedback, has been able to capture the feedback from several types of stellar feedback, examples of which are radiation energy which is deposited locally and winds. The *energy injection rate* is represented as a function which is based on the stellar population's current age and masses.

3.2.2.1 GADGET - Superwind Model

The previous discussion is used to continue the two star formation models we were discussing, as both require SNe and stellar winds to be included to make themselves self-regulating regimes, by constructing feasible methods within their models to transport hot gas into the cold gas clouds. The star formation model in `GADGET` is considered first, followed by the `GASOLINE` model.

We have derived the expression governing star formation (equation 3.2.3). A simplified model for SNe needs to be introduced for the metal enrichment of the ISM and releasing energy into the local environment surrounding star formation sites. The precise amount of energy that is released depends on the IMF chosen, which in this case has an expected average value of 4×10^{48} erg M$_{\odot}^{-1}$ for each M$_{\odot}$ in stars formed, given a canonical value of 10^{51} erg supernova $^{-1}$. The heat generated by SNe can then be expressed as:

$$\begin{aligned}
\frac{d}{dt}(\rho_h u_h)\bigg|_{SN} &= \varepsilon_{SN}\,\frac{d\rho_*}{dt} \\
&= \varepsilon_{SN}\,(1-\beta)\,\frac{d\rho_c}{dt_*} \quad , \quad \text{using (3.2.3)} \\
&= \beta\, u_{SN}\,\frac{d\rho_c}{dt_*} \quad , \quad u_{SN} = \beta^{-1}\,\varepsilon_{SN}\,(1-\beta) \qquad (3.2.5)
\end{aligned}$$

It is now possible to express u_{SN} in terms of an equivalent 'supernova temperature':

$$T_{SN} = \frac{2\,\mu\,u_{SN}}{3k} \simeq 10^8\ \mathrm{K} \qquad (3.2.6)$$

The amount of material returned by SNe to the ambient gas is still unknown and some assumptions are needed to reduce the complexity of the problem. It is assumed that the feedback energy from SNe directly heats the ambient hot phase and that thermal conduction is the dominant process for evaporating cold clouds within the hot bubbles. If the amount of hot gas released into the cold clouds is identical to the amount of cold gas which is heated, then

$$\frac{d\rho_c}{dt}\bigg|_{EV} = A\,\beta\,\frac{\rho_c}{t_*} \quad , \qquad (3.2.7)$$

where A represents the efficiency of the evaporation process. A is expected to be a function of the local environment and, for simplicity,we only consider it to have a theoretical dependence on density, $A \propto \rho^{-\frac{4}{5}}$ (McKee and Ostriker, 1977). A is treated as a parameter of the model as it is not estimated from first principles. Once a plausible temperature structure for the ISM is imposed, a limited range of values is then permissible for A.

This is the description for the stellar winds model adopted by Springel and Hernquist, 2003a. It has been demonstrated that an effective pressure is created in the multi-phase ISM by regulated star formation. This system is strongly hydrodynamically coupled, and does not produce galactic outflows naturally.

To combat this problem, Springel and Hernquist, 2003a construct a “superwind” model where fluid elements in the star- forming (SF) region are ejected from the region at a fixed speed and are simultaneously hydrodynamically decoupled until they have left the galaxy. A modification was later made by Oppenheimer and Davé, 2006 by linking the velocity dispersion of the host galaxy to the velocity of the wind and the mass loading factor. A wind with this link is referred to as a momentum-driven wind.

The inherent problem with the superwind model is that stars are formed in connection with their parent gas particles. When feedback occurs, it is possible that stars which are still tied in this fashion may be hydrodynamically accelerated, with the possibility existing that these stars could be ejected from the galaxy in which they form, which is not physical.

The blastwave model does not couple gas particles to star particles, but it does not capture the level of detail about the dynamics of the gas as the superwind model does. This leads to a possible problem where the mass of all the star particles is fixed, which could possibly lead to an under-production of stars in regions which are particularly dense, such as in star-burst galaxies (Telesco, 1988; Chapman et al., 2003). Stinson et al., 2006 tested the formula derived by Elmegreen and Efremov, 1997 which determines the fractional amount of gas which will be converted to stars, using the density and the pressure of the gas. Stinson et al., 2006 concluded that reduced star formation would only occur if the gas consumption times were less than 5 Myr, which is seldom, if ever, observed in simulations. The simulations run in this study do not encounter such a scenario, and the results are therefore not compromised by such an eventuality.

The superwind model has been extensively utilised in a number of problems, including damped Lyman-α (DLA) absorbers (Nagamine, Springel, and Hernquist, 2004a; Nagamine, Springel, and Hernquist, 2004b) and in high and low redshift studies of the enrichment of the IGM (Oppenheimer and Davé, 2006; Oppenheimer and Davé, 2009). These studies demonstrate that superwind feedback is critical in suppressing the overproduction of stars, and in recreating the cosmic star formation history (SFH) at high redshift. It also resolves the ’missing baryons’ problem at $z = 0$, by increasing the local fraction of the warm-hot IGM (WHIM) to $40 - 50$ %.

3.2.2.2 GASOLINE - Cooling Mechanisms

The superwind model is unable to include variable mass loading, which is important for modelling the quantity of wind which escapes from galaxies, and in the morphology of galaxies (Dalla Vecchia and Schaye, 2008). The superwind model has been found to struggle with such scenarios (Nagamine, Springel, and Hernquist, 2004a). One solution to this problem is the adiabatic cooling model.

Adiabatic cooling is a refined version of energetic cooling by inhibiting the gas from cooling until the hot SN bubbles can be resolved (e.g. Thacker and Couchman, 2000; Kay et al., 2002; Sommer-Larsen, Götz, and Portinari, 2003; Stinson et al., 2006). This approach has been introduced by Shen, Wadsley, and Stinson, 2010 in the `GASOLINE` code (Wadsley, Stadel, and Quinn, 2004) which is used in this study.

In `GASOLINE` the winds are produced because the ISM is accelerated by pressure generated by the hot gas. This method approaches direct ISM modelling in the high-resolution limit, and is also incorporated in the version of `GASOLINE` used in this study.

Shen, Wadsley, and Stinson, 2010 include feedback from SN II, SN Ia, and stellar winds. The Raiteri, Villata, and Navarro, 1996 model for metal enrichment from SN II and SN Ia is adopted in `GASOLINE`, but AGB stellar feedback is neglected. Any stars which have a stellar mass > 8 M$_\odot$ will explode as SN II during the actual time step, in which they are born. The explosion is modelled using the analytical model for blastwaves produced by these stars (McKee and Ostriker, 1977), which is described in detail byStinson et al., 2006. During the expansion of the SN bubble, gas cooling is suppressed. Less than half the energy of the explosion is transferred, as heat, to the ISM, $E_{SN} = 4 \times 10^{50}$ erg, while the remaining half is assumed to be radiated away. The full energy is, however, used to calculate the blast radius and cooling shut-off time.

The energy which is transferred to the ISM follows the volume weighting scheme outlined by Mashchenko, Wadsley, and Couchman, 2008. Each gas particle has a mass m_i and density ρ_i. Each gas particle affected by an explosion will receive a portion of the metals and SN energy proportional to $\frac{m_i W_{ij}}{\rho_i}$, where W_{ij} represents the SPH smoothing kernel. Wiersma et al., 2009 used a similar method for the distribution of energy and metals from SN Ia explosions. The blastwave model which is currently implemented in `GASOLINE` has a bias to suppress cooling at early epochs when compared to other methods.

Metals from SN II and SN Ia are treated differently in `GASOLINE`. In the case of SN II explosions, main sequence progenitors die and release metals and energy which are distributed to the gas within the blast radius. The yields from Woosley and Weaver, 1995 were used in the analytical fits for iron and oxygen from SN II (Raiteri, Villata, and Navarro, 1996) which are implemented in `GASOLINE`:

$$M_{\rm Fe} = 2.802 \times 10^{-4}\ M_*^{1.864} \tag{3.2.8}$$

$$M_{\rm O} = 4.586 \times 10^{-4}\ M_*^{2.721} \tag{3.2.9}$$

Stinson et al., 2006 describes the feedback from SN Ia according to Raiteri, Villata, and Navarro, 1996, which is also incorporated in `GASOLINE`. For each SN Ia, metals are ejected into the nearest gas particle, of which 0.63 $M_\odot$ is iron and 0.13 $M_\odot$ is oxygen (Thielemann, Nomoto, and Yokoi, 1986). The stellar wind feedback implemented, is based on the work by Kennicutt, Tamblyn, and Congdon, 1994, and the function derived by Weidemann, 1987 was used to calculate the returned mass fraction. The gas which is returned has the identical metallicity of the star particle. The full model for SNe and stellar winds in `GASOLINE` have been outlined and a discussion of their testing follows.

Cosmological simulations utilising the adiabatic feedback model with cooling turned off for 10 Myr for the feedback gas were conducted by Theuns et al., 2002 and Kay et al., 2002. They found that strong winds carried enough metals to produce C_{IV} absorption lines which agree with observations. The optical depth of C_{IV} and C_{III} absorption lines was investigated by Aguirre et al., 2005 using the same simulation, and was compared to observations. They found that metal-enriched hot gas in their simulation was too hot ($10^5 - 10^7$ K). The lack of metal cooling was suggested as being the reason that the simulated C_{IV} absorption lines showed discrepancies from observations.

With the inclusion of the Sutherland and Dopita, 1993 model for metal cooling, Oppenheimer and Davé, 2006 found a better agreement with observational data than Aguirre et al., 2005. The Oppenheimer and Davé, 2006 model was also used by Choi and Nagamine, 2009 to investigate the effect of metal cooling on the growth of galaxies, who found that the local SF efficiency and the accretion on to galaxies were both increased.

3.2.3 Cold Cloud Enlargement

The last processes to be discussed in the context of simulating star formation is how cold clouds come into existence and grow. The star formation and wind models might differ in `GADGET` and `GASOLINE`, but they solve very similar equations for the energy budget of the gas. The final expressions derived here (which are part of the superwind model) are comparable to the hydrodynamic energy equations solved in `GASOLINE`.

It is assumed that, in the region where the cold clouds and the hot phase coexist, a thermal instability exists. The ambient gas and cold gas clouds will therefore exchange mass between them (Field, 1965; Field, Goldsmith, and Habing, 1969; McKee and Begelman, 1990). It is shown that cold clouds grow in mass due to hot gas radiating energy, allowing it to cool from the temperature of the hot phase to that of the cold phase. The mass flux is given by

$$\begin{aligned} \left.\frac{d\rho_c}{dt}\right|_{TI} &= -\left.\frac{d\rho_h}{dt}\right|_{TI} \\ &= \frac{1}{u_h - u_c}\Lambda_{net}(\rho_h, u_h) \quad , \end{aligned} \tag{3.2.10}$$

where Λ_{net} is the cooling (or heating) function of the ambient hot medium which must be calculated separately. Kennicutt, 1989 showed that star formation obeys an observed threshold behaviour, motivating the adoption of a density threshold in this work to govern star formation once there is a thermal instability. This is chosen to depend on the total density of the gas and has the form $\rho > \rho_{th}$. This density threshold is also related to the star formation time-scale,

$$t_*(\rho) = t_0^* \left(\frac{\rho}{\rho_{th}}\right)^{-\frac{1}{2}} \quad , \tag{3.2.11}$$

where t_0^* is an additional parameter of the model outlined above. The difference in the GASOLINE implementation is that the density threshold is related to the star formation mass. Combining the previous results allows on to derive an expression for the mass evolution of the hot and cold phases:

$$\frac{d\rho_c}{dt} = -\frac{\rho_c}{t_*} - A\,\beta\,\frac{\rho_c}{t_*} + \frac{1-f}{u_h - u_c}\,\Lambda_{net}(\rho_h, u_h) \quad , \tag{3.2.12}$$

$$\frac{d\rho_h}{dt} = \beta\frac{\rho_c}{t_*} + A\,\beta\,\frac{\rho_c}{t_*} - \frac{1-f}{u_h - u_c}\,\Lambda_{net}(\rho_h, u_h) \quad . \tag{3.2.13}$$

Consider the right-hand side of the equations (3.2.12) and (3.2.13). The first term describes the processes of star formation and feedback, the second term the process of cloud evaporation, and the third term the growth of clouds resulting from the radiative cooling of the gas. The energy budget of the gas can now be expressed as

$$\frac{d}{dt}(\rho_h u_h + \rho_c u_c) = -\Lambda_{net}(\rho_h, u_h) + \beta\,\frac{\rho_c}{t_*}\,u_{SN} - (1-\beta)\,\frac{\rho_c}{t_*}\,u_c \quad , \tag{3.2.14}$$

where $\beta\,\frac{\rho_c}{t_*}\,u_{SN}$ describes the non-gravitational energy which is ejected by exploding SNe and $(1-\beta)\,\frac{\rho_c}{t_*}\,u_c$ describes the loss of energy in this gaseous phase, due to material which has been trapped in stars . By assuming that the cold clouds have a constant temperature u_c, the temperature evolution of the gas has the form

$$\rho_h\,\frac{du_h}{dt} = \beta\,\frac{\rho_c}{t_*}\,(u_{SN} + u_c - u_h) + A\,\beta\,\frac{\rho_c}{t_*}\,(u_h - u_c) - f\Lambda_{net}(\rho_h, u_h) \quad . \tag{3.2.15}$$

In order to integrate equation 3.2.15 it must be augmented by pressure forces and viscous effects. The evaporation caused by star formation in the cold clouds directly reduces their density, and so lowers the rate at which stars form. By contrast, the cooling rate increases when the density of the hot gas is higher replenishing the clouds more rapidly, thereby increasing the star formation rate. At equilibrium, the growth of cold clouds is balanced by the SN feedback which evaporates it. These equations therefore govern a self-regulated cyclic model for star formation.

This section has highlighted the differences in the two most widely used models for star formation and stellar feedback. Although both models have been proven to work in a number of scenarios, the dynamics of the ISM and IGM are not fully captured within either description. Each choice of model therefore entails as number of drawbacks that need to be taken into account in the analysis of the outcomes. Finally, the hydrodynamic energy equations solved in `GADGET` have been derived in order to show their similarity to the equations solved by `GASOLINE`, which appear in the next section.

3.3 Chemistry Cooling Model - GASOLINE Description

3.3.1 General Description of Cooling and Heating in the Code

The hydrodynamic energy equations can be written as:

$$\frac{D\epsilon}{Dt} = -\frac{\mathrm{P}}{\rho}\nabla \cdot \mathbf{u} - \frac{1}{\rho}\nabla \cdot \mathbf{F} + \frac{1}{\rho}\mathbf{\Psi} + \frac{H-\Lambda}{\rho} \quad . \tag{3.3.1}$$

Here, the specific internal energy of a fluid element of the gas is represented by ϵ, $-\frac{\mathrm{P}}{\rho}\nabla \cdot \mathbf{u}$ represents the adiabatic work done on the gas due to the change in internal energy as a result of PdV work, $\mathbf{F}$ represents the flux of heat that is conducted out of the fluid element, $\mathbf{\Psi}$ represents the viscous dissipation rate, and H and Λ represent the internal heating and cooling rates, respectively. H and Λ can be affected by a number of processes.

H and Λ are both functions of each gas particle's temperature (T), incident radiation field (J_v) and of the density, n_i, of each ion species present within it. This can be summarised as:

$$\frac{H-\Lambda}{\rho} = f(n_i, T, J_v) \quad . \tag{3.3.2}$$

The density of each ion species is dependent on the formation and destruction rates of each particular species, which are functions of n_j, T and J_v. These densities are summarised as:

$$n_i = f(n_j, T, J_v) \quad , \text{with } j \neq i \ . \tag{3.3.3}$$

Networks of differential equations are used to account for all the free electrons available for ionization of atoms, which are then used to determine the densities of the ion species. The number of elements considered in these networks can make them arbitrarily complicated (Ferland et al., 1998; Gnat and Ferland, 2012; Oppenheimer and Schaye, 2013a). The concept of non-equilibrium ionization is to carry the ionization state of every species from timestep-to-timestep as the calculation is carried out, rather than assuming ionizational equilibrium (e.g. Oppenheimer and Schaye, 2013b).

Primordial cooling is responsible for the formation of Pop III stars. The mass of these stars, and therefore the amount of metals they generate via SN explosions, is governed by the primordial chemical abundances as these affect the efficient of the gas cooling. Once these stars die via SNe the enrichment of the ISM and IGM by metals alters which coolants are dominant. Metals cool more easily and much more quickly than the primordial gas, and so become far more important in the evolution of the cosmos. They also behave very differently once an external UV background is present. Their inclusion in simulations is crucial to galaxy and structure formation, and to be able to compare simulations to observational data. Metal cooling is therefore discussed in the next subsection.

3.3.2 Metal Cooling under a UV Radiation Background

Line transitions within collisionally excited metal ions are significant coolants of the IGM (see e.g. Sutherland and Dopita, 1993). The gas dynamics are altered by metal cooling, since it affects both the gas temperature and the ionization states of the observable metal species. Calculating the metal cooling rates during simulations is not feasible, therefore tabulated cooling tables are interpolated (as in Oppenheimer and Davé, 2006; Wiersma et al., 2009; Choi and Nagamine, 2009.) The metal cooling rates are computed as functions of density, temperature, metallicity of the gas and radiation background.

However, the IGM and ISM are exposed to a UV radiation background. Wiersma, Schaye, and Smith, 2009 studied this and found that, in the temperature range $10^4 < T < 10^8$ K, the UV background, on the whole, tends to suppress the cooling rates and shifts the cooling curves' peaks to higher temperatures. This suppression is due to the UV radiation ionizing the plasma, thereby reducing the number of ions that can be collisionally excited. When the temperature $100 < T < 10^4$ K, the number density of free electrons (n_e) is increased by the UV background, thus enabling a greater cooling due to forbidden line transitions from low ionized species, such as C_{I}, C_{II}, Si_{I}, Si_{II} and O_{I}. In the enriched IGM at low temperatures, forbidden line cooling is the dominant cooling process.

In low density regions ($n_H \lesssim 10^{-4}$ cm^{-3}), some higher-ionized species with strong magnetic dipole transitions (such as Ne_{V} and Ne_{VI}) can be created by photoionization. These ions provide more efficient cooling of the plasma, producing a local cooling peak around 10^3 K (Shen, Wadsley, and Stinson, 2010). Once the density increases, these ions disappear, making the less ionized species mentioned above the dominant coolants. This is consistent with ISM cooling models (e.g. Wolfire et al., 2003).

Overall, the greatest effect of the radiation background is to substantially increase the metal cooling rate between 100 and 10^4 K over collisional ionization equilibrium (CIE). Shen, Wadsley, and Stinson, 2010 find that the adding the CIE model for metal cooling to the primordial cooling rates results in severe over and under estimations of the cooling rates, depending on the temperature. It must be noted that the UV background they adopt overestimates the effect of photoionization on the metal cooling rate, due to amplitude which is too high.

To solve for the radiative cooling, the process is split into three components:

$$\Lambda = \Lambda_{\mathrm{H,He}} + \Lambda_{\mathrm{metal}} + \Lambda_{\mathrm{Comp}} \quad , \tag{3.3.4}$$

where $\Lambda_{\mathrm{H,He}}$ represents the cooling due to the primordial H and He species (H, H^+, He, He^+, He^{++}), Λ_{metal} represents the cooling due to metals, and Λ_{Comp} refers to the net Compton heating or cooling. The primordial gas ionization, heating and cooling rates are calculated directly, using the non-equilibrium rates from Abel et al., 1997. The difference between equilibrium and non-equilibrium cooling is important to this discussion.

Equilibrium cooling assumes that the ions and free electrons are at an equilibrium value for each time-step, and so assign them Boltzmann distributions each time they are required for calculations. This has been shown to be an extremely inefficient cooling model, leaving the gas temperature almost unchanged by the time Pop III stars should form at $z \sim 20$. At high redshift, particularly around reionization, the use of non-equilibrium rates can alter the temperature by several thousand degrees. This is due to non-equilibrium methods keeping a record of the abundances of each species considered at every time-step of the simulation.

We continue the discussion of the cooling function by considering the first term. The abundance of hydrogen is unaffected by the inclusion of metals, but the abundance of He is. For this reason, the relation from Jimenez et al., 2003, Shen, Wadsley, and Stinson, 2010 estimated the helium mass abundance Y as a function of metallicity. In the case where the metal mass abundance $Z < 0.1$ ($\sim 10\ \mathrm{M}_\odot$),

$$Y = Y_{\mathrm{p}} + \left(\frac{\Delta Y}{\Delta Z}\right) Z \quad , \tag{3.3.5}$$

where $Y_{\mathrm{p}} = 0.236$ represents the helium mass abundance for the primordial gas, and $\frac{\Delta Y}{\Delta Z} = 2.1$ represents the helium mass to metal mass ratio produced in stars. In the case where $Z > 0.1$, a linear decrease is applied to Y so that $Y = 0$ when there are 100% metals ($Z = 1.0$).

The photoionization code `CLOUDY` (Ferland et al., 1998) was used to calculate the metal heating and cooling rates under a UV radiation background, producing a cooling table which was the same for every simulation run for this study. `CLOUDY` assumes that metals are in ionization equilibrium, which is a good approximation when an extragalactic UV background is used. The UV background is, generally, a function of space and time. A uniform built-in extragalactic UV background was called from `CLOUDY` to generate the metal cooling table. This UV background includes both quasar and galactic radiation. The radiation field is a function of wavelength, and is turned on at redshift $z = 8.9$. This radiation field is also used for the primordial species, and is evolved for all species until redshift $z = 0$.

Due to the time evolution of the radiation background, the metal cooling is dependent on redshift. The metal cooling utilised in (our version of) GASOLINE is the same as that of Shen, Wadsley, and Stinson, 2010 and assumes relative solar abundances for the metal cooling. The default solar composition from CLOUDY was utilized, containing the first 30 elements from the periodic table (data compiled from Grevesse and Sauval, 1998, Holweger, 2001, Allende Prieto, Lambert, and Asplund, 2001, Allende Prieto, Lambert, and Asplund, 2002; for the documentation details, see CLOUDY version 07.02 Table 9). To calculate the metal cooling rates, the primordial cooling rates were subtracted from the sum of the first 30 elements cooling rates, including those of H and He. The work by Shen, Wadsley, and Stinson, 2010 showed that the net cooling rate depends linearly on the metallicity. Therefore, the metal rates for solar abundance can be tabulated and then scaled according to the metallicity. This allows the metal cooling rates to be represented as:

$$\Lambda_{\mathrm{metal}}(T,\rho,z,Z) = \frac{Z}{Z_{\odot}}\Lambda_{\mathrm{metal},\odot}(T,\rho,z) \quad , \tag{3.3.6}$$

where T represents the temperature, ρ the density, z the redshift and Z the metallicity of the gas.

3.3.3 Turbulent Metal Diffusion

SPH uses discrete particles to model the fluid so any metals which are newly created and injected into the gas are locked within specific particles. A manifestation of this artificial process had been discussed by Aguirre et al., 2005 where the simulated metal distributions which were too inhomogeneous when compared with observations. The importance of mixing was investigated by Wiersma et al., 2009 using SPH-smoothed metallicities in comparison to conventional particle metallicities. They found a significant increase in low-metallicity material being generated by smoothing, but this approach suffers from an inability to preserve the spread of metals over time with its impact on cooling and the thermal history of the gas. The direct modelling of the turbulence within the ISM is not currently possible in cosmological simulations. Smagorinsky, 1963 proposed a subgrid turbulent diffusion model which uses a shear-dependent diffusion term to replace any unresolved turbulent mixing. The version of the GASOLINE code utilised in this work employs a variant of this method, implemented by Shen, Wadsley, and Stinson, 2010. In order for them to investigate the non-local effects of metal cooling, they calculated metal cooling based metal diffusion.

Since SPH is a Lagrangian scheme, it does not implicitly contain diffusion of scalar quantities like metals. Even simple processes such as convection and Rayleigh-Taylor instabilities have been demonstrated to have physically incorrect results (Wadsley, Veeravalli, and Couchman, 2008). Wadsley, Veeravalli, and Couchman, 2008 were able to match Eulerian grid code results (which naturally have turbulent mixing due to the use of advection estimates for the propagation of hydro dynamical quantities) to those of SPH by including a simple turbulent model. This model utilises a diffusion coefficient $D = C\ \Delta v\ h_{\mathrm{SPH}}$, where Δv represents the pairwise velocity, h_{SPH} the resolution scale, and $C \sim 0.1$. It therefore was possible to use SPH to construct entropy profiles for similar non-radiative galaxy clusters which were comparable to high- resolution grid codes. This was a major flaw in the cluster comparison made by Frenk et al., 1999. SN remnants were simulated and studied, implementing a similar scheme, by Greif et al., 2009.

As has been mentioned previously, mixing is critical for IGM studies due to galactic outflows being highly turbulent. Turbulent mixing models have long been studied in environmental and engineering fluid mechanics. The first proposed mixing estimator for the atmospheric boundary layer by Smagorinsky, 1963 formed the basis for the robust mixing estimator incorporated in GASOLINE. This atmospheric boundary layer estimator is expressed as:

$$\frac{dA}{dt}|_{\text{Diff}} = \nabla(D\nabla A) \quad ,$$

$$D = C|S_{ij}|h^2 \quad , \tag{3.3.7}$$

where A represents any scalar, S_{ij} represents the trace-free shear tensor, and h represents the measurement scale (which in this case is $\sim h_{\text{SPH}}$. The choice for S_{ij} means that no diffusion occurs for compressive or purely rotating flows. The diffusion expression for a scalar A_{p} acting on a particle p is computed in SPH as follows:

$$\widetilde{S}_{ij}|_{\text{p}} = \frac{1}{\rho_{\text{p}}} \sum_q m_q (v_j|_q - v_j|_{\text{p}}) \nabla_{\text{p},i} W_{pq} \quad ,$$

$$S_{ij}|_{\text{p}} = \frac{1}{2}\left(\widetilde{S}_{ij}|_{\text{p}} + \widetilde{S}_{ji}|_{\text{p}}\right) - \delta_{ij}\frac{1}{3}\text{Tr}\left(\widetilde{S}_{ij}|_{\text{p}}\right) \quad ,$$

$$D_{\text{p}} = C|S_{ij}|_{\text{p}} h_{\text{p}}^2 \quad ,$$

$$\frac{dA}{dt}|_{\text{Diff}} = -\sum_q m_q \frac{(D_{\text{p}} + D_q)\,(A_{\text{p}} - A_q)\,(r_{pq} \cdot \nabla_{\text{p}} W_{pq})}{\frac{1}{2}\,(\rho_{\text{p}} + \rho_q)\, r_{pq}^2} \quad , \tag{3.3.8}$$

where we sum over the SPH nearest neighbours q, δ_{ij} is the Kronecker delta, W represents the SPH kernel function, ρ_q is the density, r_{pq} refers to the separation between particles as a vector, $v_i|_q$ represents the component of the particle's velocity in the i direction, ∇_{p} represents the gradient operator of particle p (which operates on W) and $\nabla_{\text{p},i}$ represents the ith component of the resultant vector. This differs from the models adopted by Wadsley, Veeravalli, and Couchman, 2008 and Greif et al., 2009 because, instead of using a simple velocity difference to calculate the diffusion coefficient, our version of GASOLINE use the turbulent mixing model. Since the diffusion coefficient depends on the velocity shear, shearing flows which have mixing are better modelled using this scheme. In the case where two phases of fluids have no shearing motion (for example when a clumpy medium is embedded within a hot wind, and the two fluids move at identical speeds) the turbulent diffusion is not added. Shen, Wadsley, and Stinson, 2010 found that a value of 0.05 for C was sufficient for cluster comparisons, which they obtained from turbulence theory.

3.4 Streaming Models

In this section, we will outline three simulations done by Maio, Koopmans, and Ciardi, 2011, Stacy, Bromm, and Loeb, 2011 and Greif et al., 2011b. Each of them implemented streaming velocities, but in varying box sizes and with varying numbers of particles.

Their studies are all based on the work by Tseliakhovich and Hirata, 2010 who predict an rms velocity of 30 kms^{-1}, which is coherent over a few Mpc comoving. Each of these studies adds homogeneous velocities to the x-components of the gas's velocity field. The model they adopt is given in detail in Stacy, Bromm, and Loeb, 2011, but a brief outline is given here, giving the relevant expressions within their model and highlighting key points.

In order to characterise the gas collapse, the cosmological Jeans mass is used (as in section 3.2). The virial velocity V_{vir} is used to characterise the gravitational potential of a mini-halo. The gas will begin to fall into the mini-halo when

$$V_{vir} > c_s \quad \text{, where } c_s = \sqrt{\frac{k_B T}{\mu m_H}} \quad . \tag{3.4.1}$$

Here, c_s is the sound speed. Once the infall begins, c_s and V_{vir} become coupled through adiabatic heating and the density scales as c_s^3. The adiabatic phase of the evolution of the gas continues until the virial mass of the mini-halo $M_{vir} > M_J$, where M_J is the Jeans mass. In the case where there is no streaming velocity,

$$M_J = \left(\frac{\pi}{6}\right) \frac{c_s^3}{G^{\frac{3}{2}} \rho^{\frac{1}{2}}} \quad . \tag{3.4.2}$$

The adiabatic phase also has the criteria that the cooling time (driven by H_2) of the gas $t_{cool} < t_{ff}$, where t_{ff} is the free-fall time of the gas. In order for the next phase of rapid collapse to begin, both the Jeans criteria ($M_{vir} > M_J$) and the cooling criteria ($t_{cool} < t_{ff}$) must be satisfied. The gas then quickly reaches the maximum number density $n_{max} = 104\ \mathrm{cm}^{-3}$.

The difference between the non-streaming and streaming velocity cases lies in the difference in their effective velocities. When a streaming velocity is introduced, the effective velocity becomes

$$v_{eff} = \sqrt{c_s^2 + v_s^2} \ , \tag{3.4.3}$$

with $v_s = \frac{v_{s,i}}{1+z}$, so that v_s attenuates with decreasing redshift. Thus, the infall of gas is delayed. The Jeans mass in this regime is now

$$M_J = \left(\frac{\pi}{6}\right) \frac{v_{eff}^3}{G^{\frac{3}{2}} \rho^{\frac{1}{2}}} \ . \tag{3.4.4}$$

The redshifts for collapse are found using expressions for V_{vir}, and the density of the gas is also computed. The initial setups of the three studies are included as separate subsections, with the overall results being summarised in the final subsection.

3.4.1 Maio et al. 2011

Maio, Koopmans, and Ciardi, 2011 uses the three-dimensional tree-SPH code `P- GADGET2` (Springel, 2005). The initial conditions are setup using the `N-GENIC` code, at $z_i = 100$ within box sizes of 0.7 and 1 Mpc h^{-1}. A ΛCDM cosmology was considered, with $\Omega_\Lambda = 0.7$, $\Omega_m = 0.3$, $\Omega_b = 0.04$, h = $\frac{H_0}{100}$ km s^{-1} Mpc^{-1} = 0.7 (where H_0 is Hubble expansion rate at present), $\sigma_8 = 0.9$ and a spectral index $n_s = 1$. The initial conditions contain 320^3 particles for both DM and gas. Within this framework, the mass resolutions for the gas and DM are $\sim 10^2$ M$_\odot$ h^{-1} and $\sim 7.5 \times 10^2$ M$_\odot$ h^{-1}, respectively. For exploration of larger scale features and resolution studies a set of simulations was conducted within boxes of 5 Mpc h^{-1}.

They track the abundances of H, H^+, H^-, H_2, $H_2{}^+$, He, He^+, He^{++}, e^-, D, D^+ and HD, using the chemical networks and cooling terms outlined in Maio et al., 2006, Maio et al., 2007, Maio, 2009, Maio et al., 2010 and Maio et al., 2011. The chemical abundances were initialized as in Maio et al., 2007 and Maio et al., 2010.

A homogeneous streaming velocity field was added to the gas in the x-direction with $v_{s,i} = 0; 3; 6$ km s^{-1}, corresponding to velocities of 0, 30 and 60 km s^{-1} at the epoch of recombination. These were implemented in accordance with the work of Tseliakhovich and Hirata, 2010. The variance in these velocities is due to the variance in the rms value for the velocity of 30 km s^{-1} as in Tseliakhovich and Hirata, 2010, and can differ up to an order of magnitude. It is noted here that the initial redshift for simulations $z_{in} \gg 200$ is questionable and should therefore be closer to $z_{in} \sim 200$ for reliable results.

3.4.2 Stacy et al. 2011

The simulations which were carried out using the three-dimensional SPH code `GADGET` (Springel, Yoshida, and White, 2001; Springel and Hernquist, 2002). The box size chosen was 100 h^{-1} kpc (comoving) and the initial conditions included both gas and DM particles, initialized at $z = 100$ with 128^3 particles for each species. A ΛCDM cosmology was chosen with $\Omega_\Lambda = 0.7$, $\Omega_m = 0.3$, $\Omega_b = 0.04$ and h = 0.7. Two values of the fiducial normalization of the power spectrum were tested: the standard $\sigma_8 = 0.9$ and the accelerated case where $\sigma_8 = 1.4$. The accelerated case leads to mini-halo formation occurring earlier, and therefore earlier star formation. The mass of the gas particles within this framework is $m_g = 8\ \mathrm{M}_\odot$, leading to a mass resolution of $M_{res} \simeq 1.5\ \mathrm{N}_{neigh} m_g \lesssim 400\ \mathrm{M}_\odot$, with $\mathrm{N}_{neigh} \simeq 32$ is the typical number of particles in the SPH smoothing kernel (e.g. Bate and Burkert, 1997). The mass resolution here allows the tracking of the evolution of the gas up to a maximum number density of $n_{max} = 104\ \mathrm{cm}^{-3}$.

The chemical network, which was used to capture the thermal and chemical evolution of the gas, tracked the abundances of H, H^+, H^-, H_2, ${H_2}^+$, He, He^+, He^{++}, e^-, D, D^+, D^-, HD and HD^+, using the same chemical network outlined in Greif et al., 2010 and the same cooling terms.

The simulations performed tested with and without a streaming velocity. The streaming velocities implemented, at $z_i = 100$, were $v_{s,i} = 3; 10\ \mathrm{kms}^{-1}$. This was done to test the rms velocity of TH (Tseliakhovich and Hirata, 2010) which is 30 kms^{-1} at recombination. This value can vary by an order of magnitude, and so the second velocity was chosen to test the case where suppression is larger. The streaming velocities will attenuate with $z + 1$, hence the decrease from the recombination epoch. These values for $v_{s,i}$ were chosen to be in a similar range to Maio, Koopmans, and Ciardi, 2011, whose values are listed above. All the velocities were introduced in the x- direction.

3.4.3 Greif et al. 2011

Greif et al., 2011b used the moving mesh code AREPO, which is based on a set of grid points that are advected with the flow (Springel, 2010). This has a higher efficiency and accuracy compared SPH simulations, while maintaining the natural adaptivity of SPH. They argue that the Galilean invariance of AREPO is more advantageous for the study of supersonic bulk velocities than other adaptive mesh refinement simulations.

The box size chosen was 500 kpc with 256^3 particles for both DM and gas. A coarse DM simulation for each set of initial conditions was run in order to find the Lagrangian region of the first mini-halo with a virial mass $\geqslant 5 \times 10^5\ \mathrm{M}_\odot$. The particle masses were 272 $\mathrm{M}_\odot$ and the comoving gravitational softening length was 68 pc. A ΛCDM cosmology was considered, with $\Omega_\Lambda = 0.73$, $\Omega_m = 0.27$, $\Omega_b = 0.046$, h = 0.7 and $n_s = 0.96$. The five-year Wilkinson Microwave Anisotropy Probe results (Komatsu et al., 2009) were used to set the parameters above. Three values of the fiducial normalization of the power spectrum $\sigma_8 = 0.9; 1.1; 1.3$ were used in order to alter the redshift of collapse, thereby extending the scope of the simulations given that the box size is so limited. The initial conditions were computed for $z = 99$.

Once the location of a mini-halo, matching the selection criteria, is found in each simulation, the refinement criteria described in Greif et al., 2011a in order to increase the mass resolution around the target halo. The masses of the DM and gas particles are then reduced to 3.53 and 0.72 $M_\odot$, respectively. The comoving gravitational softening length within this refined region is also reduced to 17pc. It was assumed that the transfer functions for the gas and DM components were identical. Although this can substantially affect the filtering mass scale (Naoz, Perets, and Ragozzine, 2010), it was argued that the same parameters were used for all the simulations, and so the effects of the streaming velocities would affect all of them identically. Further, only the effects of the steaming velocities were studied, so the results are therefore independent of this choice.

A Streaming velocity was added to the gas in the x-direction, with $v_{s,i} = 3$ km s^{-1}. This corresponds, roughly, to the 1σ peak. To ensure that only refined particles collapse into the mini-haloes, the high-resolution region was extended in the x-direction. The chemical network, which captured the chemical and thermal evolution of the gas, tracked the abundances of H, H^+, H^-, H_2, $H_2{}^+$, He, He^+, He^{++}, e^-, D, D^+ and HD (Glover and Jappsen, 2007; Greif et al., 2011a). This network included the rotational and vibrational line cooling of H_2 and HD, collisionally-induced H_2 line emission, collisionally-induced H_2 dissociation cooling, and heating via three-body H_2 formation (see Greif et al., 2011a for further details).

3.4.4 Results

All three studies found that star formation was systematically delayed by the inclusion of a streaming velocity, with Greif et al., 2011b finding a delay of $\Delta z = 4$, who found the initial redshift of collapse at $z = 19.8$. It was concluded that a higher kinetic energy for the gas during the recombination epoch means that DM haloes retain less material, the gas condenses more slowly making molecular formation less efficient and effective, and thus resulting in less efficient cooling which delays the formation of stars. This particularly applies to small primordial haloes with masses $\sim 10^4 - 10^8$ $M_\odot$ (see Tseliakhovich and Hirata, 2010), due to the fact that their dimensions are comparable to, or smaller than, the baryon Jeans length. The gas, in this case, does not fragment within the halo, and, since only large haloes are capable of trapping such quantities of gas, the gas partially or wholly flows out of the halo. This then affects the large scale growth of the Universe by altering the small scale evolution, due to the strong suppression of the inflow and condensation of the gas. Maio, Koopmans, and Ciardi, 2011 also found that streaming velocities have practically no effect on DM- dominated haloes. Stacy, Bromm, and Loeb, 2011 found that the thermal evolution of the gas was relatively unaffected by the addition of a streaming velocity, except that, for low-density gas, the streaming velocity acted as a heating term.

Due to the spatial coherence lengths of Tseliakhovich and Hirata, 2010 streaming velocities, which correspond to many megaparsecs in the current Universe, it is plausible that both reionization and the 21cm background could both carry observalble imprints of such a streaming velocity (Furlanetto, 2006; Barkana and Loeb, 2001). There is the further possibility that these could affect conditions for observing Pop III star SNe (e.g. Bromm and Loeb, 2002). Cosmological parameters, such as those which are related to the properties of dark energy, whose parameters are based on large-scale estimates could be affected by more massive objects forming at later times inheriting such a distribution. These are due to small-scale star formation effects being able modify large-scale distributions, thereby affecting large-scale structure formation and thus cosmological parameters could be affected.

In this chapter we have discussed the numerical recipe governing the formation of stars, with the inclusion of a chemistry network. The effect this has on stellar feedback has also been outlined, thus giving a detailed description of the chemical and thermal evolution of the gas from early times. The additional study of simulations which implemented a primordial streaming velocity, provides a holistic approach for cosmic evolution from the time of decoupling and recombination. The next chapter will focus on what was done in this work, detailing the improvements made to the chemistry model, and on how a streaming velocity was added.

Chapter 4

Numerical Implementation

The additions made in this work and the setup of the simulations run to test them are laid out in this Chapter. The implementation of molecular cooling is discussed in section 4.1. Including H_2 has been done by numerous authors and the species which are required to form H_2 and into which H_2 can decay. The inclusion of HD is more complex, due to the difficulties arising from the chemical network on which it relies. This section will summarise these complexities and explain how the final chemical network was chosen. The chemical network as employed in the simulations in this study are tabulated in Appendix B. The summary of the various studies done on the effects of streaming velocities is presented in section 3.4. All these studies confirm that primordial streaming velocities have a significant impact on the evolution of the gas and stars, most importantly they delay the formation of the first stars. The implementation our streaming velocity model is detailed in section 4.2. The setups and parameters for the `GASOLINE` simulations furnished with our models are given in section 4.3.

4.1 Implementing Molecular Cooling

Adding in H_2 and HD are done via similar arguments, following the model adopted by Christensen et al., 2012 who implemented H_2 in their version of `GASOLINE`. To keep this discussion as brief and focussed as possible, each subsection introduces the idea behind the process implemented, and then contains a sub-subsection (where necessary) for H_2 and HD, respectively.

An SPH approach is adopted by Christensen et al., 2012 in their model tracking the non-equilibrium abundance of H_2, using the formation and destruction rates local to each gas particle. Dense clouds have dust grains within them which are the major contributors to H_2 formation, while photodissociation is the major branch for H_2 destruction, both heavily affecting the abundance of H_2. The dust in these clouds forms a natural shield for H_2 formation and must be included. Photodissociation for both H_2 and HD are discussed in this section, as they are important for regulated star formation. Although implemented for both, our simulations did not introduce external UV fields as this study is focussed on star formation before $z \sim 10$, which is before these UV fields are really effective. The model we adopt for HD introduces the same processes as H_2.

To illustrate this for the reader, two reaction networks are shown. The first is for He, which has a very simple network. This was chosen to illustrate that at least one creation and one destruction reaction must be included for every species. The reaction network is shown in table 4.1.

Creation Reactions	Destruction Reactions
$He^+ + e^- \longrightarrow He + \gamma$	$He + e^- \longrightarrow He^+ + 2\,e^-$
$He^+ + e^- \longrightarrow He + \gamma$ (dielectronic radiation)	

TABLE 4.1: A simple reaction network for He, illustrating that a network requires both creation and destruction rates to balance the abundance of the species. The reaction rates associated with these vary, and so the creation-to-destruction reaction ratio need not be 1:1.

To show how complicated these networks can become, the full network for H_2 is shown in table 4.2. In contrast to He, H_2 has more destruction reactions. The creation mechanisms are sufficient to increase the abundance of H_2 down to $T \sim 150$ K, where HD becomes abundant enough to be the dominant coolant, and the destruction mechanisms for HD reduce the overall H_2 abundance.

Creation Reactions	Destruction Reactions
$H + H^- \longrightarrow H_2 + e^-$	$H_2 + H_2 \longrightarrow H_2 + 2\,H$
$HD + H^+ \longrightarrow D^+ + H_2$	$H_2 + H \longrightarrow 3\,H$
$HD + H \longrightarrow D + H_2$	$H_2 + H^+ \longrightarrow {H_2}^+ + H$
	$H_2 + e^- \longrightarrow 2\,H + e^-$
	$D + H_2 \longrightarrow HD + H$
	$D^+ + H_2 \longrightarrow HD + H^+$

TABLE 4.2: A more complex reaction network is illustrated for H_2, giving the reader an idea about the difficulties involved in creating a full network. The creation-to-destruction reaction ratio is again not 1:1.

The introduction of HD into simulations is complicated by the number of species which could possible affect its abundance. It has been found that the major cooling species altering the abundance of HD are H_2 and D. To construct a sufficient model to track these abundances, H^-, D^- and D^+ are added to the chemical network. The abundance of HD depends very heavily on the abundance of H_2, with an expected abundance for HD $Y_{HD} = 10^{-2} - 10^{-3} Y_{H_2}$ (e.g. Puy et al., 1993; Galli and Palla, 1998; Flower, 2000). Lipovka, Núñez-López, and Avila-Reese, 2005 argue that HD can be as an important a coolant as H_2 at temperatures $\gtrsim 3000$ K.

Several other species have also been proposed as potentially being important. D. Savin suggested that at low gas temperatures D_2 might be important for the destruction of H_2, but the work by Glover and Abel, 2008 showed that this is not the case. The abundances of ${H_3}^+$ and HeH^+ are far too small to have any noticeable impact unless the gas density becomes particularly high (and can be resolved at such levels; Glover and Savin, 2006). Li and other heavier elements only occur in trace amounts and are again unnoticeable in cosmological simulations. We exclude the species discussed in this paragraph as they have negligible impact at the early stages we are interested in.

Christensen et al., 2012 also implemented a model for LW radiation in `GASOLINE`. Gnedin, Tassis, and Kravtsov, 2009 presented an implementation of LW radiation which is intended for AMR simulations and is too computationally intensive to be feasibly introduced into SPH simulations. Christensen et al., 2012 provided a simplified form of this model, and this study implements the same model. LW radiation introduced to resolve the over-cooling problem associated with an over-production of H_2 at low redshifts. But other models have also been proposed the H_2 over-cooling problem. Due to the lack of theoretical understanding we have decided to not included the effects of LW radiation in our setup, as it is expected to have negligible effects at high redshifts, which is where we expect the first stars to form ($z \sim 20 - 30$).

Gas-phase formation and dissociation refer to the creation and destruction (of any species in the chemical network) which rely on non-equilibrium reaction rate coefficients, which are added together to find the net change which will be added to the abundance of the species. Non-equilibrium rates are particularly effective when metals aren't included, as metal cooling is much more efficient than H and He compounds. In particular, the H_2 abundance is very sensitive to this. An increase in the abundance of H_2 naturally drives up the abundance of HD. A semi-implicit solver is implemented to calculate the H_2 abundance in each gas particle at every time step, using cooling and heating rates. The integrator then calculates the abundances of D and HD, respectively, using the same method.

The decision about which rates to include proved difficult because reaction networks often include the creation of minor species (such as $H_2{}^+$). This study chose to consider only those reactions which had our species network (H, H^+, H^-, He, He^+, He^{++}, H_2, D, D^+, D^-, HD and HD^+) which were involved on both sides of the reaction rates chosen. The rates used are obtained from different authors (e.g. Verner and Ferland, 1996; Galli and Palla, 1998; Abel et al., 1997; Glover and Abel, 2008) who apply fitting functions to observational data. The curves of "best fit" each represent a single non-equilibrium rate for a particular reaction. Glover and Abel, 2008 currently provide the most up-to-date and detailed reaction network from which we implement a reduced number of reactions (see Appendix B for the full network).

The simplified network incorporates the interactions between H_2, D, D^+, D^- HD and HD^+. Each of these rates was included separately and then test runs were made to check whether it worked and what effect it had. Quite a few of these rates caused issues with the feedback code within `GASOLINE` and had to be excluded. Some additional reactions where tested but would cause the feedback algorithm to stall and therefore had to be excluded. These rates mainly involved HD^+, which has a very small impact on the overall HD abundance in cosmological simulations due to their reduced resolution. The final network is tabulated in Appendix B.

HD^+ was basically removed, leaving just four rates in which it is involved: two creation and two destruction. It was found in testing that it remains at such a low abundance level (due to its reduced network) that it has an insignificant impact on cooling, but it does alter the abundances of the species, affecting the overall abundance of HD. It is only included in the discussion of the gas phase formation of various species within section 4.1.

The model we implement can be broken down into four components: formation on dust grains, radiation shielding, gas-phase formation and dissociation, and heating and cooling. Each of these are now examined in turn. The discussion of the HD rates only affects the gas-phase formation and dissociation directly, as these depend on the non-equilibrium rates. They affect the overall abundance of HD, which is used in both the radiation shielding and heating and cooling calculations. The H_2 abundance remains relatively unchanged by the excluded rates, but is affected (at low-temperatures) by its destruction in order to form HD. The formation on dust grains only concerns the abundance of H_2, and is therefore affected at low temperatures. Although metal cooling is often included in discussions, its purpose is to regulate the transition to regulated star formation, effective only once the first stars have formed and have ejected metals. This study is concerned with the primordial gas and the processes governing the abundances of the primordial species.

4.1.1 Dust Grain Formation

This subsection governs a formation to path for H_2 only after the introduction of metals. It is included in this study because it is an important for the regime change from primordial gas to metal enriched gas, and contributes to the amount of HD which can be formed, but is negligible in comparison to gas phase formation and dissociation in the primordial gas.

Dust grain formation is a very important formation path for H_2, but is an irrelevant path for HD and is therefore only implemented for H_2. It relies on the metals within the chemical environment of the gas. Once metal pollution is present, even in small pockets, dust grain formation will dominate over gas-phase formation. The equation for the rate of dust formation (R_d) adopted in our model follows that of Wolfire et al., 2008, which is observationally motivated by the same reasoning asGnedin, Tassis, and Kravtsov, 2009. Within this regime, dust and gas density both affect the rate of H_2 formation. The amount of dust is calculated by assuming that the ratio of dust-to-gas is a function of metallicity, Z. The subgrid clumping factor and dust's effects are both contributors to the amount of H_2 formed by this process (Christensen et al., 2012). The rate of dust formation is then,

$$R_\mathrm{d} = 3.5 \times 10^{-17} \frac{Z}{Z_\odot} C_\rho \,\mathrm{cm}^3\,\mathrm{s}^{-1} \quad , \tag{4.1.1}$$

where $Z_\odot$ is the solar metallicity and C_ρ is the gas clumping factor. The value for C_ρ is set by assuming a log-normal density structure for the gas, with $C_\rho = \mathrm{e}^{\sigma^2_{\ln\rho}}$ were, σ_ρ represents the width of the distribution. The best fitting value for C_ρ is 10.0 as shown by Gnedin, Tassis, and Kravtsov, 2009.

The radiation shielding from LW and external UV background and is implemented for H_I, H_2 and HD. However, since it is not tested in this study because it will have negligible effects at high-redshifts and has therefore been turned off, we exclude its discussion in this work. Radiation shielding is mainly effective at $z < 10$, where the external UV background and LW radiation become much more effective, increasing the photodissociation rates of the gas and providing consistent heating of the gas. We move the discussion to the gas phase formation and dissociation, since this has the greatest effect on the primordial gas.

4.1.2 Gas-phase Formation and Dissociation

4.1.2.1 H2 Non-equilibrium Formation and Destruction

Gas-phase reactions affect the abundance of H_2, and provide additional cooling to the gas, particularly in low-metallicity regions. Gas-phase formation for H_2 is governed by two processes:

$$\mathrm{H_2}^+ + \mathrm{H} \longrightarrow \mathrm{H_2} + \mathrm{H}^+ \tag{4.1.2}$$

$$\mathrm{H}^- + \mathrm{H} \longrightarrow \mathrm{H_2} + \mathrm{e}^- \tag{4.1.3}$$

For H_2 formation via H^- we use the rate coefficient $k_1 0$ for the production of H^- and $k_1 1$ for 4.1.3, which can both be found in Appendix B, table B.2. We assume that the H_2 abundance is primarily independent of the H^+ abundance.H_2 is not only destroyed via photodissociation, but also through collisions with H_2, H_I, H^+ and e^-. The rate coefficients for these collisions were originally taken from Lepp and Shull, 1983, Dove and Mandy, 1986, Abel et al., 1997 and Donahue and Shull, 1991,respectively, but are now replaced by the rates from Martin, Keogh, and Mandy, 1998 and Shapiro and Kang, 1987, Lepp and Shull, 1983 and Mac Low and Shull, 1986, Savin et al., 2004, and Trevisan and Tennyson, 2002a. The resulting evolution equation for the abundance ratio $X^{\mathrm{gp}}_{\mathrm{H_2}}$ is:

$$\dot{X}^{\mathrm{gp}}_{\mathrm{H_2}} = n_{\mathrm{H}}(k_{10} n_{\mathrm{H^-}} + k_{26} n_{\mathrm{HD}}) + k_{25} n_{\mathrm{H^+}} n_{\mathrm{HD}} - n_{\mathrm{H_2}}(k_{12} n_{\mathrm{H_2}} + k_{13} n_{\mathrm{H}} \tag{4.1.4}$$

$$+ k_{14} n_{\mathrm{H^+}} + k_{15} n_{\mathrm{e}} + k_{16} n_{\mathrm{D}} + k_{17} n_{\mathrm{D^+}}) \quad , \tag{4.1.5}$$

where $n_{\mathrm{H^-}}$ is the equilibrium number density of H^- (Abel et al., 1997). The collisional formation rates are given by k_{10}, k_{25} and k_{26}. The collisional dissociation rates are given by k_{12}, k_{13}, k_{14}, k_{15}, k_{16} and k_{17}. The numbering of these rate coefficients correspond to the numbers in our chemical network table (Appendix B, table B.2). Following the work of Glover and Abel, 2008, we assume that the ortho-to-para hydrogen ratio is constantly 3:1 for all gas-phase calculations. This is the ratio holds unless the gas is extremely cold ($<$ 30 K), when the amount of para-hydrogen increases, becoming 1 at 0 K. If the ratio were taken into account, a model would need to be developed to modify the way in which H_2 would react when it was only in its para-hydrogen state.

4.1.2.2 HD Non-equilibrium Formation and Destruction

The main formation mechanisms for HD are:

$$
\begin{aligned}
H_2 + D^+ &\longrightarrow HD + H^+ && (4.1.6)\\
H_2 + D &\longrightarrow HD + H && (4.1.7)
\end{aligned}
$$

The species D and D^+ cannot be implemented on their own, as they rely on D^-, so the evolution equations for all of these species are added to the model. HD^+ is also included, but it has already been mentioned that its contribution is negligibly small. The collisional interactions for each species are thus provided by: D interacting with H, H^+, H^- and H_2, D^+ with H, D^- and H_2, and D^- with H, H^+, D^+ and H_2. HD^+ interacts with H, H^+, H^-, D, D^+ and e^-. The gas phase equations for these species are given below (with rates adopted from Glover and Abel, 2008).

For D,

$$
\begin{aligned}
\dot{X}^{\rm gp}_{\rm D} =& n_{\rm D^-}(k_{20}n_{\rm D^+} + k_{23}n_{\rm H^+}) + n_{\rm H}(k_{21}n_{\rm D^+} + k_{22}n_{\rm D^-} + k_{26}n_{\rm HD}) + n_{\rm e^-}(k_{32}n_{\rm D^+} + k_{27}n_{\rm HD^+})\\
&- n_{\rm D}(k_{16}n_{\rm H_2} + k_{18}n_{\rm H^+} + k_{19}n_{\rm H^-} + k_{30}n_{\rm H} + k_{29}n_{\rm e} + k_{31}n_{\rm H^+}) \quad . \qquad (4.1.8)
\end{aligned}
$$

The collisional formation rates are given by k_{20}, k_{21}, k_{22}, k_{23}, k_{26}, k_{27} and k_{32}. The collisional dissociation rates are given by k_{16}, k_{18}, k_{19}, k_{30}, k_{29} and k_{31}. The numbering of these rate coefficients correspond to the numbers in our chemical network table (Appendix B, table B.2).

For D^+,

$$
\dot{X}^{\rm gp}_{\rm D^+} = n_{\rm H^+}(k_{18}n_{\rm D} + k_{25}n_{\rm HD}) - n_{\rm D^+}(k_{17}n_{\rm H_2} + k_{20}n_{\rm D^-} + k_{21}n_{\rm H} + k_{32}n_{\rm e}) \quad . \qquad (4.1.9)
$$

The collisional formation rates are given by k_{18} and k_{25}. The collisional dissociation rates are given by k_{17}, k_{20}, k_{21} and k_{32}. The numbering of these rate coefficients correspond to the numbers in our chemical network table (Appendix B, table B.2).

For D^-,

$$
\dot{X}^{\rm gp}_{\rm D^-} = n_{\rm D}(k_{19}n_{\rm H^-} + k_{29}n_{\rm e^-}) - n_{\rm D^-}(k_{20}n_{\rm D^+} + k_{22}n_{\rm H} + k_{24}n_{\rm H} + k_{23}n_{\rm H^+}) \quad . \qquad (4.1.10)
$$

The collisional formation rates are given by k_{19} and k_{29}. The collisional dissociation rates are given by k_{20}, k_{22}, k_{23} and k_{24}. The numbering of these rate coefficients correspond to the numbers in our chemical network table (Appendix B, table B.2).

For HD^+,

$$\dot{X}^{gp}_{D^-} = k_{31} n_D n_{H^+} + k_{33} n_{D^+} n_H - n_{HD^+} (k_{27} n e^- + k_{28} n_{H^-}) \quad . \tag{4.1.11}$$

The collisional formation rates are given by k_{31} and k_{33}. The collisional dissociation rates are given by k_{27} and k_{28}. The numbering of these rate coefficients correspond to the numbers in our chemical network table (Appendix B, table B.2).

With these equations now setup, the gas-phase formation equation for HD can finally be represented as:

$$\begin{aligned}\dot{X}^{gp}_{HD} =& n_{H_2} (k_{16} n_D + k_{17} n_{D^+}) + n_H (k_{30} n_D + k_{24} n_{D^-}) + k_{28} n_{HD^+} n_{H^-} \\ & - n_{HD} (k_{25} n_{H^+} + k_{26} n_H) \quad ,\end{aligned} \tag{4.1.12}$$

The collisional formation rates are given by k_{16}, k_{17}, k_{30}, k_{24}, and k_{28}. The collisional dissociation rates are given by k_{25} and k_{26}. The numbering of these rate coefficients correspond to the numbers in our chemical network table (Appendix B, table B.2).

4.1.3 Heating and Cooling

4.1.3.1 H2 Implementation

H_2 cooling in the code includes both the collisional processes of dissociation and excited line emission. H_2 collisional reactions are of particular importance in cooling when $200 < T < 5000$ K and $\rho \gtrsim 10$ a.m.u cm^{-3} (Gnedin and Kravtsov, 2010). The rates and amount of emission outlined in (Abel et al., 1997) for collisions with H_2, H, H^+ and e^-, were used to calculate the dissociative cooling due to collisions. The collisionally induced line-cooling rates were calculated for H_2 and its interactions with H_2, H, H^+, He_I and e^-, using the low-density cooling rates presented by Glover and Mac Low, 2007. Glover and Mac Low, 2007 presented cooling rates which were determined using values calculated by Wrathmall, Gusdorf, and Flower, 2007 which were based on the Mielke, Garrett, and Peterson, 2002 potential surface. These rates have a substantial increase from those determined by Galli and Palla, 1998. Heating due to H_2 is also included, along with the already existing photoionization for atomic and ionized hydrogen and helium.

Christensen et al., 2012 ignored Deuterium cooling due to the inability of their simulations to resolve the high densities needed for it to become a dominant coolant. In our simulations, we aim to show that Deuterium and Hydrogen-Deuteride (HD) are indeed resolvable, and modify the evolution of the gas and affect star formation.

4.1.3.2 HD Implementation

HD cooling is particularly important for temperatures in the range $10 < T < 200$ K. Line cooling was included for H_2, but proves inefficient for HD (Glover and Abel, 2008). This is due to the fact that H_2 has ortho and para-hydrogen states, where HD does not have this separation of spin states.

The effects of a UV background on D are assumed to be identical to those of H_I. For HD, the same regime as H_2 is adopted for an external UV background. The difference is that the energy lost during H_2 dissociation is 4.476 eV (Glover and Abel, 2008), while HD loses 5.086 eV during its dissociation Trevisan and Tennyson, 2002b).

A detailed review of the modifications made to the cooling code within `GASOLINE`, including a description of how the cooling is handled, is given in Appendix A. Simulations were run to test this implementation of molecular cooling against the atomic and metal cooling version of `GASOLINE`. The setup is described in section 4.3.

4.2 Streaming Velocities

This section discusses how a streaming velocity is introduced into the initial conditions for simulations. It follows similar lines to the work by Maio, Koopmans, and Ciardi, 2011, Stacy, Bromm, and Loeb, 2011 and Greif et al., 2011b.

From the work by Tseliakhovich and Hirata, 2010, the rms velocity is $v_{rms} = 30$ km s^{-1}. We assume that this is the velocity is generated at $z_{rms} = 1000$. The initial redshift of the simulation, z_i, is used to calculate the appropriate streaming velocity at that redshift from the expression:

$$v_s = \frac{v_{rms}}{1 + \frac{z_{rms}}{z_i}} \quad . \tag{4.2.1}$$

This homogeneous velocity field is added to the velocity generated for the initial conditions. This study adds a constant homogeneous velocity field, arbitrarily chosen to be in the x-direction.

4.3 Simulation Setup and Parameters

We used the `GASOLINE` code to run high-resolution, 3-D, hydrodynamical simulations which incorporate stellar evolution, star formation and efficient SN feedback. A full description for metal pollution, primordial molecular chemistry (following e^-, H,H^+, H^-, He^+, He^{++}, H_2, D, D^+, D^-, HD and HD^+)and fine structure metal transition cooling via equilibrium cooling using `CLOUDY` are also included. *Metals*-run contains everything except molecular cooling, *HD*-run adds molecular cooling, and V_{Stream}-run adds a streaming velocity of 30 km S^{-1}.

The simulations were conducted within a cubic volume of 200 kpc on a side, starting at redshift of 100 with 128^3 particles for both gas and the same number for the DM. Consequently, the mass per gas particle is $\sim 52\ M_\odot$. Similarly, the mass for the DM particle is $\sim 276\ M_\odot$. The initial abundances for H_I, He and D were set to 0.76, 0.06, and 4×10^{-5}, respectively. The rest of the species had an initial abundance of 0. We adopt a ΛCDM matter cosmology with $\Omega_\Lambda = 0.6825$, $\Omega_m = 0.3175$, $\Omega_b = 0.049$ and h = 0.671.

The density threshold for star formation is chosen to be $\sim 10^{-1}$ cm^{-3}. For the star formation to be modelled in a physically justifiable way, each SPH particle must give rise to two or more star particles. In our simulations, each star is allocated $\frac{1}{3}$ of the mass of the gas particle giving rise to it. A minimum mass per gas particle is set so that gas particles do not become too small, which is now explained in detail. For each original gas particle g_i (at the beginning of the simulation) set by the initial conditions (ICs) to have a mass m_i, g_i can never have its mass reduced by star formation to the point where it is $< \frac{1}{9}m_i$. If this occurs then the gas particle in question is removed and its mass assigned to the nearest neighbours within the tree.

For the V_{Stream}-run simulation a constant streaming velocity is added to the velocity field of the ICs in the HD-run simulation ($v_{x,i} = v_x + v_{Stream}$). Thus any differences between the outcomes of the HD-run and V_{Stream}-run simulation are due solely to the streaming velocity. Since this run begins at redshift $z = 100$, the streaming velocity can be shown to be $v_s = 2.727 \sim 3$ km s^{-1}, which is in agreement with the streaming velocities used by Maio, Koopmans, and Ciardi, 2011, Stacy, Bromm, and Loeb, 2011 and Greif et al., 2011b.

In this chapter a detailed molecular cooling model has been proposed, which will significantly accelerate the time of formation and number of Pop III stars compared to approaches which ignore the effect of molecular cooling on primordial star formation. In addition to that, primordial streaming velocities have been introduced which may may decelerate star formation (the implementation of the streaming velocities discussed here may be oversimplified - a future more rigorous treatment will possibly reveal acceleration and deceleration of the primordial star formation at the same time, depending on the fine structure of the streaming velocity field.) The simulations discussed in the next chapter will reveal how these adverse processes affect early star formation.

Chapter 5

Results

This chapter is broken into two sections discussing the effects of the inclusion of molecules (section 5.1) and of the implementation primordial streaming velocities (section 5.2). The main features we are interested in are: formation times of the first stars; thermal evolution of the gas; and halo density and distribution. We find that molecular cooling accelerates star formation by cooling the gas much more efficiently. The increase of the feedback due to higher star formation activity at earlier times is able to expel larger amounts of gas from the star forming regions and thus causes a delay in the formation of the second generation of stars.The inclusion of a streaming velocity also delays star formation and produces, in combination with the accelerated star formation due to the inclusion of primordial chemistry, a similar distribution for the gas temperature, density and metallicity to the simulation neglecting molecular cooling and a streaming velocity. The ordering of the results within this chapter is by-no-means the only way to present them, but was chosen in this way in order to show the logical steps taken to ensure that the data obtained made sense. The simulations will be referred to following the nomenclature introduced Chapter 4, namely: *Metals*-run referring to the simulation with the base code (excluding molecular cooling), *HD*-run being the simulation containing molecular cooling, and V_{Stream}-run indicating the simulation with molecular cooling and a streaming velocity of 30 km s $^{-1}$.

5.1 Effects Resulting from the Inclusion of Molecular Cooling

5.1.1 Evolution of the Temperature Distribution of the Gas

It is well understood that DM will collapse under gravity, providing DM haloes into which the gas particles will eventually fall.The gas gradually sinks to the centre of the halo, where run-away cooling is observed followed by rapid collapse in the gas form stars. Run-away cooling and collapse happen far too fast in simulations for the time-steps to be close enough together to pick this up. This is where molecular cooling is dominant and it is difficult to capture it directly. Molecular cooling does, however, leave a traceable signature in the temperature function for the gas. This can be examined by constructing a thermal distribution for the gas. Once the first stars form, the temperature function will spread out, with the bulk of the gas between 30 and 1000 K, with very little gas above 10000 K. The histograms for *Metals*-run (blue) and *HD*-run (red) are presented plotted against one another for redshifts from $z = 36$ to $z = 6$, which are shown in figure 5.1.

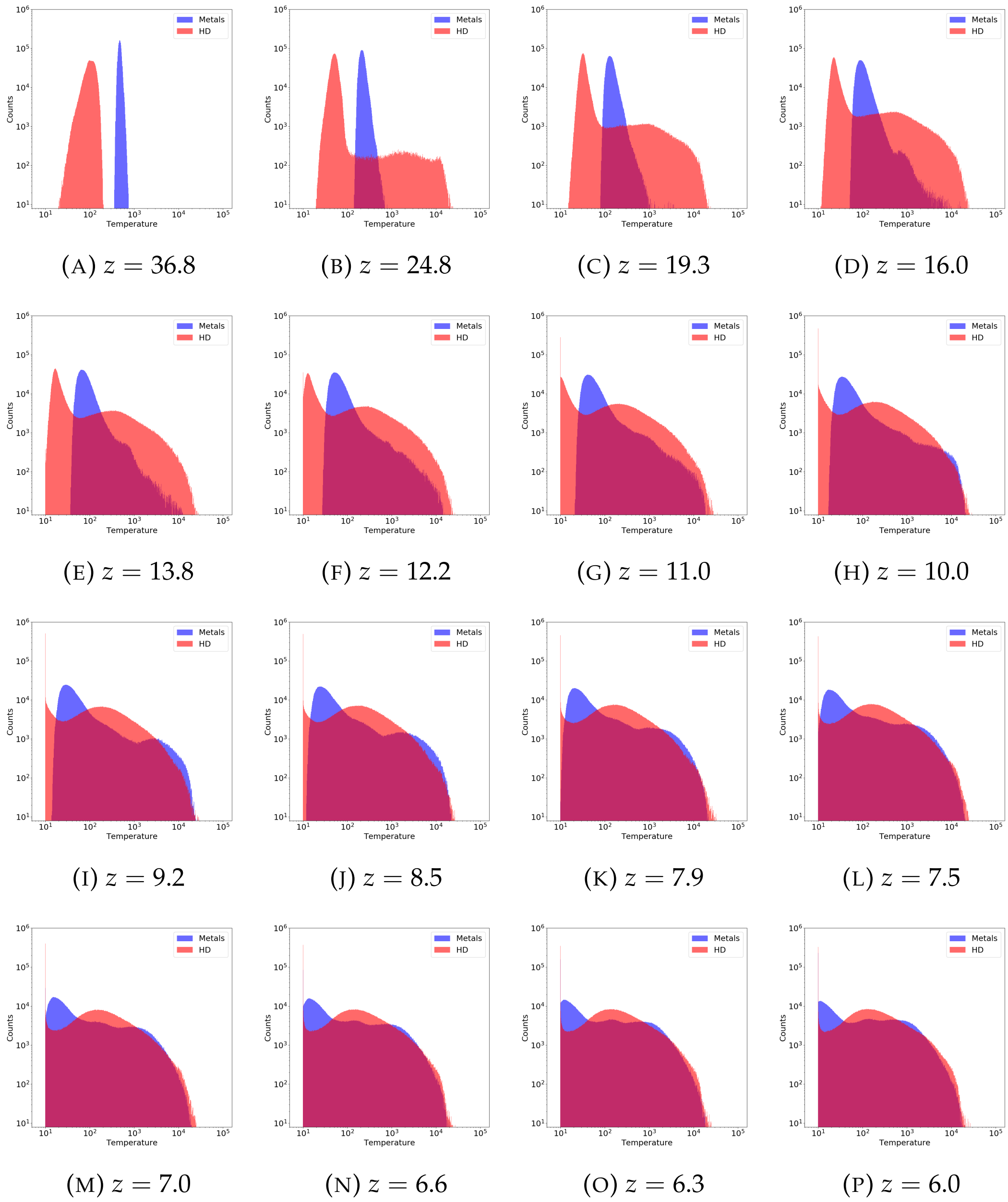

(A) $z = 36.8$ (B) $z = 24.8$ (C) $z = 19.3$ (D) $z = 16.0$

(E) $z = 13.8$ (F) $z = 12.2$ (G) $z = 11.0$ (H) $z = 10.0$

(I) $z = 9.2$ (J) $z = 8.5$ (K) $z = 7.9$ (L) $z = 7.5$

(M) $z = 7.0$ (N) $z = 6.6$ (O) $z = 6.3$ (P) $z = 6.0$

FIGURE 5.1: The thermal distribution of the gas particles at various redshifts, with *Metals*-run in blue and *HD*-run in red. In the beginning the major peaks in *Metals*-run and *HD*-run show a large separation and then merge at $z = 6$, indicating a similar thermal evolution from that point on. Figure 5.1a shows an elongated distribution for *HD*-run, foreshadowing the immediate star formation indicated by the sudden high-temperatures seen in figure 5.1b due to SNe events. It can clearly be seen that molecules accelerate star formation and alter the high-redshift thermal evolution, while tending towards the same low-redshift distribution as *Metals*-run which is as expected.

In figure 5.1, the first key feature is that the bulk of the gas has a temperature $T < 1000$ K, which is expected. Furthermore, the main peak temperature for *HD*-run starts out at about 100 K at $z = 36$ and steadily decreases to the threshold temperature of 30 K at $z = 6$. *Metals*-run follow a similar trend, but start out at a higher base around 600 K at $z = 36$, reducing gradually to the threshold temperature of 30 K at $z = 6$. This illustrates that the two simulations differ greatly at high redshifts, but match more closely at low redshifts, indicating that the thermal evolutions will coincide eventually which is expectedand also desired otherwise the results of the cosmological simulations of galaxy formation would be questionable. Considering figure 5.1a, the effect of molecular cooling can be clearly seen in comparison to the *Metals*-run with the elongation of the distribution and peak being at a significantly lower temperature. This indicates that star formation is immediate, which is indeed the case as is seen in 5.1b, where supernova events have taken place. Another interesting feature is the "double-peak" which is present throughout most of the *HD*-run, but only appears in *Metals*-run at low redshifts. This is due to the advent of a halo in which there is consistent star birth and death. The gas is constantly in a flux of run-away cooling and SNe heating, leading to the trough between these two states. These plots clearly indicate the effectiveness of molecules at high redshifts, drastically altering the thermal evolution of the gas at high redshifts, but returning to a similar evolution to *Metals*-run at low redshifts, indicating that the two will coincide in their evolutions at $z = 0$. They also indicate that the star formation histories will differ at high-redshifts, with *HD*-run being significantly earlier. This will be the focus of the next set of results.

5.1.2 Star Formation History

Star formation within a simulation is categorised by two main features: the time when the earliest stars form, and the rate at which the stars form. To investigate both of these, we plot the distribution of the individual star formation times as a function of redshift, by linearly binning these formation time by redshift. *Metals*-run are plotted in blue and *HD*-run in red. The x-axis runs from redshift $z = 40 - 6$, and the y-axis is the number of stars in the bins. The histograms are displayed in figure 5.2.

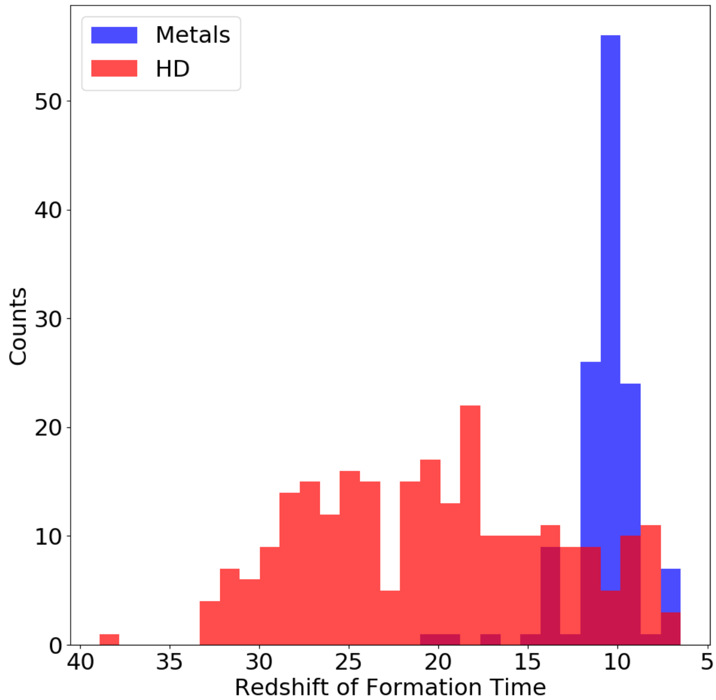

FIGURE 5.2: Star formation history distributions for *Metals*-run and *HD*-run (the colour difference shows the regions of overlap between the two histograms). Star formation happens much earlier when molecules are included, and the star formation rate at high redshifts is also increased, which is seen by the consistent number of stars produced at high redshifts. *Metals*-run show a sudden spike in star formation around $z \sim 10$. It is expected that molecular cooling accelerates star formation and that it will increase the star formation rate, both of which are confirmed by this data. The consistent production of large numbers of stars in *HD*-run suggests that the evolution of the gas's temperature, density and metallicity will all be very different from the *Metals*-run.

Figure 5.2 shows that *HD*-run forms stars much earlier than *Metals*-run, and that it continuously produces large numbers of stars at high redshifts. The star formation rate is therefore also increased by introducing molecular cooling. The single star formed around $z \sim 38$, seem to be associated with an extremely high dark matter density peak and confirms the ability of molecules to very efficiently cool the gas in sufficiently dense environments. The spike in star formation at $z \sim 10$ in the *Metals*-run indicates that it takes much longer for the gas to cool and produce stars, illustrating the inefficiency of H and He as efficient coolants at low temperatures. This burst of star formation is caused by the SN explosions of the earlier stars which pollute the environment with metals, thereby allowing much more efficient cooling of the gas.

The consistently high number of stars produced almost continuously in the *HD*-run suggests that the temperature, density and metallicity evolution of the gas is very different from that of the *Metals*-run. The next few subsections will illustrate that this is indeed the case.

5.1.3 Evolution of the DM

Before studying the evolution and properties of the gas, the DM distribution is investigated. This will provide information about the structures forming within the simulation volume and indicate whether there are any significant differences between the *Metals*-run and *HD*-run DM evolutions. It is anticipated that the difference between the DM distributions of the two runs will be rather small. To plot the DM distribution, the DM particles are gridded according to their position within the box, and then a colour-map is applied based on the number-density of particles within a particular grid. The plots are projections along the entire z-axis of the box, showing the distributions in the $x - y$ plane, in units of Mpc. These are displayed in figure 5.3, where the two runs are plotted 2 x 2, with *HD*- run on the left and *Metals*-run on the right.

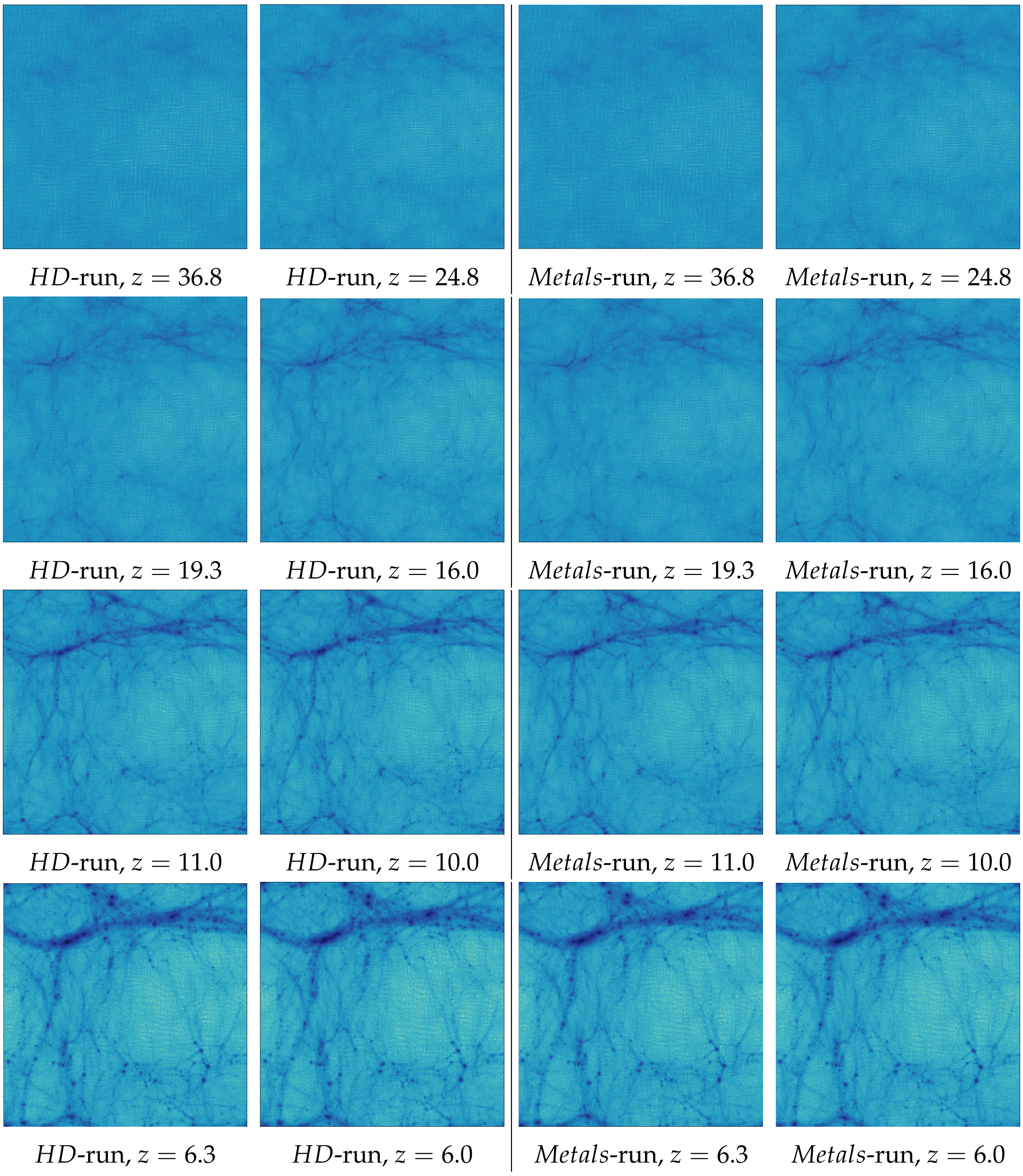

FIGURE 5.3: DM density maps constructed by gridding the positions of the particles and then colouring them according to number density.They are projected along the z-axis through the entire box and show the distribution in the x-y plane. One side of the square map corresponds to 200 kpc. Each row has the two panels on the left being the *HD*-run evolution, and the two on the right being *Metals*-run. It is illustrated that the DM distributions for *Metals*-run and *HD*-run are identical, reinforcing the fact that any gaseous distribution differences will be the result of molecular cooling.

The evolution depicted in figure 5.3 shows no difference between the DM distributions of the two runs. Therefore it can be anticipated that any changes in the gas distributions will be due to the changes between the cooling mechanisms. It has already been shown , by previous studies using GASOLINE, that the *Metals*-run code evolves galaxy formation to $z = 0$ which matches features seen in observational data, confirming that the data produce can be trusted (as is expected, otherwise the studies would have been abandoned). Since the DM distribution for the *HD*-run is so similar to that of the *Metals*-run, this indicates that the *HD*-run would also match observational data at $z = 0$. This was not done in this study, but would provide a stronger argument for the *HD*-run evolution being more accurate than the *Metals*-run. To investigate the distribution of the gas, and whether the two evolutions are as similar as this data, the thermal, density and metallicity evolutions of the gas are considered.

5.1.4 Thermal and Density Evolution of the Gas

So far, it has been demonstrated that the DM distributions are identical, but that the temperature distributions are very different at high redshifts, but tend towards each other at low redshifts, indicating an evolution which my match up at $z = 0$, which is what is wanted for comparison to observational data. The star formation histories were completely different, indicating that the evolution of the gas should be very different. This section shows that this is the case by considering the thermal and density evolutions of the gas.

5.1.4.1 Thermal Evolution

The thermal evolution is illustrated by a sequence of plots which apply a uniform grid to the box and find the mean temperature density of each grid cell. A projection is made through the entire box along the z-axis, showing the temperature distribution of the gas in the $x - y$ plane, with the axes in units of Mpc. On top of these we over-plot the positions of the star particles showing that the hottest points correspond to the locations of the stars. These temperature maps are illustrated in figure 5.4, with *HD*-run and *Metals*-run plotted in the same fashion as figure 5.3.

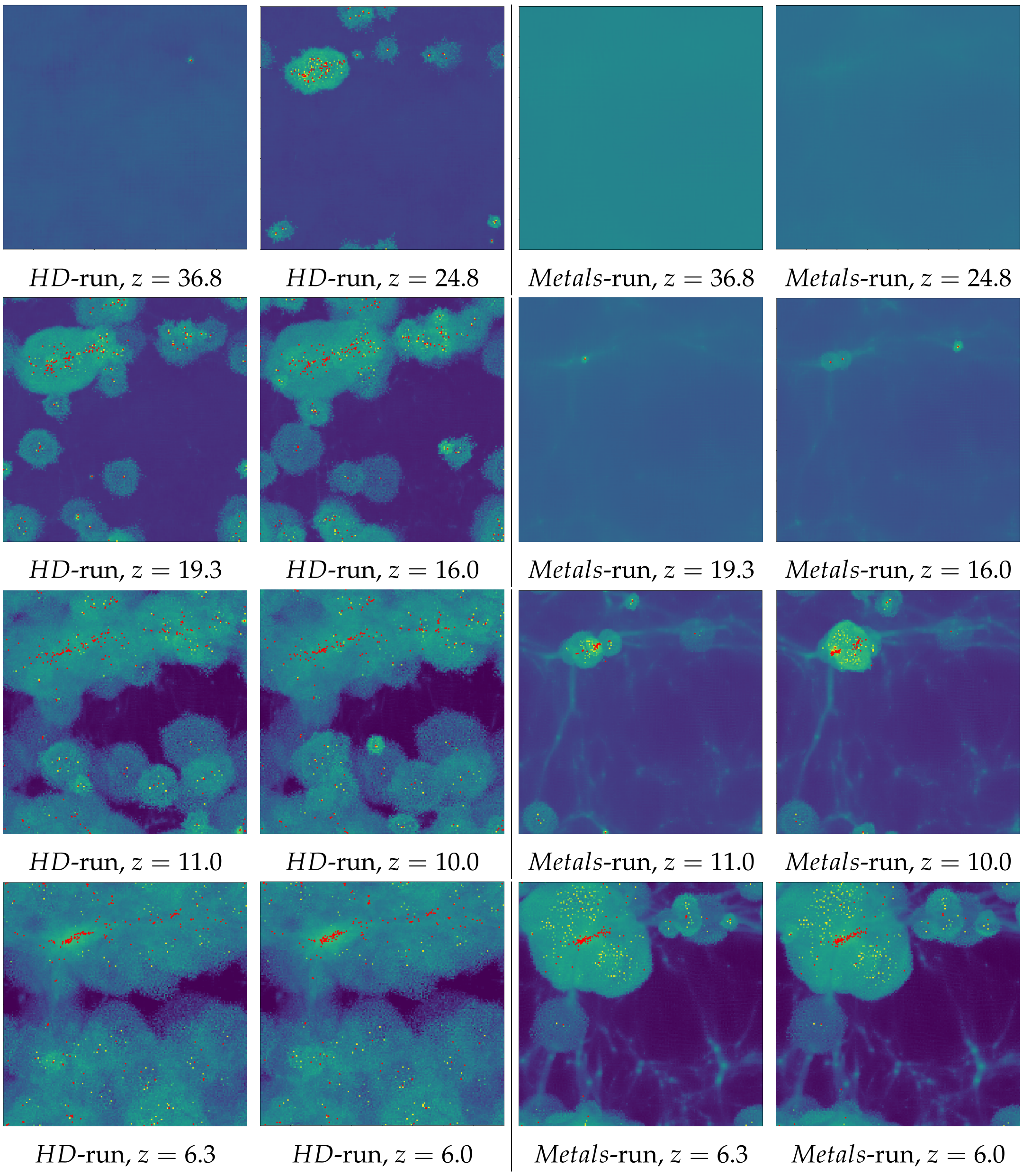

FIGURE 5.4: Temperature maps illustrating the thermal evolution of the gas. Each cell represents the mean temperature density projected through the z-axis of the entire box. The bright spots indicate high temperatures. The over-plotted red dots represent the positions of the stars. One side of the square map corresponds to 200 kpc. Each row has the two panels on the left being the *HD*-run evolution, and the two on the right being *Metals*-run. Molecular cooling increases star production at high redshifts, increasing the number of SN explosions which re-distribute the gas all of the box. The *HD*-run shows a temperature distribution which is more dispersed, due to the small DM haloes being unable to trap the SN ejections as effectively at high redshifts in comparison to the *Metals*-run. Smaller DM haloes in the *HD*-run are are able to trap the gas more easily due to the increased efficiency of molecular cooling.

The temperature maps in figure 5.4 illustrate a massive difference in where the hot gas is located within the box. The formation of stars happening so much earlier, and so much more frequently, in the *HD*-run run means that the DM haloes are smaller and are not able to trap the SN gas expelled within their haloes. The gas is therefore blow out very frequently, re-distributing it throughout the box. This is seen very clearly at low redshifts, where most of the gas within the box is at high temperatures. The fact that the more efficient cooling allows smaller DM haloes to more effectively trap the gas also influences the time and location of star formation, contributing to the more dispersed temperature distribution seen in the *HD*-run.

In comparison, the *Metals*-run gas collects into filaments and one very large halo, with some smaller haloes appearing around it. The delay in the first stars allows more gas to be trapped within the DM haloes, leading to a more "structured" distribution in the gas. A detailed discussion of the evolution of the gas below $z \sim 9$ is incomplete due to the lack of an external UV background. It looks as though the two distributions will begin to mirror one another with the decrease in the star formation rate for *HD*-run, as indicated by the clustering of the stars in a similar position to the *Metals*-run. Molecules do clearly modify the thermal evolution of the gas.

5.1.4.2 Gas Density Evolution

The density evolution of the gas is constructed by a sequence of plots which apply a uniform grid to the box and find the mean density of each grid cell. A projection is made through the entire box along the z-axis, showing the density distribution of the gas in the $x - y$ plane, with the axes in units of Mpc. The density maps are shown in figure 5.5, with *HD*-run and *Metals*-run plotted in the same fashion as figure 5.4.

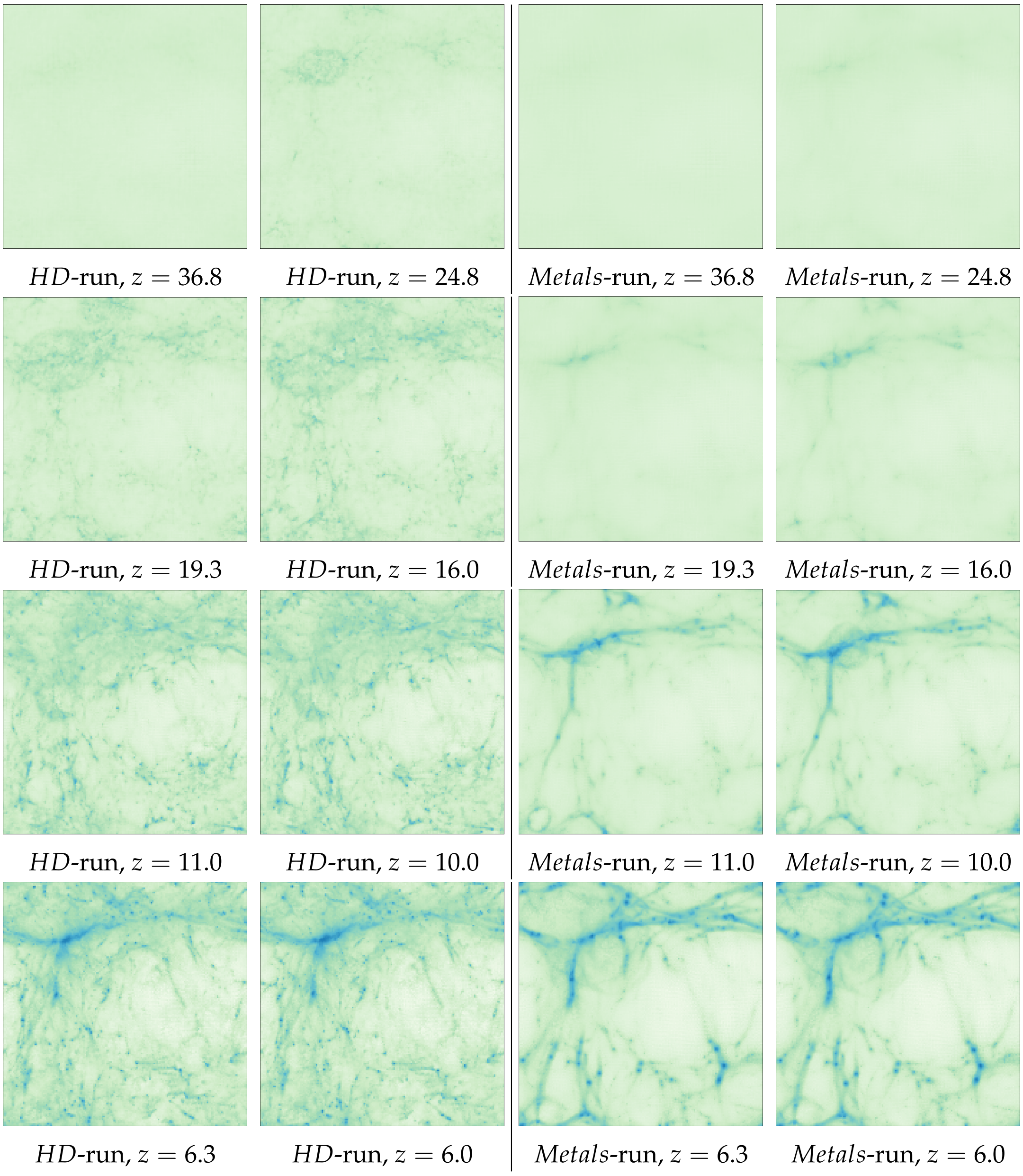

FIGURE 5.5: Density maps of the density evolution of the gas particles are shown, with each cell representing the mean temperature density projected along the z-axis of the entire box. The blue and white regions indicate high and low densities, respectively. One side of the square map corresponds to 200 kpc. Each row has the two panels on the left being the *HD*-run evolution, and the two on the right being *Metals*-run. These illustrate the same effects seen in the temperature maps, where the *HD*-run has a more disrupted density distribution in comparison to the smooth gas density field in the *Metals*-run, with stars formed all over the box. Molecules therefore have a significant impact on the density evolution of the gas.

The density maps in figure 5.5 illustrate the same large differences as was shown in the temperature distributions. The same arguments about high redshift star formation and efficient molecular cooling in the *HD*-run apply here. The effect is that the *HD*-run shows a more disrupted gas density field in comparison to *Metals*-run. This reinforces the conclusions drawn from the temperature maps. Once again, the lack of UV background limits the discussion about the evolution beyond $z \sim 9$.

5.1.5 Evolution of the Gas Metallicity

Having seen that the temperature and density evolutions have been altered so much, and concluding that smaller DM haloes can trap the gas, leading to more wide-spread star formation, the effects of metal pollution become important. They have the ability to make gas cooling even more efficient, which could explain the large difference in the distributions of the gas density fields between *HD*-run and *Metals*-run.

The evolution of the gas metallicity is illustrated by a sequence of plots which apply a uniform grid to the box and find the mean metallicity of each grid cell. A projection is made through the entire box along the z-axis, showing the distribution of metals in the $x - y$ plane, with the axes in units of Mpc. We once more over-plot the positions of the star particles showing the locations of the stars. These metallicity maps are illustrated in figure 5.6 with *HD*-run and *Metals*-run plotted in the same fashion as figures 5.4 and 5.5.

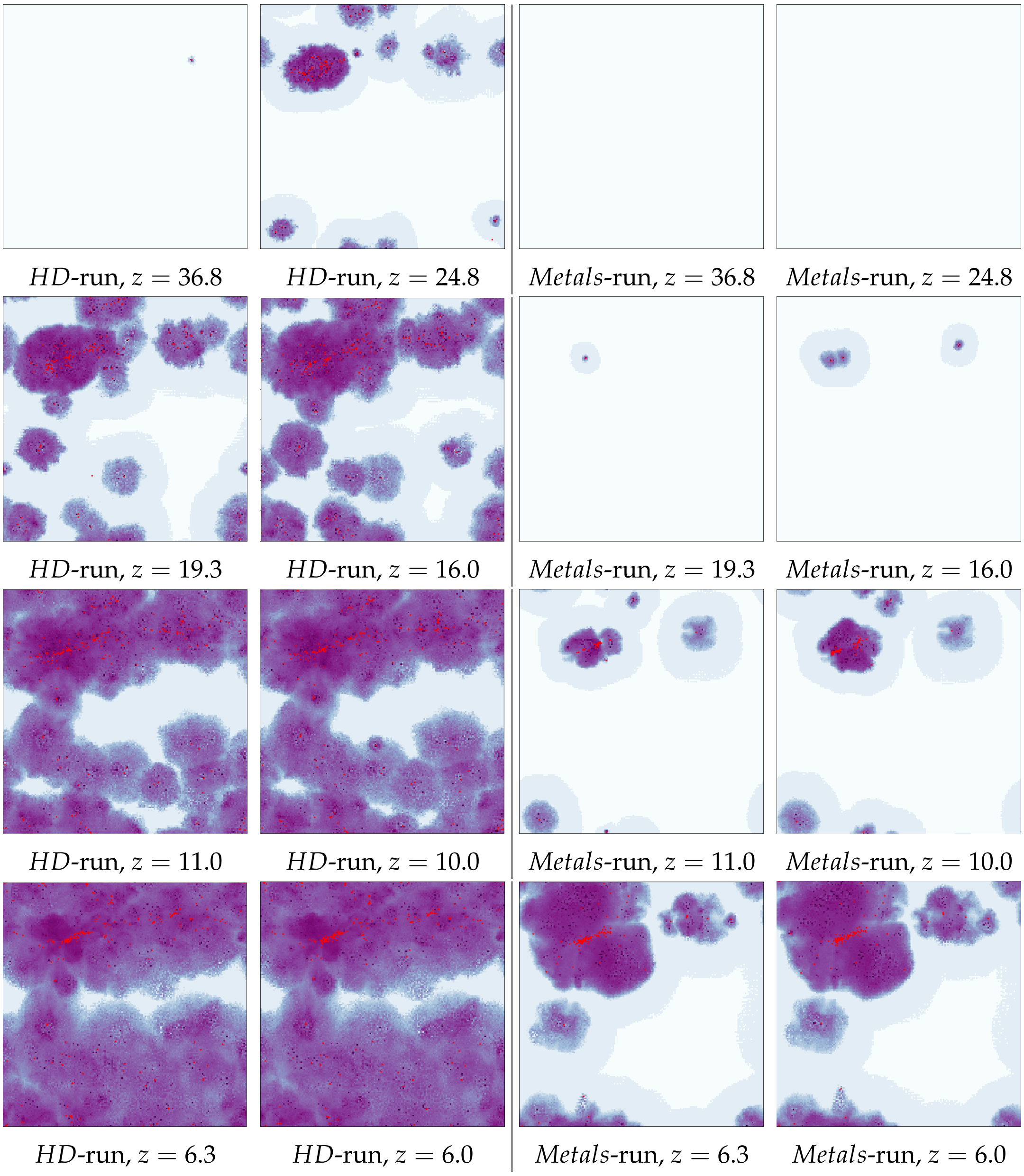

FIGURE 5.6: Metallicity maps illustrating the distribution metals in the box by placing a uniform grid on it. Each cell represents the mean metallicity projected along the z-axis of the entire box. One side of the square map corresponds to 200 kpc.. The darker the region, the more metals that are present within it. The red dots represent the positions of the stars. Each row has the two panels on the left being the *HD*-run evolution, and the two on the right being *Metals*-run. The greater pollution by metals in the *HD*-run, and the fact that they get spread out so much, means stars can form all over the box. This results in a greater production of stars, and in a very different evolution for the gas, resulting from the inclusion of molecular cooling.

The metallicity maps in figure 5.4 show the same structural differences between the *HD*-run and metals as were seen before, due ot the same arguments. These maps show that the distribution of metals happens much earlier *HD*-run, thereby cooling the gas even more, and allowing stars to form earlier and more rapidly. The extra time taken for stars to form in the *Metals*-run is responsible for the reduction in metal pollution, leading to rapid star formation only within the largest haloes. The wide-spread distribution of metals in the *HD*-run allows much smaller haloes to produce stars. It is therefore clear that molecular cooling modifies the evolution of the gas in all aspects.

5.1.6 Summary

It has been illustrated in this section that molecular cooling has an enormous impact on the evolution of the gas and stars, but leaves the DM evolution untouched. Stars form much earlier when molecular is included as DM haloes can more effectively trap the gas due to its more efficient cooling. Earlier star formation creates SN explosions which populate the gas with metals much earlier. The SN explosions also evacuate the gas from the DM haloes, since the haloes are too small to stop the gas from doing so. This results in wide-spread high-temperature gas containing metals. This happens almost continuously from $z \sim 30$, leading to maps for the temperatures and densities which are more dispersed. This follows from the small DM halo argument. Molecules therefore drastically change the evolution of the gas and are crucial to studying the advent of Pop III stars, which agrees well with the results of Nakauchi, Inayoshi, and Omukai, 2014. These results indicate that, overall, our implementation of molecular cooling has been successful.

5.2 The Effects of the Streaming Velocity

To compare the *HD*-run and V_{Stream}-runs, the same plots are constructed in the same manner as the previous section. The plots are therefore shown in their own subsections and the discussion of them is delayed to the end of the section where we make a summary.

5.2.1 Evolution of the Temperature Distribution of the Gas

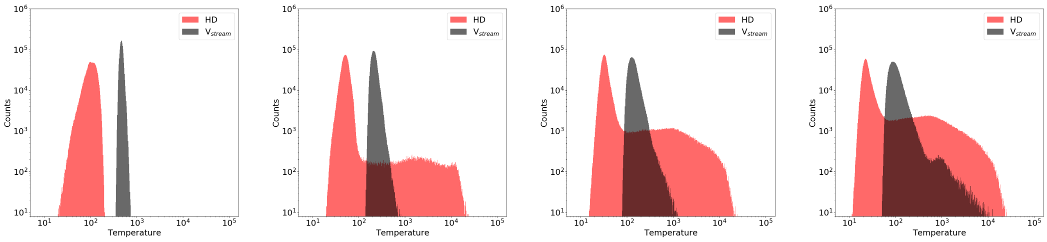

(A) $z = 36.8$ (B) $z = 24.8$ (C) $z = 19.3$ (D) $z = 16.0$

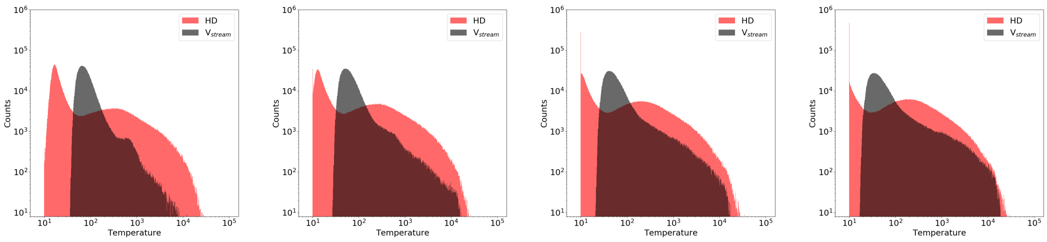

(E) $z = 13.8$ (F) $z = 12.2$ (G) $z = 11.0$ (H) $z = 10.0$

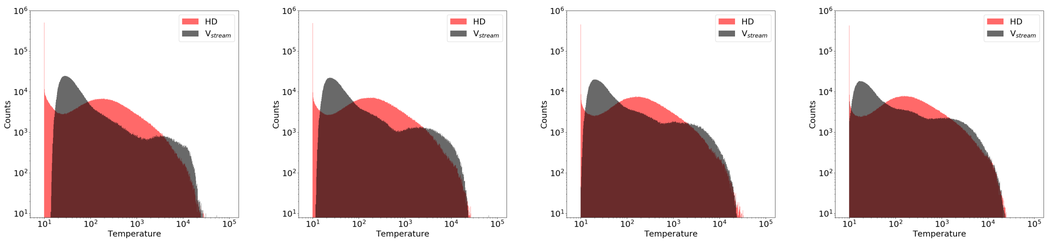

(I) $z = 9.2$ (J) $z = 8.5$ (K) $z = 7.9$ (L) $z = 7.5$

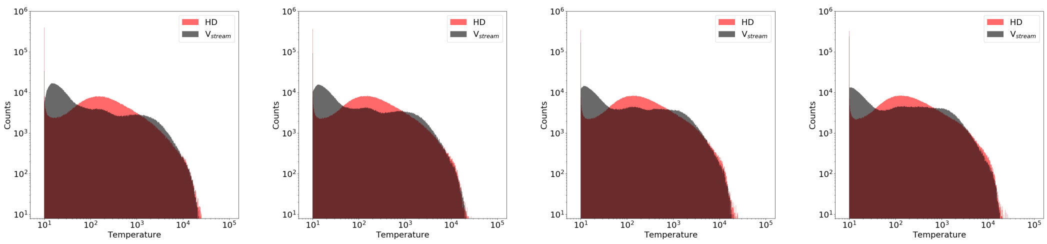

(M) $z = 7.0$ (N) $z = 6.6$ (O) $z = 6.3$ (P) $z = 6.0$

FIGURE 5.7: The thermal distribution of the gas particles at various redshifts, with the V_{Stream}-run in black and *HD*-run in red. The major peaks in V_{Stream}-run and *HD*-run start substantially far apart, and then merge at $z = 6$, indicating a similar thermal evolution from that point. The *HD*-run is clearly ahead at high redshifts, indicating that there is a delay when a streaming velocity is included, as is expected.

5.2.2 Star Formation History

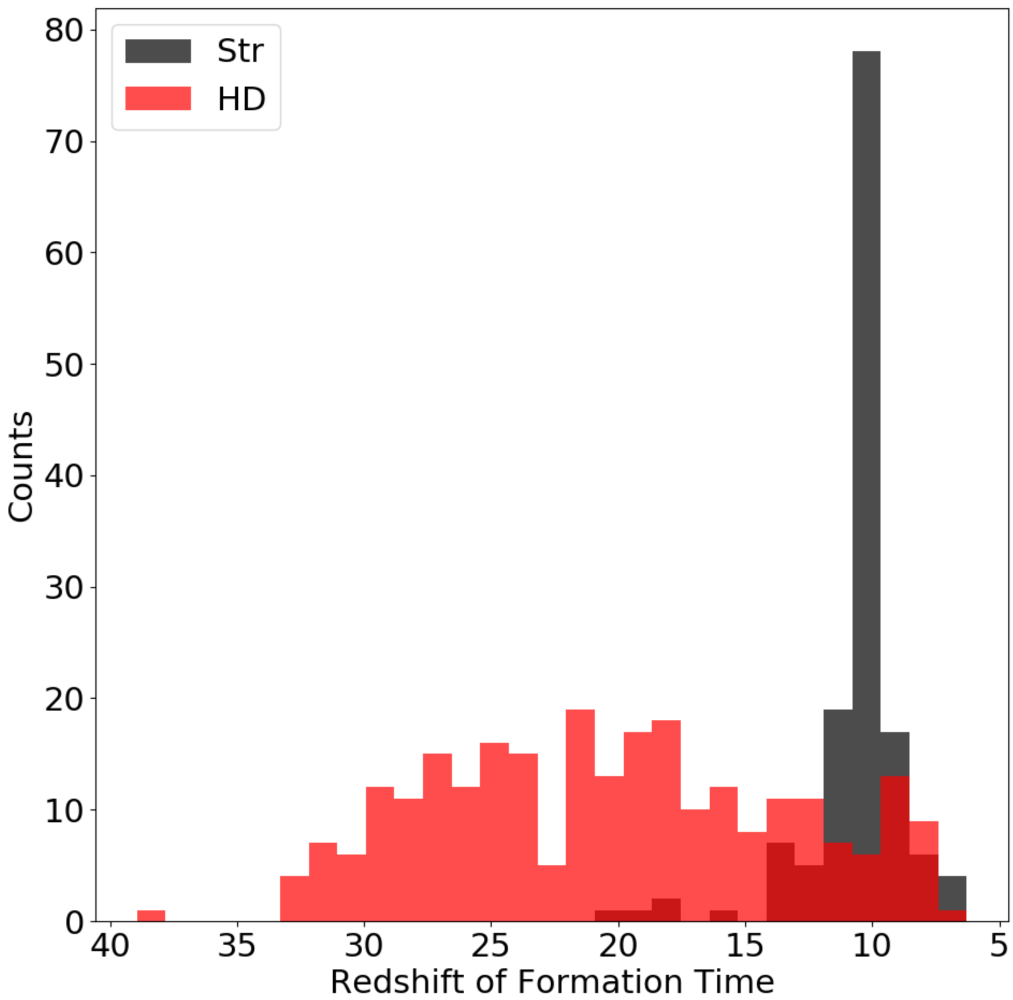

FIGURE 5.8: Star formation history distributions for V_{Stream}-run and *HD*-run (the colour difference shows the regions of overlap between the two histograms). Star formation happens much later when a streaming velocity is included. V_{Stream}-run shows a sudden spike in star formation around $z \sim 10$, which shows some similarity to the *Metals*-run. This illustrates the expected behaviour of the gas when a streaming velocity is included.

5.2.3 Evolution of the DM

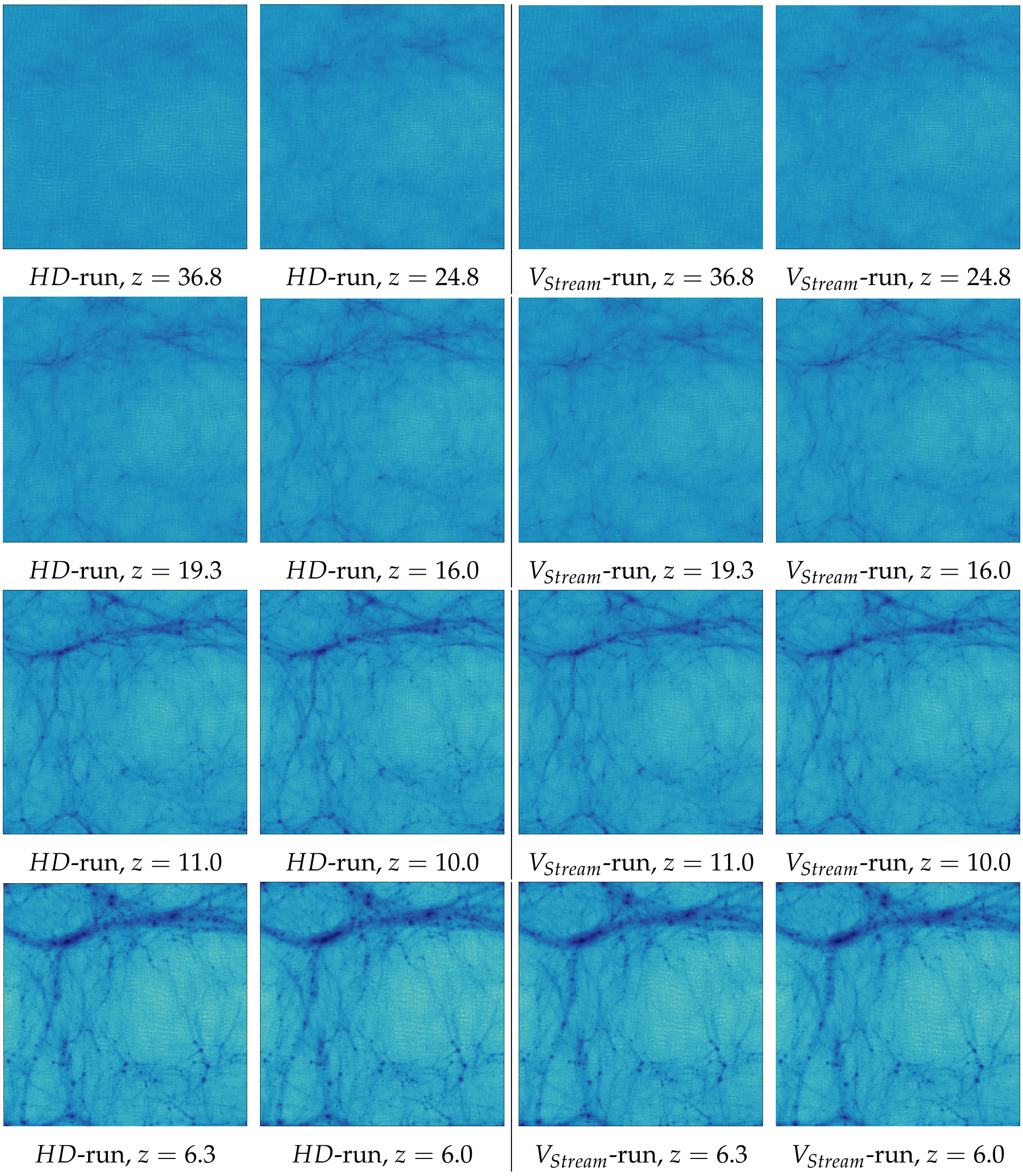

FIGURE 5.9: DM density maps constructed by gridding the positions of the particles and then colouring them according to number density. They are projected along the z-axis of the box and show the distribution in the x-y plane. One side of the square map corresponds to 200 kpc. Each row has the two panels on the left being the HD-run evolution, and the two on the right being V_{Stream}-run. It is illustrated that the DM distributions for HD-run and V_{Stream}-run are identical, reinforcing the fact that any gaseous distribution differences will be the result of the streaming velocity.

5.2.4 Thermal and Density Evolution of the Gas

5.2.4.1 Thermal Evolution

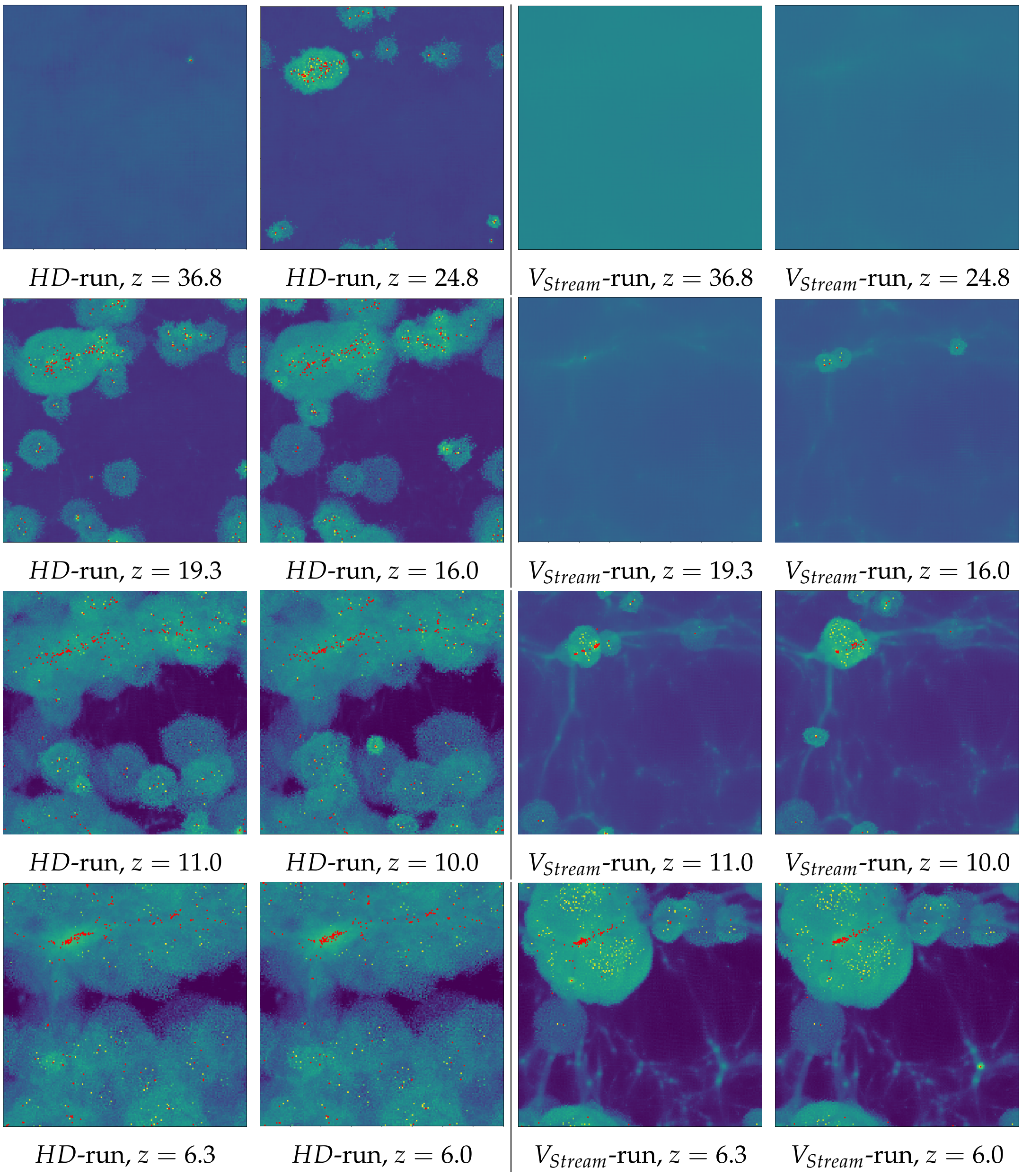

FIGURE 5.10: Temperature maps illustrating the thermal evolution of the gas. Each cell represents the mean temperature density projected through the z-axis of the entire box. The bright spots indicate high temperatures. The over-plotted red dots represent the positions of the stars. One side of the square map corresponds to 200 kpc. Each row has the two panels on the left being the *HD*-run evolution, and the two on the right being V_{Stream}-run. The streaming velocity delays the formation of stars, creating a similar distribution of temperatures in comparison the *Metals*-run.

5.2.4.2 Gas Density Evolution

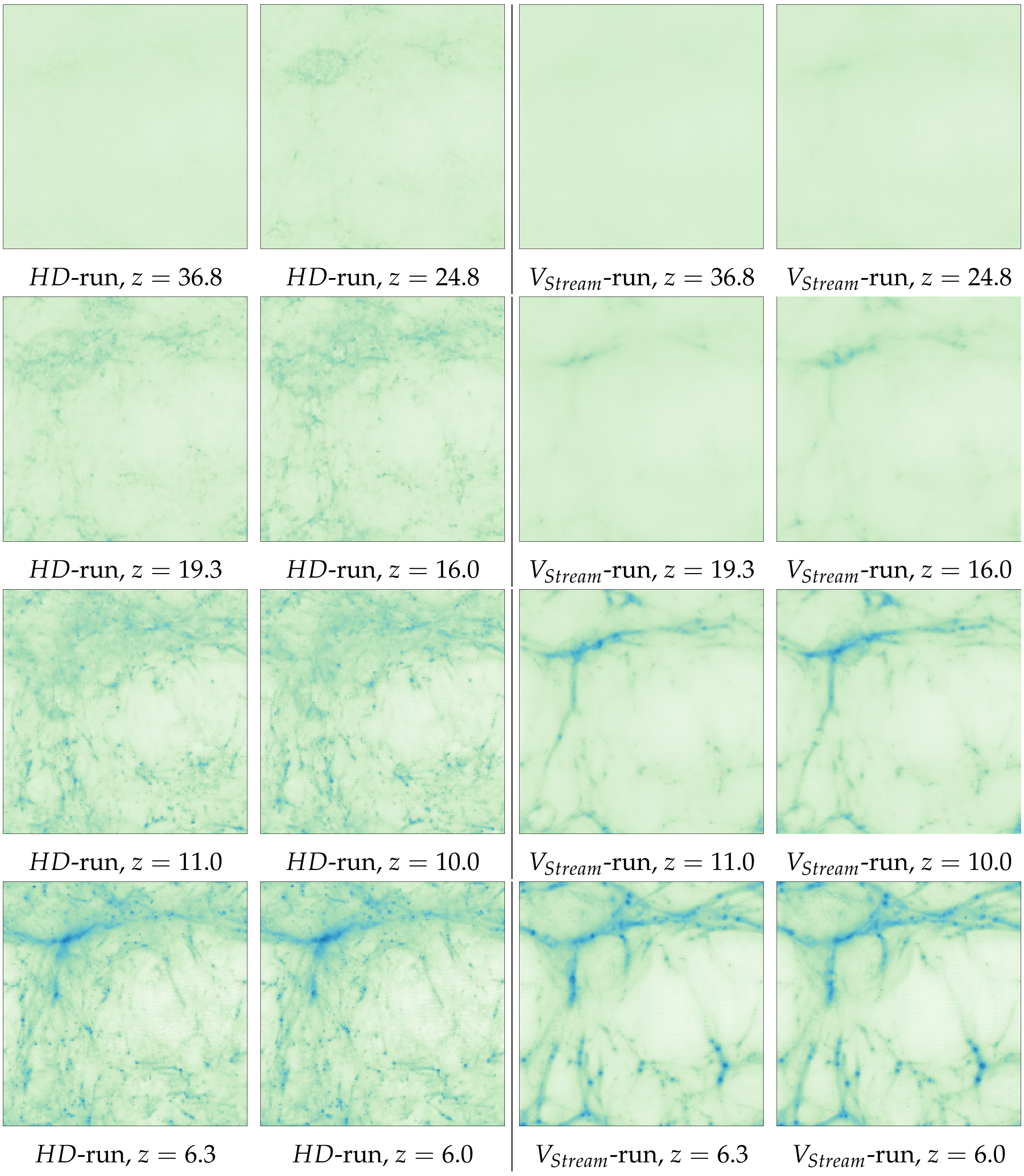

FIGURE 5.11: Density maps of the density evolution of the gas particles are shown, with each cell representing the mean temperature density projected along the z-axis of the entire box. The blue and white regions indicate high and low densities, respectively. One side of the square map corresponds to 200 kpc. Each row has the two panels on the left being the HD-run evolution, and the two on the right being *Metals*-run. These illustrate the same effects seen in the temperature maps, where the *Metals*-run have a less dispersed density field, with the HD-run having star form all over the box. The streaming velocity delays the formation of stars by suppressing star formation in small DM haloes at high redshifts. This results in a similar gas density field in comparison to the *Metals*-run.

5.2.4.3 Difference in Gas Density Evolutions

To get a picture of where the HD-run and V_{Stream}-runs differ in their density evolution, a plot is made where the density maps for V_{Stream}-run are subtracted from those of *HD*-run. Since the features will be similar for the temperature and metallicity maps, these density maps are the best illustration and the others are neglected. These are shown in figure 5.12.

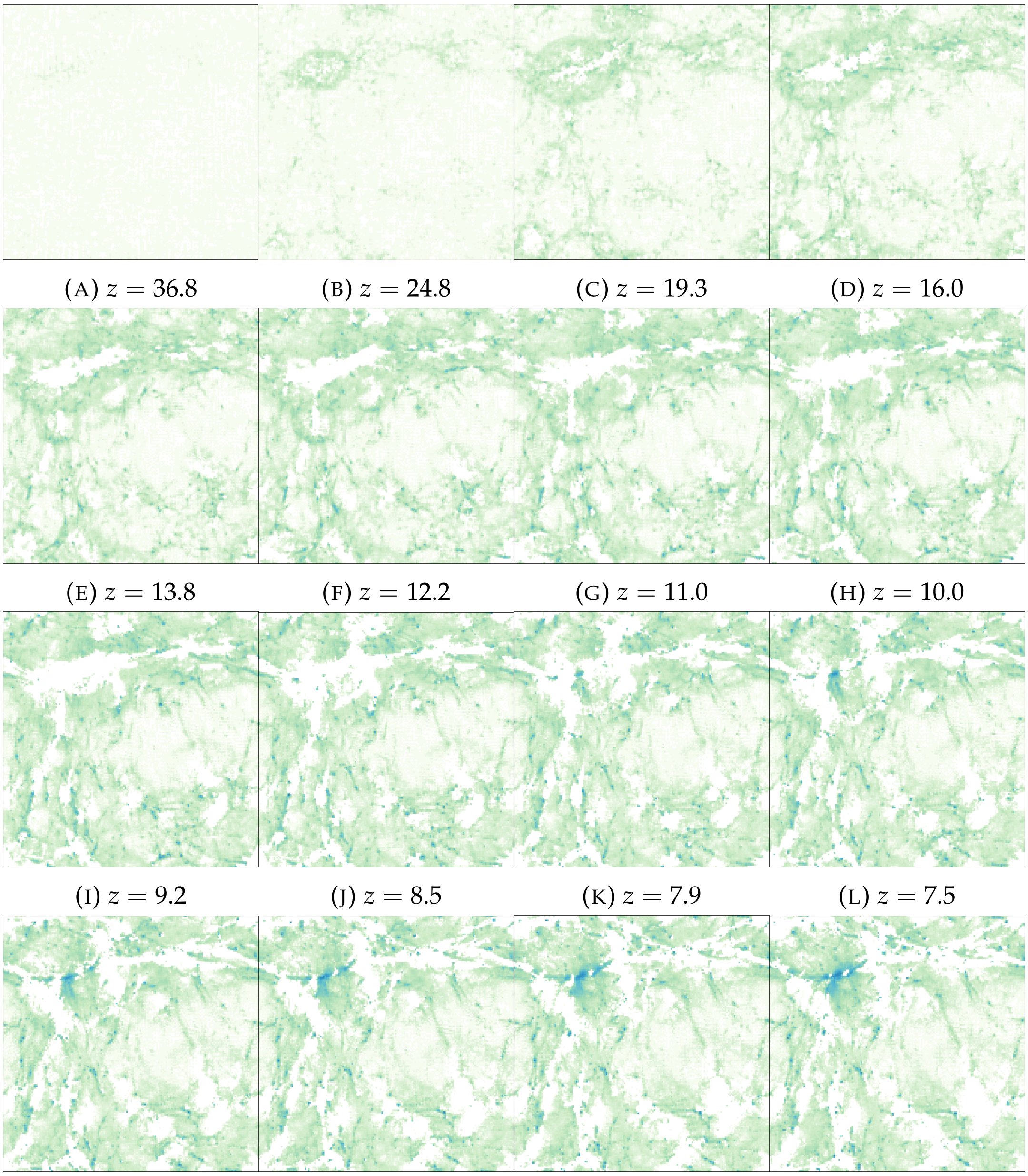

(A) $z = 36.8$ (B) $z = 24.8$ (C) $z = 19.3$ (D) $z = 16.0$

(E) $z = 13.8$ (F) $z = 12.2$ (G) $z = 11.0$ (H) $z = 10.0$

(I) $z = 9.2$ (J) $z = 8.5$ (K) $z = 7.9$ (L) $z = 7.5$

(M) $z = 7.0$ (N) $z = 6.6$ (O) $z = 6.3$ (P) $z = 6.0$

FIGURE 5.12: Gas density maps showing where the contributions from V_{Stream}-run have been removed from the *HD*-run maps. One side of the square map corresponds to 200 kpc. The areas which are white indicate where the maps are the same, while the coloured regions show where *HD*-run differs. This clearly illustrates the wide-spread star formation present in *HD*-run and that the inclusion of a streaming velocity makes it more difficult for the DM haloes to trap the gas, wiping out star formation in high-redshift small DM haloes.

5.2.5 Evolution of the Gas Metallicity

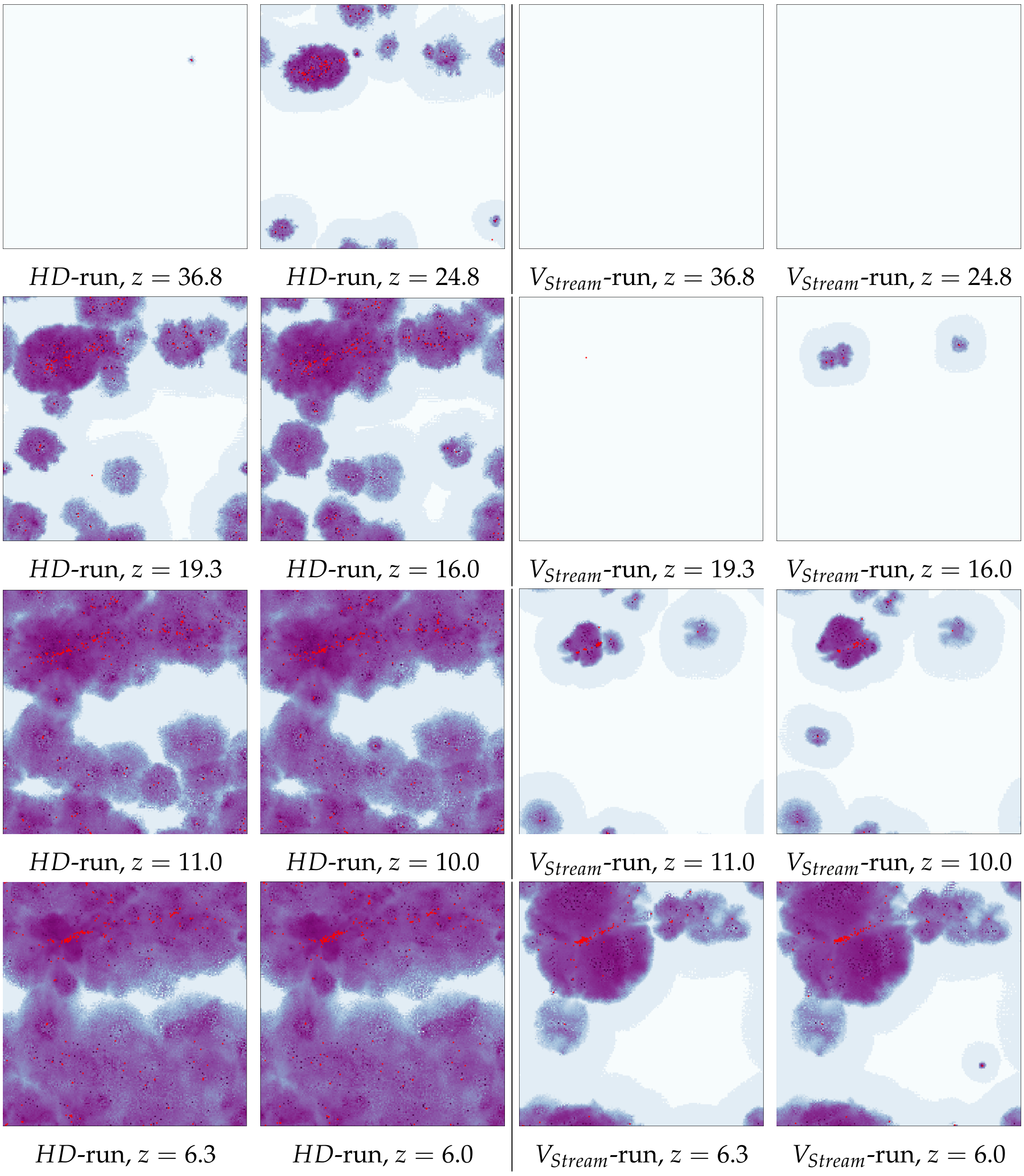

FIGURE 5.13: Metallicity maps illustrating the distribution metals in the box by placing a uniform grid on it. Each cell represents the mean metallicity projected along the z-axis of the entire box. One side of the square map corresponds to 200 kpc.. The darker the region, the more metals that are present within it. The red dots represent the positions of the stars. Each row has the two panels on the left being the HD-run evolution, and the two on the right being V_{Stream}-run. The streaming velocity delays the formation of stars, reducing the effects of metal pollution in the V_{Stream}-run. This also results in a similar metallicity distribution in comparison to the *Metals*-run.

This summary will consider each figure in turn and draw the conclusions from it. The final result will then be discussed and compared to the results of the previous studies from chapter 3, section 3.4.

The temperature distribution of the gas by redshift (figure 5.7), shows the same evolution for *HD*-run as before, with a clear delay in the formation of stars in V_{Stream}-run. These plots suggest that the first stars form around $z \sim 19$. It is important that the two simulations tend towards a similar evolution, and these two do by $z = 6$, suggesting that they will be comparable to observations at $z = 0$. The lack of a peak in the HD-run is due to the increase in the amount of gas trapped within small DM haloes, leading to larger amounts of gas at higher temperatures. This will lead to the earlier star formation seen before.

The star formation history (figure 5.8) supports the previous conclusions, showing a delay of $\Delta z \sim 10 - 15$ for the V_{Stream}-run. The peak star formation is at $z \sim 10$, suggesting that the delay in formation time delays the introduction of metals into the gas.

The DM distributions are compared in figure 5.9 and show that the two runs had identical DM evolutions. It is therefore concluded that only the changes to the gas can account for any structural changes which occur.

The temperature and density maps in figures 5.10 and 5.11 indicate a large difference in the dispersions of these fields within the two runs. The delay in star formation in V_{Stream}-run is shown once more, with the stars mostly forming within the large halo in the upper left hand corner. Star formation within small mass primordial haloes (such as the star formed in the *HD*-run at $z = 38$, have been entirely suppressed by the inclusion of a streaming velocity. A much less disrupted evolution of the fields is observed in the V_{Stream}-run. This is confirmed in the density map constructed by subtracting the V_{Stream}-run mean density in each cell from its opposite number in the *HD*-run (figure 5.12). The white areas indicate identical distributions, with the increasing colour (blue being the largest difference) indicating the divergence of the evolutions. The gas is clearly more spread-out in the *HD*-run, and shows that it is gathering much intensely in the regions of the large DM haloes by $z = 6$. The V_{Stream}-run doesn't have this feature as the gas is spread more evenly in the large halo which is already present.

The two temperature distributions show that the *HD*-run and V_{Stream}-run have similar distributions at high temperatures, where the DM haloes trap the gas to form the same large structures, but that the voids are very different. The voids are much smaller and less well-defined in the *HD*-run. This difference corresponds to the much earlier star formation, leading to the gas being much hotter due to the SNe. The gas had longer to fall into DM haloes in the V_{Stream}-run, so that the SNe from stars ejected less material at later times, due to the larger haloes more effectively stopping slower material leaving the halo. At earlier times, this would not have occurred as easily, and so more gas would have escaped the halo. The amount of hot gas being so widely spread in the *HD*-run is an indication of this.

Finally, the metallicities are compared in figure 5.13. The star formation in the V_{Stream}-run is clearly delayed, and shows a much less dispersion in the distribution of metals. The *HD*-run has a much more wide-spread distribution, with stars forming all over the box as opposed to the concentrated star formation within the large halo and some minor haloes in the V_{Stream}-run. The lack of metals also delays the transition from Pop III stars to the later generations. The same small-mass halo suppression of star formation is highlighted by these maps.

The streaming velocity therefore delayed star formation which agrees well with the studies made by Maio, Koopmans, and Ciardi, 2011, Stacy, Bromm, and Loeb, 2011 and Greif et al., 2011b. The delay being $\Delta z \sim 10-15$ is larger than that observed by Greif et al., 2011b, but since simulations are difficult to compare, our value does not seem unreasonable, especially since the time of collapse in the V_{Stream}-run was at $z = 21$ (very close to their value of $z = 19.8$).

The smoother density, temperature and metallicity distributions (as appeared in the *Metals*-run), along with the star formation history and temperature distribution, suggest that the DM haloes have to grow in size before stars can form, removing star formation from small DM haloes. This is illustrated by the early stars which form in the *HD*-run appearing in remote regions of the box, which do not appear in the V_{Stream}-run, indicating a suppression of star formation in small mass DM haloes. We find excellent agreement with Maio, Koopmans, and Ciardi, 2011, Stacy, Bromm, and Loeb, 2011 and Greif et al., 2011b in this regard as well. This has the net effect of producing an evolution which superficially appears to be similar to the *Metals*-run. Since no analysis was done to confirm this, one cannot claim that is so, but it is interesting to see the similarity, and suggests that the removal of molecules has a similar evolution to molecules with a streaming velocity. This would be very promising because the inclusion of a streaming velocity would delay star formation, but not alter the structure formation so much that it doesn't match observations at $z = 0$.

The effects of UV backgrounds have been excluded, as previously stated. Christensen et al., 2012 introduced an expression which would simulate the UV background for nearby stars, and a UV background from the epoch of re-ionisation can also be turned on between redshifts 8 and 10. The effects these would have in such a small volume, and how relevant the expressions are in such cases needs to be investigated, and will be considered in future work. The effects associated with UV fields, magnetic fields, and turbulence are of great importance in star formation, and need to be addressed in further studies. With reference to these effects, the mass resolution in this study may look small enough (a gas mass resolution of $\sim 2\,M_{\odot}$, but numerical simulations do not resolve individual stars, but groups of stars. The effects from magnetic fields and turbulent gases are therefore too simple for such scenarios, and need to be investigated in more detail so that these effects can be captured in further works.

The only point on which we differ with the previous studies is about the thermal evolution of the gas. The *HD*-run had an entirely different gas distributions to that of the V_{Stream}-run, which was not found to be the case in the Maio, Koopmans, and Ciardi, 2011, Stacy, Bromm, and Loeb, 2011 and Greif et al., 2011b studies.

Chapter 6

Conclusions

The cosmological simulations in this study were conducted within a cubic volume of 200 kpc on a side, starting at redshift of 100 with 128^3 particles for both gas and the same number for the DM, resulting in a mass per gas particle of $\sim 52\ M_\odot$, and a mass per DM particle of $\sim 276\ M_\odot$. Three simulations were run: *Metals*-run (with no molecular cooling), *HD*-run (with molecular cooling) and V_{Stream}-run (with molecular cooling and an homogeneous streaming velocity in the x-direction). The molecular cooling network consisted of the species e^-, H,H^+, H^-, He^+, He^{++}, H_2, D, D^+, D^-, HD and HD^+.

The inclusion of molecular cooling, and in particular the addition of HD to the chemical network, has a large impact on when Pop III stars form. The formation time in this study was found to be around $z = 38$, in comparison to $z = 21$ in the *Metals*-run. This completely altered the thermal, density and metallicity evolution of the gas, as the early introduction of metals meant that smaller DM haloes were able to cool the gas more efficiently and thus produce large numbers of stars over a longer period. This resulted in a wide-spread distribution of metals, due to SN explosions continuously pumping the hot gas out of their DM haloes, and dispersed the distributions for the temperature and density fields. Nevertheless, we find good agreement with Nakauchi, Inayoshi, and Omukai, 2014 that the inclusion of HD is an important coolant for the study of Pop III stars.

Adding a streaming velocity, using the same molecular cooling code as discussed above, delayed star formation by $\Delta z \sim 10 - 15$. This was larger than the delay of $\Delta z = 4$ found by Greif et al., 2011b, but we are in excellent agreement with them about the formation of the first stars, our study putting it at $z = 21$ and there's at $z = 19.8$. Certainly these differences are stochastic in nature as the simulation volume is very small. This delay is attributed to small DM haloes being unable to trap the gas as effectively at high redshifts due to the addition of a rampressure (which removes the gas). These findings agree well with previous studies by Maio, Koopmans, and Ciardi, 2011, Stacy, Bromm, and Loeb, 2011 and Greif et al., 2011b. Further investigations are needed to investigate whether molecular cooling totally compensates for the streaming velocity.

The thermal, density and metallicity evolutions of the gas were found to differ substantially between the runs with and without the streaming velocity. The reasons behind the suppression of gas structure within the molecular cooling code is that DM halos have more time to grow when a streaming velocity is included, allowing the gas to be trapped more effectively within larger haloes once the first SN explosions occur. The metallicity of the gas will be suppressed within this regime, since the formation of Pop II-I stars is delayed. This delay traps the metals within the large DM haloes, producing a more pronounced structure formation for the gas.

At completion of the current research project several avenues become apparent for future research. One avenue is to improve star formation within simulations in particular the use of the IMF for this high resolution - low particle mass regime must be revised. Simulations which implement more accurate turbulence models may be soon able to resolve the formation of individual stars which then would provide the mass spectrum of the stars self-consistently. Another avenue is to focus on the improvement of the wind description. The current model assumes a homogeneous streaming velocity field which is certainly a simplification. A way forward here is the utilisation of the analytical model by Ahn, 2016 for the implementation of the initial conditions of the simulations. This will lead not only to the sweeping away of gas from dark matter halos but also to accumulation of gas at other locations possible leading to an acceleration of star formation.

Appendix A

Cooling in the GASOLINE code

This appendix is designed to give an overview of the way in which the cooling and heating of the gas are handled within GASOLINE. This is by-no-means a user manual or technical guide, but a brief summary of the relevant functions, and details about the changes which have been made to the cooling code to incorporate molecules into the chemical network. It is also intended to be read with the reader in possession of the source code. The full code is not given in this appendix, and very few clippings from the code exist here. This is more of a discussion about what the functions do and how their contents were modified. With this in mind, we begin by looking at how the code is compiled to include molecular cooling.

A.1 Makefile Options

We begin with the Makefile and discussing the important cooling options. The two most important ones dictate whether or not molecular cooling is present within the calculations or not. To turn on cooling which contains hydrogen and helium (and their various ions), and metals from a table constructed by CLOUDY, use these compilation options:

```
COOLING_OBJ = cooling_metal.o
COOLING_DEF = −DCOOLING_METAL
```

This calls the metal cooling file `cooling_metal.c` with its header file `cooling_metal.h`. To turn on cooling including H_2 and HD, use these compilation options:

```
COOLING_OBJ = cooling_metal_H2.o
COOLING_DEF = −DCOOLING_MOLECULARH
```

This calls the metal cooling file `cooling_metal_H2.c` with its header file `cooling_metal_H2.h`. We will discuss these cooling files after discussing two more molecular cooling options.

`-DCOOLDEBUG` turns on the option to output two textfiles during the cooling calculations: one which outputs every calculation step and one which outputs a custom cooling table for the non-equilibrium species (which can be modified by the user). In its present configuration, the first column outputs the temperature of the current step, the next 9 columns are the abundances of every species within the chemical network and the rest of the columns output the energies of each rate in the reaction network and the photoionization rates.

textmyfont-DRADIATIVEBOX is an option made available by changes from Christensen et al., 2012 which allows an additional Lyman-Werner UV background to be added to the code. This is done to reduce the H_2 abundance once the first SNe events occur. For full details on how this works, see Christensen et al., 2012.

The rest of the compilation options within the Makefile are standard for the code and need not be discussed in this work. We will now move on to a discussion of the `cooling_metal_H2.c` and `cooling_metal_H2.h` files.

A.2 Molecular Cooling Files

This section describes the relevant functions within the cooling `.c` and `.h` files. The code will not be given in full (as this would take up an inordinate amount of space and add little value). Instead, this will act as a guide to the code assuming that the full code is available to the reader. Note that the cooling code for molecular cooling builds on the cooling code for metals, and so the two are almost identical, with the molecular cooling adding in a few functions and more cooling and heating terms. It will be pointed out where these changes occur.

The creators of `GASOLINE` chose an object-oriented programming (OOP) approach to structure the code. All the objects are declared within the header files and then called in the `.c` files. Reading objects in `C` proves difficult when the variable types are unknown, so a discussion of the objects in the header file seems the best place to start.

A.2.1 The Header File

The beginning of the file consists of defining constants. These are either cosmological (e.g. $Z_\odot$) or threshold values (e.g. minimum temperatures, error tolerances, and so on), and need not be discussed.

ThetextmyfontCOOLPARAM object contains all the parameters associated with cooling. Apart from the already existing parameters, three additional parameters were added:

```
    int    bSelfShield;   /* Set to true to include self-shielding  */
    int    bShieldHI;    /* Set to true to allow dust to shield HI */

#ifdef  RADIATIVEBOX
    double dLymanWernerFrac; /* Fraction of Lyman Werner radiation that escapes birth cloud.
        0.5 is a good choice of value.  - MU */
    int bAgeFromMass;          /* Set to true to determine age of star  particle  from mass
        compared to formation mass when calculating LW radiation, particularly useful with
        ICs which already have stars. - MU*/
```

```
    #endif
```

The notation for parameters in GASOLINE is *b* for **boolean**, *n* for **integer** and *d* for **double**, with all boolean-variables being integers with values 0 or 1. The comments pertaining to the above lines are self-explanatory. The ifdef defined here links directly to the one mentioned in Appendix A.1 above.

The COOLPARTICLE object contains all of the cooling variables for working out the abundances of ions within gas particles, and whether or not a Lyman-Werner (LW) flux will affect the gas particle.

```
    typedef struct CoolingParticleStruct {
        FLOAT f_HI,f_HeI,f_HeII;  /* Cooling−metals abundances of ions */
        FLOAT f_H2, f_D,f_HD;       /* Abundance of molecular ions add − MU */
        #ifdef  RADIATIVEBOX
        double      dLymanWerner; /* Flux of Lyman Werner radiation for a particular gas
            particle  − MU */
        #endif
} COOLPARTICLE;
```

The PERBARYON object has a similar structure to that of COOLPARTICLE, except that it uses **double** types. There is no LW flux here, merely abundances, and variables for molecular cooling were added.

The UVSPECTRUM object contains the photoionization rates for the various species considered. The photoionization variables for H_2, D and HD were added.

The RATES_NO_T and RATES_T objects are very similar. RATES_NO _T contains one temperature independent collisional ionization rate for each species. RATES_T contains all the temperature dependent non-equilibrium rates associated with each species (see Appendix B). Both of these objects use a custom variable type called CL_RT_FLOAT, which is of type **double**. The RATES_T object is related to the RATES object, which uses the **double** type for all the rates instead of the CL_RT_FLOAT variable type. Molecular cooling variables were added to both RATES_T and RATES.

The COOL object contains all of the cooling data from COOLPARAM, but extends it to include all of the cooling threshold values. The RADIATIVEBOX compilation option was added once more, along with a variable related to LW radiation:

```
    double      dInitStarMass; /* Mass of star  particle  at  formation time,  Used when
        calculating LW radiation − MU */
```

The COOLDEBUG compilation option is added here to allow the interaction with all the particle data by using a **struct**.

The final additions are that each rate has its own function and each of these is added in the header file.

A.2.2 The .c File

As in the header file, the beginning of this file declares all the constants which will be used, along with all the appropriate headers and libraries. The following constants were added:

```
#define CL_eH2    (4.476*CL_eV_erg) /*Energy lost during H2 dissociation, Shapira &
        Kang (1987) through Abel 1997, page 194 - MU */
#define CL_eHD    (5.086*CL_eV_erg) /*Energy lost during HD dissociation Trevisan & Tennyson
    (2002b) */
#define CL_eD     (13.60*CL_eV_erg) /* Energy lost during D dissociation - MU */
```

which represent the energies lost during dissociation for these species, and are converted from eVs to ergs.

Just a note on functions: functions beginning with `COOL` or `Cool` are private functions, while functions beginning with `cl` are public functions.

The `CoolInit` function initialises the integration for cooling. The size of the derivatives array was increased from 4 to 7, to allow the tracking of the species H_2, D and HD (in that order).

The `CoolPERBARYONtoPARTICLE` and `CoolPARTICLEtoPERBARYON` functions calculate the abundances of species within a gas particle, based on the overall abundances, and vice verse. Here, the abundances of H_2, D and HD are given in terms of the total abundance of H_I.

Although we do not alter the cooling table, the reading of it is the next step. The table is in *XDR* format. The various parameters given for the cooling table are defined by local variables, followed by reading the various sections of the table into a local 3D **array**. This **array** is then called by various rates functions later on.

The `clInitUV` function initializes the table for UV background, and has additional variables added to it for the photoionization heating of H_2, D and HD.

The `clInitRatesTable` function initializes the `RATES` object, added in all the rates which are independent of temperature first, followed by all of the non-equilibrium rates which are temperature dependent. Both of these contain entries for H_2, D and HD as additions. This function contains the option to have cubic interpolation turned on. This sacrifices speed for a more accurate interpolation between the values contained within the cooling table. In order to understand the significance of this, a brief outline of a cooling table is given. Essentially, a cooling table contains a number of columns. The first column is either redshift or scale factor, the second is rho, the third is temperature, and then the additional columns will each represent a single species. For each redshift, density and temperature, the values in the other columns represent the energies which are lost (or gained). The ordering of the redshift z is from high to low values, while density and temperature are ordered from low to high values. If the current time-step within a simulation is between two redshift (or scale-factor), density and temperature values, the energy must be interpolated. Thus, the two methods are linear and cubic interpolations, and linear is default. Because the different methods are dealt with separately within `clInitRatesTable`, the various rates have to be inputted within each *if statement*, meaning they appear twice overall.

The `clRatesTableError` function checks that the table values are within the thresholds, and that the errors are acceptable, particularly after interpolation. This function was untouched in this work.

The `clRatesRedshift` function contains all the information relating to the UV heating of the various species, and the Compton cooling of the metal species. Once more, interpolation is used for the UV values, allowing linear and logarithmic interpolation. The photoheating of H_2, D and HD were all added to this function, with D following H_I, and HD following H_2.

The `clRates` function contains all of the rates which will be used in calculating the net loss or gain of energy by each particle within the simulation. It too contains linear and cubic interpolations. The H_2, D and HD species rates were all added, including LW radiation and shielding (where appropriate).

The interpolating functions were not altered . They interpolate the rates and return energy values, and can perform linear and cubic interpolations. The `clRateMetalTable` function was also untouched. It returns the energies associated with the metals found in the cooling table constructed by `CLOUDY`.

The `clHeatTotal` and `clCoolTotal` functions are now deprecated, but rates for H_2, D and HD were added to both of them anyway. `clHeatTotal` returns the total heating of the gas via interaction with a UV source as a single heating term. At high redshifts, this will be zero. `clCoolTotal` returns the total cooling via collisional, dissociational and radiative processes. These are computed by adding together all of these rates to form the cooling term, which is what is returned.

The next two functions are both useful for debugging. The first is `clPrintCool` which outputs to the terminal all the cooling occurring at the current step of the calculation within the simulation. This proves tricky when running on a cluster. The second function is `clPrintCoolFile` is more useful because it outputs everything in `clPrintCool` to a file written in the same directory as the simulation is being run. This makes it extremely useful in checking for rates which could be causing problems.

The `clAbunds` function calculates the current abundances of all the species in the `clDerivs` array (in this work it is the 7 species tracked explicitly). It then returns all of the new abundances by updating the relevant object.

The `clSelfShield` and `clDustShield` functions are implementations of the Christensen et al., 2012. After these, every rate equation has its own function. These are all temperature dependent. Included within these are line cooling, radiative recombination and a low temperature approximation for metals, along with the addition of LW radiation.

The `clEdotInstant_Table` and `clEdotInstant` functions both return the net energy loss or gain by subtracting all the cooling rates from the heating rates. The former contains interpolation where the latter does not. These replace the `clHeatTotal` and `clCoolTotal` functions as they combine them both in one function.

The next function which was altered was `clDerivs`. This calculates the derivatives of each species which will be integrated at each time-step. These will alter the abundances of the various species. They take the form:

$$\begin{aligned} dx_{species} = &\sum(\text{formation rates } \times \text{abundances of each species involved}) \\ &- \sum(\text{destruction rates } \times \text{abundances of each species involved}) \end{aligned} \quad \text{(A.2.1)}$$

The minor species, such as H^-, are tracked in a similar manner, but are not added to an array and so are traced only within the current calculation by using the abundances of the major species and the rates pertaining to the formation and destruction of the minor species.

The `clJacobn` function is used to make sure that the derivatives which are calculated match certain error tolerances and thresholds. H_2, D and HD were added here and were scaled, along with the rest of the species already implemented, so that the overall abundances were never too high or too low. `clSetyscale` and `clIntegrateEnergy` both have similar forms to `clJacobn`, and also check tolerances. The same additions were made to these functions.

The final functions link all of the above `cl` functions together and then link them to the external files. They were unaltered.

This concludes this Appendix. We have covered the compilation options needed to turn on molecular cooling, and have then discussed all of the major functions needed for molecular (and atomic) cooling.

Appendix B

Chemical Network

This Appendix details all the rates which already exist within the `GASOLINE` code and tabulates all the rates and where they come from (Table B.1). It also tabulates the rates implemented in this work and where they come from (Table B.2). Within the code, each rate is expressed as a function of temperature, and is called in the relevant places (see Appendix A for details).

Reaction	Rate	Rate Equation	Reference
$H + e^- \longrightarrow H^+ + 2e^-$	k_1	$k_1 = \exp[-32.71396786 + 13.536556 \ln(T)$ $-5.73932875 \ln(T)^2$ $+1.56315498 \ln(T)^3$ $-0.2877056 \ln(T)^4$ $+3.48255977 \times 10^{-2} \times \ln(T)^5$ $-2.63197617 \times 10^{-3} \times ln(T)^6$ $+1.11954395 \times 10^{-4} \ln(T)^7$ $-2.03914985 \times 10^{-6} \ln(T)^8]$ cm^3 s^{-1}	1
$He + e^- \longrightarrow He^+ + 2e^-$	k_2	$k_2 = \exp[-44.09864886 + 23.91596563 \ln(T)$ $-10.7532302 \ln(T)^2$ $+3.05803875 \ln(T)^3$ $-0.56851189 \ln(T)^4$ $+6.79539123 \times 10^{-2} \times \ln(T)^5$ $-5.00905610 \times 10^{-3} \times ln(T)^6$ $+2.06723616 \times 10^{-4} \ln(T)^7$ $-3.64916141 \times 10^{-6} \ln(T)^8]$ cm^3 s^{-1}	1
$He^+ + e^- \longrightarrow He^{++} + 2e^-$	k_3	$k_3 = \exp[-68.71040990$ $+43.93347633 \ln(T)$ $-18.4806699 \ln(T)^2$ $+4.70162649 \ln(T)^3$ $-0.76924663 \ln(T)^4$ $+8.113042 \times 10^{-2} \times \ln(T)^5$ $-5.32402063 \times 10^{-3} \times ln(T)^6$ $+1.97570531 \times 10^{-4} \ln(T)^7$ $-3.16558106 \times 10^{-6} \ln(T)^8]$ cm^3 s^{-1}	2

Continued on next page

Table B.1 – continued from previous page

Reaction	Rate	Rate Equation	Reference
$H^- + e^- \longrightarrow H + 2e^-$	k_4	$k_4 = \exp[-18.01849334273$ $+2.360852208681 \ln(T)$ $-0.2827443061704 \ln(T)^2$ $+0.01623316639567 \ln(T)^3$ $-0.03365012031362999 \ln(T)^4$ $+0.01178329782711 \times \ln(T)^5$ $-0.001656194699504 \times ln(T)^6$ $+0.0001068275202678 \ln(T)^7$ $-2.631285809207 \times 10^{-6} \ln(T)^8]$ $\mathrm{cm^3\,s^{-1}}$	2
$H^- + H^+ \longrightarrow 2H$	k_5	$k_5 = 7.0 \times 10^{-8} e^{-\frac{T}{100}}$	25
$H^+ + e^- \longrightarrow H + \gamma$	k_6	$k_8 = 7.982 \times 10^{-11}/[\sqrt{T} \times 0.563615$ $\times (1 + \sqrt{T} \times 0.563615)^{0.252}$ $\times (1 + \sqrt{T} \times 1.192167 \times 10^{-3})^{1.748}]$	3
$He^+ + e^- \longrightarrow He + \gamma$	k_7	$k_9 = \mathrm{dex}[10.3217$ $+0.749031 \log(T)$ $-1.66439 \log(T)^2$ $+1.13114 \log(T)^3$ $-0.459420 \log(T)^4$ $+0.114337 \times \log(T)^5$ $-0.0174612 \times log(T)^6$ $+0.00158680 \log(T)^7$ $-7.86098 \times 10^{-5} \times \log(T)^8$ $+1.63398 \times 10^{-6} \times \log(T)^9]$ $\mathrm{cm^3\,s^{-1}}$	3
$He^+ + e^- \longrightarrow He + \gamma$	k_8	$k_{10} = 1.9 \times 10^{-3} \times T^{-1.5}$ $\times e^{-4.7\times10^5 \times \frac{1}{T}} \times (1 + 0.3 \times e^{-9.4\times10^4 \times \frac{1}{T}})$	4
$He^{++} + e^- \longrightarrow He^+ + \gamma$	k_9	$k_{11} = 1.891 \times 10^{-10}/[\sqrt{T} \times 0.326686$ $\times (1 + \sqrt{T} \times 0.326686)^{0.2476}$ $\times (1 + \sqrt{T} \times 6.004084 \times 10^{-4})^{1.7524}]$	3

TABLE B.1: Already existing chemical network in GASOLINE. The references are listed below.

[a] $\mathrm{dex}(x) \equiv 10^x$
[1] Janev et al., 1987 through Abel et al., 1997
[2] (Abel et al., 1997)
[3] Verner and Ferland, 1996
[4] Aldrovandi and Pequignot, 1973 through Black, 1981

Reaction	Rate	Rate Equation	Reference
$H + e^- \longrightarrow H^- + \gamma$	k_{10}	$k_6 = 1.429 \times 10^{-18} \times$ $T^{0.762} \times T^{0.1523\times\log(T)} \times T^{-3.274\times10^{-2}\times(\log(T))^2}$ $\mathrm{cm^3\ s^{-1}}$, $T \leq 6000$ K $= 3.802 \times 10^{-17} T^{0.1998\times\log(T)} \times$ dex $[4.0415 \times 10^{-5} \times (\log(T))^6$ $-5.447 \times 10^{-3} \times \times (\log(T))^4]$ $\mathrm{cm^3\ s^{-1}}$, $T > 6000$ K	2
$H + H^- \longrightarrow H_2 + e^-$	k_{11}	$k_7 = \exp[-20.06913897587003$ $+0.2289800603272916 \ln(T)$ $+0.03599837721023835 \ln(T)^2$ $-0.004555120027032095 \ln(T)^3$ $-0.0003105115447124016 \ln(T)^4$ $+0.0001073294010367247 \times \ln(T)^5$ $-8.36671960467864 \times 10^{-6} \times ln(T)^6$ $+2.238306228891639 \times 10^{-7} \ln(T)^7]$ $\mathrm{cm^3\ s^{-1}}$, $T > 0.1$ eV $= 1.428 \times 10^{-9}\ \mathrm{cm^3\ s^{-1}}$, $T < 0.1$ eV	2
$H_2 + H_2 \longrightarrow H_2 + 2\,H$	k_{12}	$k_{12} = \frac{5.996\times10^{-30} T^{4.1881}}{(1.0+6.761\times10^{-6} T)^{5.6881}} e^{-\frac{54657.4}{T}}$, $\nu = 0$ $= 1.3 \times 10^{-9} e^{-\frac{53300}{T}}$, LTE	5 6
$H_2 + H \longrightarrow 3\,H$	k_{13}	$k_{13} = 6.67 \times 10^{-12} \times T^{0.5} \times e^{-\left(1+\frac{63593.0}{T}\right)}$, $\nu = 0$ $= 3.52 \times 10^{-9} e^{-\frac{43900.0}{T}}$, LTE	18 19
$H_2 + H^+ \longrightarrow H_2^+ + H$	k_14	$k_{14} = [-3.3232183e-7$ $+3.3735382e-7 \times \log(T)$ $-1.4491368e-7 \times \log(T)^2$ $+3.4172805e-8 \times \log(T)^3$ $-4.7813720e-9 \times \log(T)^4$ $+3.9731542e-10 \times \log(T)^5$ $-1.8171411e-11 \times \log(T)^6$ $+3.5311932e-13 \times \log(T)^7] e^{-\frac{21237.15}{T}}$	7
$H_2 + e^- \longrightarrow 2\,H + e^-$	k_{15}	$k_{15} = 4.49 \times 10^{-9} T^{0.11} e^{-\frac{101858.0}{T}}$, $\nu = 0$ $= 1.19 \times 10^{-9} T^{0.136} e^{-\frac{53407.1}{T}}$, LTE	8
$D + H_2 \longrightarrow HD + H$	k_{16}	$k_{16} = 3.17 \times 10^{-10} e^{-\frac{5207.0}{T}}$, $T > 2000$ K = dex$[-56.4737$ $+5.88886 \times \log(T)$ $+7.19692 \times \log(T)^2$ $+2.25069 \times \log(T)^3$ $-2.16903 \times \log(T)^4$ $+0.317887 \times \log(T)^5]$, $T \leq 2000$ K [a]	17
$D^+ + H_2 \longrightarrow HD + H^+$	k_{17}	$k_{17} = [0.417 + 0.846 \log(T)$ $-0.137 \log(T)^2] \times 10^{-9}$	9

Continued on next page

Table B.2 – continued from previous page

Reaction	Rate	Rate Equation	Reference
$H^+ + D \longrightarrow H + D^+$	k_{18}	$k_{18} = 3.44 \times 10^{-10} T^{0.35}$, $T > 20000$ K $= 2.0 \times 10^{-10} T^{0.402} e^{-\frac{37.1}{T}} - 3.31 \times 10^{-17} T^{1.48}$, $T \leq 20000$ K	10
$H^- + D \longrightarrow H + D^-$	k_{19}	$k_{19} = 6.4 \times 10^{-9} (\frac{T}{300.0})^{0.41}$	11
$D^+ + D^- \longrightarrow 2\,D$	k_{20}	$k_{20} = \frac{7.0 \times 10^{-8}}{\sqrt{\frac{T}{100.0}}}$	17
$H + D^+ \longrightarrow H^+ + D$	k_{21}	$k_{21} = 2.06 \times 10^{-10} T^{0.396} e^{-\frac{33.0}{T}}$ $+2.03 \times 10^{-9} T^{-0.332}$	10
$H + D^- \longrightarrow H^- + D$	k_{22}	$k_{22} = 26.4 \times 10^{-9} (\frac{T}{300.0})^{0.41}$	11
$H^+ + D^- \longrightarrow D + H$	k_{23}	$k_{23} = \frac{7.0 \times 10^{-8}}{\sqrt{\frac{T}{100.0}}}$	17
$H + D^- \longrightarrow HD + e^-$	k_{24}	$k_{24} = \frac{1}{2} \exp[-20.06913897587003$ $+0.2289800603272916 \ln(T)$ $+0.03599837721023835 \ln(T)^2$ $-0.004555120027032095 \ln(T)^3$ $-0.0003105115447124016 \ln(T)^4$ $+0.0001073294010367247 \times \ln(T)^5$ $-8.36671960467864 \times 10^{-6} \times ln(T)^6$ $+2.238306228891639 \times 10^{-7} \ln(T)^7]$, $T > 0.1$ eV $= 1.428 \times 10^{-9}$, $T \leq 0.1$ eV	2
$HD + H^+ \longrightarrow D^+ + H_2$	k_{25}	$k_{25} = 1.1 \times 10^{-9} e^{-\frac{488.0}{T}}$	9
$HD + H \longrightarrow D + H_2$	k_{26}	$k_{26} = 5.25 \times 10^{-11} e^{-\frac{4430.0}{T} + \frac{173900.0}{T^2}}$, $T > 200$ K $= 5.25 \times 10^{-11} e^{-\frac{4430.0}{T}}$, $T < 200$ K	12
$HD^+ + e^- \longrightarrow H + D$	k_{27}	$k_{27} = 7.2 \times 10^{-8} T^{\frac{1}{2}}$	13
$HD^+ + H^- \longrightarrow H + HD$	k_{28}	$k_{28} = 1.5 \times 10^{-7} (\frac{T}{300.0})^{\frac{1}{2}}$	17
$D + e^- \longrightarrow D^- + \gamma$	k_{29}	$k_{29} = 1.429 \times 10^{-18} \times$ $T^{0.762} \times T^{0.1523 \times \log(T)} \times T^{-3.274 \times 10^{-2} \times (\log(T))^2}$ $cm^3\ s^{-1}$, $T \leq 6000$ K $= 3.802 \times 10^{-17} T^{0.1998 \times \log(T)} \times$ dex $[4.0415 \times 10^{-5} \times (\log(T))^6$ $-5.447 \times 10^{-3} \times (\log(T))^4]$ $cm^3\ s^{-1}$, $T > 6000$ K	15

Continued on next page

Table B.2 – continued from previous page

Reaction	Rate	Rate Equation	Reference
$D + H \longrightarrow HD + \gamma$	k_{30}	$k_{30} = 10^{-25}\exp[507.207$ $-370.889\ln(T)$ $+104.854\ln(T)^2$ $-14.4192\ln(T)^3$ $+0.971469\ln(T)^4$ $-0.0258076 \times \ln(T)^5]$, $T > 200$ K $= 10^{-25}\exp[2.30202$ $-6.63697\ln(T)$ $+4.75619\ln(T)^2$ $-1.39325\ln(T)^3$ $+0.178259\ln(T)^4$ $-0.00817097 \times \ln(T)^5]$, $T \leq 200$ K	16
$D + H^+ \longrightarrow HD^+ + \gamma$	k_{31}	$k_{31} = 3.9 \times 10^{-19}(\frac{T}{300.0})^{1.8} \times e^{\frac{20.0}{T}}$	17
$D^+ + e^- \longrightarrow D + \gamma$	k_{32}	$k_{32} = 7.982 \times 10^{-11}[\sqrt{T} \times 0.563615$ $\times(1+\sqrt{T} \times 0.563615)^{0.252}$ $\times(1+\sqrt{T} \times 1.192167 \times 10^{-3})^{1.748}]$	14
$D^+ + H \longrightarrow HD^+ + \gamma$	k_{33}	$k_{33} = 3.9 \times 10^{-19}(\frac{T}{300.0})^{1.8} \times e^{\frac{20.0}{T}}$	17

TABLE B.2: Molecular Chemical Network added to GASOLINE.

[a] $\mathrm{dex}(x) \equiv 10^x$
[2] (Abel et al., 1997)
[5] Martin, Keogh, and Mandy, 1998 through Glover and Abel, 2008
[6] Shapiro and Kang, 1987 through Glover and Abel, 2008
[7] Savin et al., 2004 through Glover and Abel, 2008
[8] Trevisan and Tennyson, 2002a through Glover and Abel, 2008
[9] Gerlich, 1982 through Glover and Abel, 2008
[10] Savin, 2002 through Glover and Abel, 2008
[11] Dalgarno and McDowell, 1956 through Glover and Abel, 2008
[12] Shavitt, 1959 through Glover and Abel, 2008
[13] Strömholm et al., 1995 through Glover and Abel, 2008
[14] Ferland et al., 1992 through Glover and Abel, 2008
[15] Wishart, 1979 through Glover and Abel, 2008
[16] Dickinson, 2005 through Glover and Abel, 2008
[17] Glover and Abel, 2008
[18] Mac Low and Shull, 1986 through Glover and Abel, 2008
[19] Lepp and Shull, 1983 through Glover and Abel, 2008

Bibliography

Abel, T., G. L. Bryan, and M. L. Norman (2002). “The Formation of the First Star in the Universe”. In: *Science* 295, pp. 93–98. DOI: 10.1126/science.295.5552.93. eprint: astro-ph/0112088.

Abel, T., J. H. Wise, and G. L. Bryan (2007). “The H II Region of a Primordial Star”. In: ApJ 659, pp. L87–L90. DOI: 10.1086/516820. eprint: astro-ph/0606019.

Abel, T. et al. (1997). “Modeling primordial gas in numerical cosmology”. In: New A 2, pp. 181–207. DOI: 10.1016/S1384-1076(97)00010-9. eprint: astro-ph/9608040.

Aguirre, A. (1999a). “Intergalactic Dust and Observations of Type IA Supernovae”. In: ApJ 525, pp. 583–593. DOI: 10.1086/307945. eprint: astro-ph/9904319.

Aguirre, A. and J. Schaye (2007). “How Did the IGM become Enriched?” In: *EAS Publications Series*. Ed. by E. Emsellem et al. Vol. 24. EAS Publications Series, pp. 165–175. DOI: 10.1051/eas:2007024. eprint: astro-ph/0611637.

Aguirre, A. et al. (2001a). “Enrichment of the Intergalactic Medium by Radiation Pressure-driven Dust Efflux”. In: ApJ 556, pp. L11–L15. DOI: 10.1086/322860. eprint: astro-ph/0006346.

Aguirre, A. et al. (2001b). “Metal Enrichment of the Intergalactic Medium at z=3 by Galactic Winds”. In: ApJ 560, pp. 599–605. DOI: 10.1086/323070. eprint: astro-ph/0006345.

Aguirre, A. et al. (2001c). “Metal Enrichment of the Intergalactic Medium in Cosmological Simulations”. In: ApJ 561, pp. 521–549. DOI: 10.1086/323370. eprint: astro-ph/0105065.

Aguirre, A. et al. (2004). “Metallicity of the Intergalactic Medium Using Pixel Statistics. III. Silicon”. In: ApJ 602, pp. 38–50. DOI: 10.1086/380961. eprint: astro-ph/0310664.

Aguirre, A. et al. (2005). “Confronting Cosmological Simulations with Observations of Intergalactic Metals”. In: ApJ 620, pp. L13–L17. DOI: 10.1086/428498. eprint: astro-ph/0411076.

Aguirre, A. N. (1999b). “Dust versus Cosmic Acceleration”. In: ApJ 512, pp. L19–L22. DOI: 10.1086/311862. eprint: astro-ph/9811316.

Ahn, K. (2016). “How the Density Environment Changes the Influence of the Dark Matter-Baryon Streaming Velocity on Cosmological Structure Formation”. In: ApJ 830, 68, p. 68. DOI: 10.3847/0004-637X/830/2/68. arXiv: 1603.09356.

Aldrovandi, S. M. V. and D. Pequignot (1973). “Radiative and Dielectronic Recombination Coefficients for Complex Ions”. In: A&A 25, p. 137.

Allende Prieto, C., D. L. Lambert, and M. Asplund (2001). “The Forbidden Abundance of Oxygen in the Sun”. In: ApJ 556, pp. L63–L66. DOI: 10.1086/322874. eprint: astro-ph/0106360.

– (2002). “A Reappraisal of the Solar Photospheric C/O Ratio”. In: ApJ 573, pp. L137–L140. DOI: 10.1086/342095. eprint: astro-ph/0206089.

Barkana, R. and A. Loeb (2001). “In the beginning: the first sources of light and the reionization of the universe”. In: Phys. Rep. 349, pp. 125–238. DOI: 10.1016/S0370-1573(01)00019-9. eprint: astro-ph/0010468.

Bate, M. R. and A. Burkert (1997). "Resolution requirements for smoothed particle hydrodynamics calculations with self-gravity". In: MNRAS 288, pp. 1060–1072. DOI: 10.1093/mnras/288.4.1060.

Binney, J. J. (1997). "Report of IAU Commission 33: Structure and dynamics of the galactic system." In: *Transactions of the International Astronomical Union, Series A* 23, pp. 417–427.

Black, J. H. (1981). "The physical state of primordial intergalactic clouds". In: MNRAS 197, pp. 553–563. DOI: 10.1093/mnras/197.3.553.

Boothroyd, A. I. et al. (1996). "A refined H_3 potential energy surface". In: J. Chem. Phys. 104, pp. 7139–7152. DOI: 10.1063/1.471430.

Bovino, S. et al. (2014). "Dark-matter halo mergers as a fertile environment for low-mass Population III star formation". In: MNRAS 441, pp. 2181–2187. DOI: 10.1093/mnras/stu714. arXiv: 1402.4403.

Bromm, V., P. S. Coppi, and R. B. Larson (1999). "Forming the First Stars in the Universe: The Fragmentation of Primordial Gas". In: ApJ 527, pp. L5–L8. DOI: 10.1086/312385. eprint: astro-ph/9910224.

– (2002). "The Formation of the First Stars. I. The Primordial Star-forming Cloud". In: ApJ 564, pp. 23–51. DOI: 10.1086/323947. eprint: astro-ph/0102503.

Bromm, V. and R. B. Larson (2004). "The First Stars". In: ARA&A 42, pp. 79–118. DOI: 10.1146/annurev.astro.42.053102.134034. eprint: astro-ph/0311019.

Bromm, V. and A. Loeb (2002). "The Expected Redshift Distribution of Gamma-Ray Bursts". In: ApJ 575, pp. 111–116. DOI: 10.1086/341189. eprint: astro-ph/0201400.

Bromm, V., N. Yoshida, and L. Hernquist (2003). "The First Supernova Explosions in the Universe". In: ApJ 596, pp. L135–L138. DOI: 10.1086/379359. eprint: astro-ph/0305333.

Brooks, A. M. et al. (2007). "The Origin and Evolution of the Mass-Metallicity Relationship for Galaxies: Results from Cosmological N-Body Simulations". In: ApJ 655, pp. L17–L20. DOI: 10.1086/511765. eprint: astro-ph/0609620.

Brooks, A. M. et al. (2009). "The Role of Cold Flows in the Assembly of Galaxy Disks". In: ApJ 694, pp. 396–410. DOI: 10.1088/0004-637X/694/1/396. arXiv: 0812.0007.

Cantalupo, S. (2010). "Stars quenching stars: how photoionization by local sources regulates gas cooling and galaxy formation". In: MNRAS 403, pp. L16–L20. DOI: 10.1111/j.1745-3933.2010.00806.x. arXiv: 0912.4149.

Cen, R. (1992). "A hydrodynamic approach to cosmology - Methodology". In: ApJS 78, pp. 341–364. DOI: 10.1086/191630.

Cen, R. and J. P. Ostriker (1993). "Cold Dark Matter Cosmogony with Hydrodynamics and Galaxy Formation: Galaxy Properties at Redshift Zero". In: ApJ 417, p. 415. DOI: 10.1086/173322.

Chapman, S. C. et al. (2003). "A median redshift of 2.4 for galaxies bright at submillimetre wavelengths". In: Nature 422, pp. 695–698. DOI: 10.1038/nature01540. eprint: astro-ph/0304235.

Choi, J.-H. and K. Nagamine (2009). "Effects of metal enrichment and metal cooling in galaxy growth and cosmic star formation history". In: MNRAS 393, pp. 1595–1607. DOI: 10.1111/j.1365-2966.2008.14297.x. arXiv: 0806.3460.

Christensen, C. et al. (2012). "Implementing molecular hydrogen in hydrodynamic simulations of galaxy formation". In: MNRAS 425, pp. 3058–3076. DOI: 10.1111/j.1365-2966.2012.21628.x. arXiv: 1205.5567.

Ciardi, B. and A. Ferrara (2005). "The First Cosmic Structures and Their Effects". In: Space Sci. Rev. 116, pp. 625–705. DOI: 10.1007/s11214-005-3592-0. eprint: astro-ph/0409018.

Couchman, H. M. P. and M. J. Rees (1986). “Pregalactic evolution in cosmologies with cold dark matter”. In: MNRAS 221, pp. 53–62. DOI: 10.1093/mnras/221.1.53.

Courant, Richard, Eugene Isaacson, and Mina Rees (1952). “On the solution of nonlinear hyperbolic differential equations by finite differences”. In: *Communications on Pure and Applied Mathematics* 5.3, pp. 243–255. ISSN: 1097-0312. DOI: 10.1002/cpa.3160050303. URL: http://dx.doi.org/10.1002/cpa.3160050303.

Dalgarno, A. and M. R. C. McDowell (1956). “Charge Transfer and the Mobility of H^- Ions in Atomic Hydrogen”. In: *Proceedings of the Physical Society A* 69, pp. 615–623. DOI: 10.1088/0370-1298/69/8/306.

Dalla Vecchia, C. and J. Schaye (2008). “Simulating galactic outflows with kinetic supernova feedback”. In: MNRAS 387, pp. 1431–1444. DOI: 10.1111/j.1365-2966.2008.13322.x. arXiv: 0801.2770.

Davé, R. et al. (1998). “Constraining the Metallicity of the Low-Density Lyα Forest Using O VI Absorption”. In: ApJ 509, pp. 661–677. DOI: 10.1086/306524. eprint: astro-ph/9803257.

de Souza, R. S., N. Yoshida, and K. Ioka (2011). “Populations III.1 and III.2 gamma-ray bursts: constraints on the event rate for future radio and X-ray surveys”. In: A&A 533, A32, A32. DOI: 10.1051/0004-6361/201117242. arXiv: 1105.2395.

Dickinson, A. S. (2005). “Radiative association of H and D”. In: *Journal of Physics B Atomic Molecular Physics* 38, pp. 4329–4334. DOI: 10.1088/0953-4075/38/23/014.

Donahue, M. and J. M. Shull (1991). “New photoionization models of intergalactic clouds”. In: ApJ 383, pp. 511–523. DOI: 10.1086/170809.

Dove, J. E. and M. E. Mandy (1986). “The rate of dissociation of molecular hydrogen by hydrogen atoms at very low densities”. In: ApJ 311, pp. L93–L96. DOI: 10.1086/184805.

Dunkley, J. et al. (2009). “Five-Year Wilkinson Microwave Anisotropy Probe Observations: Likelihoods and Parameters from the WMAP Data”. In: ApJS 180, pp. 306–329. DOI: 10.1088/0067-0049/180/2/306. arXiv: 0803.0586.

Efstathiou, G. (1992). “Suppressing the formation of dwarf galaxies via photoionization”. In: MNRAS 256, 43P–47P. DOI: 10.1093/mnras/256.1.43P.

Ellison, S. L. et al. (2000). “The Enrichment History of the Intergalactic Medium-Measuring the C IV/H I Ratio in the Lyα Forest”. In: AJ 120, pp. 1175–1191. DOI: 10.1086/301511. eprint: astro-ph/0005448.

Elmegreen, B. G. and Y. N. Efremov (1997). “A Universal Formation Mechanism for Open and Globular Clusters in Turbulent Gas”. In: ApJ 480, pp. 235–245. DOI: 10.1086/303966.

Ferland, G. J. et al. (1992). “Anisotropic line emission and the geometry of the broad-line region in active galactic nuclei”. In: ApJ 387, pp. 95–108. DOI: 10.1086/171063.

Ferland, G. J. et al. (1998). “CLOUDY 90: Numerical Simulation of Plasmas and Their Spectra”. In: PASP 110, pp. 761–778. DOI: 10.1086/316190.

Field, G. B. (1965). “Thermal Instability.” In: ApJ 142, p. 531. DOI: 10.1086/148317.

Field, G. B., D. W. Goldsmith, and H. J. Habing (1969). “Cosmic-Ray Heating of the Interstellar Gas”. In: ApJ 155, p. L149. DOI: 10.1086/180324.

Flower, D. R. (2000). “HD in the primordial gas”. In: MNRAS 318, pp. 875–878. DOI: 10.1046/j.1365-8711.2000.03765.x.

Forrey, R. C. et al. (1997). “Quantum Mechanical Calculations of Rotational Transitions in H-H_2 Collisions”. In: ApJ 489, pp. 1000–1003. DOI: 10.1086/304827.

Frenk, C. S. et al. (1999). “The Santa Barbara Cluster Comparison Project: A Comparison of Cosmological Hydrodynamics Solutions”. In: ApJ 525, pp. 554–582. DOI: 10.1086/307908. eprint: astro-ph/9906160.

Furlanetto, S. R. (2006). "The global 21-centimeter background from high redshifts". In: MNRAS 371, pp. 867–878. DOI: 10.1111/j.1365-2966.2006.10725.x. eprint: astro-ph/0604040.

Galli, D. and F. Palla (1998). "The chemistry of the early Universe". In: A&A 335, pp. 403–420. eprint: astro-ph/9803315.

Gerlich, D. (1982). "Calculations of reactive cross sections and rate coefficients for isotopic variants of the H+ + H2 system in the energy range 2meV - 1.8 eV". In: *Symposium on Atomic and Surface Phys., 1982 Contrib.* Ed. by W. Lindinger et al.

Glover, S. (2005). "The Formation Of The First Stars In The Universe". In: Space Sci. Rev. 117, pp. 445–508. DOI: 10.1007/s11214-005-5821-y. eprint: astro-ph/0409737.

Glover, S. and D. W. Savin (2006). "H3+ cooling in primordial gas". In: *Philosophical Transactions of the Royal Society of London Series A* 364, pp. 3107–3112. DOI: 10.1098/rsta.2006.1867.

Glover, S. C., D. W. Savin, and A.-K. Jappsen (2006). "Cosmological Implications of the Uncertainty in H^- Destruction Rate Coefficients". In: ApJ 640, pp. 553–568. DOI: 10.1086/500166. eprint: astro-ph/0506221.

Glover, S. C. O. and T. Abel (2008). "Uncertainties in H_2 and HD chemistry and cooling and their role in early structure formation". In: MNRAS 388, pp. 1627–1651. DOI: 10.1111/j.1365-2966.2008.13224.x. arXiv: 0803.1768.

Glover, S. C. O. and P. W. J. L. Brand (2001). "On the photodissociation of H_2 by the first stars". In: MNRAS 321, pp. 385–397. DOI: 10.1046/j.1365-8711.2001.03993.x. eprint: astro-ph/0005576.

Glover, S. C. O. and P. C. Clark (2012). "Is molecular gas necessary for star formation?" In: MNRAS 421, pp. 9–19. DOI: 10.1111/j.1365-2966.2011.19648.x. arXiv: 1105.3073.

Glover, S. C. O. and A.-K. Jappsen (2007). "Star Formation at Very Low Metallicity. I. Chemistry and Cooling at Low Densities". In: ApJ 666, pp. 1–19. DOI: 10.1086/519445. arXiv: 0705.0182.

Glover, S. C. O. and M.-M. Mac Low (2007). "Simulating the Formation of Molecular Clouds. I. Slow Formation by Gravitational Collapse from Static Initial Conditions". In: ApJS 169, pp. 239–268. DOI: 10.1086/512238. eprint: astro-ph/0605120.

Gnat, O. and G. J. Ferland (2012). "Ion-by-ion Cooling Efficiencies". In: ApJS 199, 20, p. 20. DOI: 10.1088/0067-0049/199/1/20. arXiv: 1111.6980 [astro-ph.IM].

Gnedin, N. Y. and N. Hollon (2012). "Cooling and Heating Functions of Photoionized Gas". In: ApJS 202, 13, p. 13. DOI: 10.1088/0067-0049/202/2/13. arXiv: 1201.5116.

Gnedin, N. Y. and A. V. Kravtsov (2010). "On the Kennicutt-Schmidt Relation of Low-Metallicity High-Redshift Galaxies". In: ApJ 714, pp. 287–295. DOI: 10.1088/0004-637X/714/1/287. arXiv: 0912.3005.

Gnedin, N. Y., K. Tassis, and A. V. Kravtsov (2009). "Modeling Molecular Hydrogen and Star Formation in Cosmological Simulations". In: ApJ 697, pp. 55–67. DOI: 10.1088/0004-637X/697/1/55. arXiv: 0810.4148.

Governato, F. et al. (2007). "Forming disc galaxies in ΛCDM simulations". In: MNRAS 374, pp. 1479–1494. DOI: 10.1111/j.1365-2966.2006.11266.x. eprint: astro-ph/0602351.

Governato, F. et al. (2009). "Forming a large disc galaxy from a $z < 1$ major merger". In: MNRAS 398, pp. 312–320. DOI: 10.1111/j.1365-2966.2009.15143.x. arXiv: 0812.0379.

Governato, F. et al. (2010). "Bulgeless dwarf galaxies and dark matter cores from supernova-driven outflows". In: Nature 463, pp. 203–206. DOI: 10.1038/nature08640. arXiv: 0911.2237.

Greif, T. H. et al. (2008). “The first galaxies: assembly, cooling and the onset of turbulence”. In: MNRAS 387, pp. 1021–1036. DOI: 10.1111/j.1365-2966.2008.13326.x. arXiv: 0803.2237.

Greif, T. H. et al. (2009). “Chemical mixing in smoothed particle hydrodynamics simulations”. In: MNRAS 392, pp. 1381–1387. DOI: 10.1111/j.1365-2966.2008.14169.x. arXiv: 0808.0843.

– (2010). “The First Galaxies: Chemical Enrichment, Mixing, and Star Formation”. In: ApJ 716, pp. 510–520. DOI: 10.1088/0004-637X/716/1/510. arXiv: 1003.0472.

Greif, T. H. et al. (2011a). “Simulations on a Moving Mesh: The Clustered Formation of Population III Protostars”. In: ApJ 737, 75, p. 75. DOI: 10.1088/0004-637X/737/2/75. arXiv: 1101.5491.

Greif, T. H. et al. (2011b). “The Delay of Population III Star Formation by Supersonic Streaming Velocities”. In: ApJ 736, 147, p. 147. DOI: 10.1088/0004-637X/736/2/147. arXiv: 1101.5493.

Grevesse, N. and A. J. Sauval (1998). “Standard Solar Composition”. In: Space Sci. Rev. 85, pp. 161–174. DOI: 10.1023/A:1005161325181.

Haardt, F. and P. Madau (1996). “Radiative Transfer in a Clumpy Universe. II. The Ultraviolet Extragalactic Background”. In: ApJ 461, p. 20. DOI: 10.1086/177035. eprint: astro-ph/9509093.

– (2012). “Radiative Transfer in a Clumpy Universe. IV. New Synthesis Models of the Cosmic UV/X-Ray Background”. In: ApJ 746, 125, p. 125. DOI: 10.1088/0004-637X/746/2/125. arXiv: 1105.2039.

Haiman, Z., M. J. Rees, and A. Loeb (1997). “Destruction of Molecular Hydrogen during Cosmological Reionization”. In: ApJ 476, pp. 458–463. DOI: 10.1086/303647. eprint: astro-ph/9608130.

Haiman, Z., A. A. Thoul, and A. Loeb (1996). “Cosmological Formation of Low-Mass Objects”. In: ApJ 464, p. 523. DOI: 10.1086/177343. eprint: astro-ph/9507111.

Heckman, T. M. (2001). “Galactic Superwinds at Low and High Redshift”. In: *Gas and Galaxy Evolution*. Ed. by J. E. Hibbard, M. Rupen, and J. H. van Gorkom. Vol. 240. Astronomical Society of the Pacific Conference Series, p. 345. eprint: astro-ph/0009075.

Heckman, T. M., L. Armus, and G. K. Miley (1990). “On the nature and implications of starburst-driven galactic superwinds”. In: ApJS 74, pp. 833–868. DOI: 10.1086/191522.

Hirano, S. et al. (2014). “One Hundred First Stars: Protostellar Evolution and the Final Masses”. In: ApJ 781, 60, p. 60. DOI: 10.1088/0004-637X/781/2/60. arXiv: 1308.4456 [astro-ph.CO].

Hirasawa, T., K. Aizu, and M. Taketani (1969). “Formation of Galaxies from Hydrogen Gas”. In: *Progress of Theoretical Physics* 41, pp. 835–838. DOI: 10.1143/PTP.41.835.

Holweger, H. (2001). “Photospheric abundances: Problems, updates, implications”. In: *Joint SOHO/ACE workshop “Solar and Galactic Composition”*. Ed. by R. F. Wimmer-Schweingruber. Vol. 598. American Institute of Physics Conference Series, pp. 23–30. DOI: 10.1063/1.1433974. eprint: astro-ph/0107426.

Hosokawa, T. et al. (2011). “Protostellar Feedback Halts the Growth of the First Stars in the Universe”. In: *Science* 334, p. 1250. DOI: 10.1126/science.1207433. arXiv: 1111.3649.

Hosokawa, T. et al. (2012). “Protostellar Feedback and Final Mass of the Second-generation Primordial Stars”. In: ApJ 760, L37, p. L37. DOI: 10.1088/2041-8205/760/2/L37. arXiv: 1210.3035.

Hu, W. and N. Sugiyama (1995). "Anisotropies in the cosmic microwave background: an analytic approach". In: ApJ 444, pp. 489–506. DOI: 10.1086/175624. eprint: astro-ph/9407093.

Inayoshi, K. and K. Omukai (2011). "Effect of cosmic ray/X-ray ionization on supermassive black hole formation". In: MNRAS 416, pp. 2748–2759. DOI: 10.1111/j.1365-2966.2011.19229.x. arXiv: 1106.2812.

Janev, R. K. et al., eds. (1987). *Elementary processes in hydrogen-helium plasmas: Cross sections and reaction rate coefficients*. Vol. 4.

Jappsen, A.-K. et al. (2007). "Star Formation at Very Low Metallicity. II. On the Insignificance of Metal-Line Cooling During the Early Stages of Gravitational Collapse". In: ApJ 660, pp. 1332–1343. DOI: 10.1086/513085. eprint: astro-ph/0511400.

Jasche, J., B. Ciardi, and T. A. Enßlin (2007). "Cosmic rays and the primordial gas". In: MNRAS 380, pp. 417–429. DOI: 10.1111/j.1365-2966.2007.12058.x. arXiv: 0705.4541.

Jimenez, R. et al. (2003). "The Cosmic Production of Helium". In: *Science* 299, pp. 1552–1555. DOI: 10.1126/science.1080866. eprint: astro-ph/0303179.

Johnson, J. L. and V. Bromm (2006). "The cooling of shock-compressed primordial gas". In: MNRAS 366, pp. 247–256. DOI: 10.1111/j.1365-2966.2005.09846.x. eprint: astro-ph/0505304.

Johnson, J. L., C. Dalla Vecchia, and S. Khochfar (2013). "The First Billion Years project: the impact of stellar radiation on the co-evolution of Populations II and III". In: MNRAS 428, pp. 1857–1872. DOI: 10.1093/mnras/sts011. arXiv: 1206.5824.

Karlsson, T., V. Bromm, and J. Bland-Hawthorn (2013). "Pregalactic metal enrichment: The chemical signatures of the first stars". In: *Reviews of Modern Physics* 85, pp. 809–848. DOI: 10.1103/RevModPhys.85.809. arXiv: 1101.4024.

Katz, N., D. H. Weinberg, and L. Hernquist (1996). "Cosmological Simulations with TreeSPH". In: ApJS 105, p. 19. DOI: 10.1086/192305. eprint: astro-ph/9509107.

Kay, S. T. et al. (2002). "Including star formation and supernova feedback within cosmological simulations of galaxy formation". In: MNRAS 330, pp. 113–128. DOI: 10.1046/j.1365-8711.2002.05070.x. eprint: astro-ph/0106462.

Kennicutt Jr., R. C. (1989). "The star formation law in galactic disks". In: ApJ 344, pp. 685–703. DOI: 10.1086/167834.

– (1998). "The Global Schmidt Law in Star-forming Galaxies". In: ApJ 498, pp. 541–552. DOI: 10.1086/305588. eprint: astro-ph/9712213.

Kennicutt Jr., R. C., P. Tamblyn, and C. E. Congdon (1994). "Past and future star formation in disk galaxies". In: ApJ 435, pp. 22–36. DOI: 10.1086/174790.

Kitayama, T. et al. (2004). "The Structure and Evolution of Early Cosmological H II Regions". In: ApJ 613, pp. 631–645. DOI: 10.1086/423313. eprint: astro-ph/0406280.

Komatsu, E. et al. (2009). "Five-Year Wilkinson Microwave Anisotropy Probe Observations: Cosmological Interpretation". In: ApJS 180, pp. 330–376. DOI: 10.1088/0067-0049/180/2/330. arXiv: 0803.0547.

Kravtsov, A. V. (1999). "High-resolution simulations of structure formation in the universe". PhD thesis. NEW MEXICO STATE UNIVERSITY.

Kroupa, P., C. A. Tout, and G. Gilmore (1993). "The distribution of low-mass stars in the Galactic disc". In: MNRAS 262, pp. 545–587. DOI: 10.1093/mnras/262.3.545.

Krumholz, M. R., A. K. Leroy, and C. F. McKee (2011). "Which Phase of the Interstellar Medium Correlates with the Star Formation Rate?" In: ApJ 731, 25, p. 25. DOI: 10.1088/0004-637X/731/1/25. arXiv: 1101.1296.

Lepp, S. and J. M. Shull (1983). "The kinetic theory of H2 dissociation". In: ApJ 270, pp. 578–582. DOI: 10.1086/161149.
Lipovka, A., R. Núñez-López, and V. Avila-Reese (2005). "The cooling function of HD molecule revisited". In: MNRAS 361, pp. 850–854. DOI: 10.1111/j.1365-2966.2005.09226.x. eprint: astro-ph/0503682.
Mac Low, M.-M. and A. Ferrara (1999). "Starburst-driven Mass Loss from Dwarf Galaxies: Efficiency and Metal Ejection". In: ApJ 513, pp. 142–155. DOI: 10.1086/306832. eprint: astro-ph/9801237.
Mac Low, M.-M. and R. S. Klessen (2004). "Control of star formation by supersonic turbulence". In: *Reviews of Modern Physics* 76, pp. 125–194. DOI: 10.1103/RevModPhys.76.125. eprint: astro-ph/0301093.
Mac Low, M.-M. and J. M. Shull (1986). "Molecular processes and gravitational collapse in intergalactic shocks". In: ApJ 302, pp. 585–589. DOI: 10.1086/164017.
Machida, M. N. et al. (2005). "Low-Mass Star Formation Triggered by Supernovae in Primordial Clouds". In: ApJ 622, pp. 39–57. DOI: 10.1086/428030. eprint: astro-ph/0412282.
Mackey, J., V. Bromm, and L. Hernquist (2003). "Three Epochs of Star Formation in the High-Redshift Universe". In: ApJ 586, pp. 1–11. DOI: 10.1086/367613. eprint: astro-ph/0208447.
Madau, P., A. Ferrara, and M. J. Rees (2001). "Early Metal Enrichment of the Intergalactic Medium by Pregalactic Outflows". In: ApJ 555, pp. 92–105. DOI: 10.1086/321474. eprint: astro-ph/0010158.
Maio, U. (2009). "Switching on the first light in the Universe". PhD thesis. Ludwig Maximilian University <EMAIL>umaio@mpe.mpg.de</EMAIL>.
Maio, U., L. V. E. Koopmans, and B. Ciardi (2011). "The impact of primordial supersonic flows on early structure formation, reionization and the lowest-mass dwarf galaxies". In: MNRAS 412, pp. L40–L44. DOI: 10.1111/j.1745-3933.2010.01001.x. arXiv: 1011.4006.
Maio, U. et al. (2006). "Early structure formation in quintessence models and its implications for cosmic reionization from first stars". In: MNRAS 373, pp. 869–878. DOI: 10.1111/j.1365-2966.2006.11090.x. eprint: astro-ph/0607409.
Maio, U. et al. (2007). "Metal and molecule cooling in simulations of structure formation". In: MNRAS 379, pp. 963–973. DOI: 10.1111/j.1365-2966.2007.12016.x. arXiv: 0704.2182.
Maio, U. et al. (2010). "The transition from population III to population II-I star formation". In: MNRAS 407, pp. 1003–1015. DOI: 10.1111/j.1365-2966.2010.17003.x. arXiv: 1003.4992.
Maio, U. et al. (2011). "The interplay between chemical and mechanical feedback from the first generation of stars". In: MNRAS 414, pp. 1145–1157. DOI: 10.1111/j.1365-2966.2011.18455.x. arXiv: 1011.3999.
Martin, P. G., W. J. Keogh, and M. E. Mandy (1998). "Collision-induced Dissociation of Molecular Hydrogen at Low Densities". In: ApJ 499, pp. 793–798. DOI: 10.1086/305665.
Mashchenko, S., J. Wadsley, and H. M. P. Couchman (2008). "Stellar Feedback in Dwarf Galaxy Formation". In: *Science* 319, p. 174. DOI: 10.1126/science.1148666. arXiv: 0711.4803.
McKee, C. F. and M. C. Begelman (1990). "Steady evaporation and condensation of isolated clouds in hot plasma". In: ApJ 358, pp. 392–398. DOI: 10.1086/168995.
McKee, C. F. and J. P. Ostriker (1977). "A theory of the interstellar medium - Three components regulated by supernova explosions in an inhomogeneous substrate". In: ApJ 218, pp. 148–169. DOI: 10.1086/155667.

McKee, C. F. and J. C. Tan (2008). "The Formation of the First Stars. II. Radiative Feedback Processes and Implications for the Initial Mass Function". In: ApJ 681, 771-797, pp. 771–797. DOI: 10.1086/587434. arXiv: 0711.1377.

Mielke, S. L., B. C. Garrett, and K. A. Peterson (2002). "A hierarchical family of global analytic Born-Oppenheimer potential energy surfaces for the $H+H_2$ reaction ranging in quality from double-zeta to the complete basis set limit". In: J. Chem. Phys. 116, pp. 4142–4161. DOI: 10.1063/1.1432319.

Mo, H., F. C. van den Bosch, and S. White (2010). *Galaxy Formation and Evolution*.

Monaghan, J. J. (1992). "Smoothed particle hydrodynamics". In: ARA&A 30, pp. 543–574. DOI: 10.1146/annurev.aa.30.090192.002551.

Murray, N., E. Quataert, and T. A. Thompson (2005). "On the Maximum Luminosity of Galaxies and Their Central Black Holes: Feedback from Momentum-driven Winds". In: ApJ 618, pp. 569–585. DOI: 10.1086/426067. eprint: astro-ph/0406070.

Nagakura, T. and K. Omukai (2005). "Formation of Population III stars in fossil HII regions: significance of HD". In: MNRAS 364, pp. 1378–1386. DOI: 10.1111/j.1365-2966.2005.09685.x. eprint: astro-ph/0505599.

Nagamine, K., V. Springel, and L. Hernquist (2004a). "Abundance of damped Lyman α absorbers in cosmological smoothed particle hydrodynamics simulations". In: MNRAS 348, pp. 421–434. DOI: 10.1111/j.1365-2966.2004.07393.x. eprint: astro-ph/0302187.

– (2004b). "Star formation rate and metallicity of damped Lyman α absorbers in cosmological smoothed particle hydrodynamics simulations". In: MNRAS 348, pp. 435–450. DOI: 10.1111/j.1365-2966.2004.07180.x. eprint: astro-ph/0305409.

Nakamura, F. and M. Umemura (2002). "The Stellar Initial Mass Function in Primordial Galaxies". In: ApJ 569, pp. 549–557. DOI: 10.1086/339392. eprint: astro-ph/0201497.

Nakauchi, D., K. Inayoshi, and K. Omukai (2014). "Conditions for HD cooling in the first galaxies revisited: interplay between far-ultraviolet and cosmic ray feedback in Population III star formation". In: MNRAS 442, pp. 2667–2679. DOI: 10.1093/mnras/stu1042. arXiv: 1405.6901.

Nakauchi, D. et al. (2012). "Long-duration X-Ray Flash and X-Ray-rich Gamma-Ray Bursts from Low-mass Population III Stars". In: ApJ 759, 128, p. 128. DOI: 10.1088/0004-637X/759/2/128. arXiv: 1207.2835 [astro-ph.HE].

Naoz, S., H. B. Perets, and D. Ragozzine (2010). "The Observed Orbital Properties of Binary Minor Planets". In: ApJ 719, pp. 1775–1783. DOI: 10.1088/0004-637X/719/2/1775. arXiv: 1001.2558 [astro-ph.EP].

Nath, B. B. and N. Trentham (1997). "On the enrichment of the intergalactic medium by galactic winds". In: MNRAS 291, p. 505. DOI: 10.1093/mnras/291.3.505. eprint: astro-ph/9707177.

Navarro, J. F. and M. Steinmetz (1997). "The Effects of a Photoionizing Ultraviolet Background on the Formation of Disk Galaxies". In: ApJ 478, pp. 13–28. DOI: 10.1086/303763. eprint: astro-ph/9605043.

Navarro, J. F. and S. D. M. White (1993). "Simulations of Dissipative Galaxy Formation in Hierarchically Clustering Universes - Part One - Tests of the Code". In: MNRAS 265, p. 271. DOI: 10.1093/mnras/265.2.271.

Omukai, K. and R. Nishi (1999). "Photodissociative Regulation of Star Formation in Metal-free Pregalactic Clouds". In: ApJ 518, pp. 64–68. DOI: 10.1086/307285. eprint: astro-ph/9904303.

Omukai, K. and F. Palla (2001). "On the Formation of Massive Primordial Stars". In: ApJ 561, pp. L55–L58. DOI: 10.1086/324410.

– (2003). "Formation of the First Stars by Accretion". In: ApJ 589, pp. 677–687. DOI: 10.1086/374810. eprint: astro-ph/0302345.

Oppenheimer, B. D. and R. Davé (2006). "Cosmological simulations of intergalactic medium enrichment from galactic outflows". In: MNRAS 373, pp. 1265–1292. DOI: 10.1111/j.1365-2966.2006.10989.x. eprint: astro-ph/0605651.

– (2009). "The nature and origin of low-redshift OVI absorbers". In: MNRAS 395, pp. 1875–1904. DOI: 10.1111/j.1365-2966.2009.14676.x. arXiv: 0806.2866.

Oppenheimer, B. D. and J. Schaye (2013a). "AGN proximity zone fossils and the delayed recombination of metal lines". In: MNRAS 434, pp. 1063–1078. DOI: 10.1093/mnras/stt1150. arXiv: 1303.0019.

– (2013b). "Non-equilibirum ionization and cooling of metal-enriched gas in the presence of a photoionization background". In: MNRAS 434, pp. 1043–1062. DOI: 10.1093/mnras/stt1043. arXiv: 1302.5710.

O'Shea, B. W. and M. L. Norman (2007). "Population III Star Formation in a ΛCDM Universe. I. The Effect of Formation Redshift and Environment on Protostellar Accretion Rate". In: ApJ 654, pp. 66–92. DOI: 10.1086/509250. eprint: astro-ph/0607013.

– (2008). "Population III Star Formation in a ΛCDM Universe. II. Effects of a Photodissociating Background". In: ApJ 673, 14-33, pp. 14–33. DOI: 10.1086/524006. arXiv: 0706.4416.

O'Shea, B. W. et al. (2004). "Introducing Enzo, an AMR Cosmology Application". In: *ArXiv Astrophysics e-prints*. eprint: astro-ph/0403044.

O'Shea, B. W. et al. (2005). "Forming a Primordial Star in a Relic H II Region". In: ApJ 628, pp. L5–L8. DOI: 10.1086/432683. eprint: astro-ph/0503330.

O'Shea, B. W. et al. (2008). "First Stars III Conference Summary". In: *First Stars III*. Ed. by B. W. O'Shea and A. Heger. Vol. 990. American Institute of Physics Conference Series, p. xiii. DOI: 10.1063/1.2940787. arXiv: 0801.2124.

Peebles, P. J. E. and R. H. Dicke (1968). "Origin of the Globular Star Clusters". In: ApJ 154, p. 891. DOI: 10.1086/149811.

Pettini, M. et al. (2001). "The Rest-Frame Optical Spectra of Lyman Break Galaxies: Star Formation, Extinction, Abundances, and Kinematics". In: ApJ 554, pp. 981–1000. DOI: 10.1086/321403. eprint: astro-ph/0102456.

Pettini, M. et al. (2003). "The C IV Mass Density of the Universe at Redshift 5". In: ApJ 594, pp. 695–703. DOI: 10.1086/377043. eprint: astro-ph/0305413.

Pontzen, A. et al. (2008). "Damped Lyman α systems in galaxy formation simulations". In: MNRAS 390, pp. 1349–1371. DOI: 10.1111/j.1365-2966.2008.13782.x. arXiv: 0804.4474.

Pontzen, A. et al. (2010). "The nature of HIabsorbers in gamma-ray burst afterglows: clues from hydrodynamic simulations". In: MNRAS 402, pp. 1523–1535. DOI: 10.1111/j.1365-2966.2009.16017.x. arXiv: 0909.1321.

Puy, D. et al. (1993). "Formation of primordial molecules and thermal balance in the early universe". In: A&A 267, pp. 337–346.

Raiteri, C. M., M. Villata, and J. F. Navarro (1996). "Simulations of Galactic chemical evolution. I. O and Fe abundances in a simple collapse model." In: A&A 315, pp. 105–115.

Rees, M. J. (1986). "Lyman absorption lines in quasar spectra - Evidence for gravitationally-confined gas in dark minihaloes". In: MNRAS 218, 25P–30P. DOI: 10.1093/mnras/218.1.25P.

Rees, M. J. and J. P. Ostriker (1977). "Cooling, dynamics and fragmentation of massive gas clouds - Clues to the masses and radii of galaxies and clusters". In: MNRAS 179, pp. 541–559. DOI: 10.1093/mnras/179.4.541.

Ritter, J. S. et al. (2012). "Confined Population III Enrichment and the Prospects for Prompt Second-generation Star Formation". In: ApJ 761, 56, p. 56. DOI: 10.1088/0004-637X/761/1/56. arXiv: 1203.2957.

Roškar, R. et al. (2008). "Riding the Spiral Waves: Implications of Stellar Migration for the Properties of Galactic Disks". In: ApJ 684, L79, p. L79. DOI: 10.1086/592231. arXiv: 0808.0206.

Salpeter, E. E. (1955). "The Luminosity Function and Stellar Evolution." In: ApJ 121, p. 161. DOI: 10.1086/145971.

Savin, D. W. (2002). "Rate Coefficients for D(1s)+$H^+ \leftrightarrows D^+$+H(1s) Charge Transfer and Some Astrophysical Implications". In: ApJ 566, pp. 599–603. DOI: 10.1086/324218.

Savin, D. W. et al. (2004). "Rate Coefficient for H^+ + $H_2(X^1\Sigma^+{}_g$, ν = 0, J = 0) –> H(1s) + $H^+{}_2$ Charge Transfer and Some Cosmological Implications". In: ApJ 606, pp. L167–L170. DOI: 10.1086/421108. eprint: astro-ph/0404288.

Scannapieco, E. and T. Broadhurst (2001a). "Linking the Metallicity Distribution of Galactic Halo Stars to the Enrichment History of the Universe". In: ApJ 550, pp. L39–L42. DOI: 10.1086/319487. eprint: astro-ph/0012152.

– (2001b). "The Role of Heating and Enrichment in Galaxy Formation". In: ApJ 549, pp. 28–45. DOI: 10.1086/319043. eprint: astro-ph/0003104.

Scannapieco, E., A. Ferrara, and T. Broadhurst (2000). "The Influence of Galactic Outflows on the Formation of Nearby Dwarf Galaxies". In: ApJ 536, pp. L11–L14. DOI: 10.1086/312725. eprint: astro-ph/0004289.

Schaye, J., R. F. Carswell, and T.-S. Kim (2007). "A large population of metal-rich, compact, intergalactic CIV absorbers - evidence for poor small-scale metal mixing". In: MNRAS 379, pp. 1169–1194. DOI: 10.1111/j.1365-2966.2007.12005.x. eprint: astro-ph/0701761.

Schaye, J. et al. (2000). "The Detection of Oxygen in the Low-Density Intergalactic Medium". In: ApJ 541, pp. L1–L4. DOI: 10.1086/312892. eprint: astro-ph/0008011.

Schaye, J. et al. (2003). "Metallicity of the Intergalactic Medium Using Pixel Statistics. II. The Distribution of Metals as Traced by C IV". In: ApJ 596, pp. 768–796. DOI: 10.1086/378044. eprint: astro-ph/0306469.

Seager, S., D. D. Sasselov, and D. Scott (1999). "A New Calculation of the Recombination Epoch". In: ApJ 523, pp. L1–L5. DOI: 10.1086/312250. eprint: astro-ph/9909275.

– (2000). "How Exactly Did the Universe Become Neutral?" In: ApJS 128, pp. 407–430. DOI: 10.1086/313388. eprint: astro-ph/9912182.

Shapiro, P. R. and H. Kang (1987). "Hydrogen molecules and the radiative cooling of pregalactic shocks". In: ApJ 318, pp. 32–65. DOI: 10.1086/165350.

Shavitt, I. (1959). "A Calculation of the Rates of the Ortho-Para Conversions and Isotope Exchanges in Hydrogen". In: J. Chem. Phys. 31, pp. 1359–1367. DOI: 10.1063/1.1730599.

Shchekinov, Y. A. and E. O. Vasiliev (2006). "Formation of HD molecules in merging dark matter haloes". In: MNRAS 368, pp. 454–460. DOI: 10.1111/j.1365-2966.2006.10117.x. eprint: astro-ph/0505619.

Shen, S., J. Wadsley, and G. Stinson (2010). "The enrichment of the intergalactic medium with adiabatic feedback - I. Metal cooling and metal diffusion". In: MNRAS 407, pp. 1581–1596. DOI: 10.1111/j.1365-2966.2010.17047.x. arXiv: 0910.5956.

Simcoe, R. A. (2006). "High-Redshift Intergalactic C IV Abundance Measurements from the Near-Infrared Spectra of Two z ~ 6 QSOs". In: ApJ 653, pp. 977–987. DOI: 10.1086/508983. eprint: astro-ph/0605710.

Simcoe, R. A., W. L. W. Sargent, and M. Rauch (2004). "The Distribution of Metallicity in the Intergalactic Medium at z~2.5: O VI and C IV Absorption in the Spectra of Seven QSOs". In: ApJ 606, pp. 92–115. DOI: 10.1086/382777. eprint: astro-ph/0312467.

Smagorinsky, J. (1963). "General Circulation Experiments with the Primitive Equations". In: *Monthly Weather Review* 91, p. 99. DOI: 10.1175/1520-0493(1963)091<0099:GCEWTP>2.3.CO;2.

Sommer-Larsen, J., M. Götz, and L. Portinari (2003). "Galaxy Formation: Cold Dark Matter, Feedback, and the Hubble Sequence". In: ApJ 596, pp. 47–66. DOI: 10.1086/377685. eprint: astro-ph/0204366.

Songaila, A. and L. L. Cowie (1996). "Metal enrichment and Ionization Balance in the Lyman Alpha Forest at Z = 3". In: AJ 112, p. 335. DOI: 10.1086/118018. eprint: astro-ph/9605102.

Springel, V. (2005). "The cosmological simulation code GADGET-2". In: MNRAS 364, pp. 1105–1134. DOI: 10.1111/j.1365-2966.2005.09655.x. eprint: astro-ph/0505010.

– (2010). "E pur si muove: Galilean-invariant cosmological hydrodynamical simulations on a moving mesh". In: MNRAS 401, pp. 791–851. DOI: 10.1111/j.1365-2966.2009.15715.x. arXiv: 0901.4107.

Springel, V. and L. Hernquist (2002). "Cosmological smoothed particle hydrodynamics simulations: the entropy equation". In: MNRAS 333, pp. 649–664. DOI: 10.1046/j.1365-8711.2002.05445.x. eprint: astro-ph/0111016.

– (2003a). "Cosmological smoothed particle hydrodynamics simulations: a hybrid multiphase model for star formation". In: MNRAS 339, pp. 289–311. DOI: 10.1046/j.1365-8711.2003.06206.x. eprint: astro-ph/0206393.

– (2003b). "The history of star formation in a Λ cold dark matter universe". In: MNRAS 339, pp. 312–334. DOI: 10.1046/j.1365-8711.2003.06207.x. eprint: astro-ph/0206395.

Springel, V., N. Yoshida, and S. D. M. White (2001). "GADGET: a code for collisionless and gasdynamical cosmological simulations". In: New A 6, pp. 79–117. DOI: 10.1016/S1384-1076(01)00042-2. eprint: astro-ph/0003162.

Stacy, A. and V. Bromm (2007). "Impact of cosmic rays on Population III star formation". In: MNRAS 382, pp. 229–238. DOI: 10.1111/j.1365-2966.2007.12247.x. arXiv: 0705.3634.

Stacy, A., V. Bromm, and A. Loeb (2011). "Effect of Streaming Motion of Baryons Relative to Dark Matter on the Formation of the First Stars". In: ApJ 730, L1, p. L1. DOI: 10.1088/2041-8205/730/1/L1. arXiv: 1011.4512.

Stacy, A., T. H. Greif, and V. Bromm (2012). "The first stars: mass growth under protostellar feedback". In: MNRAS 422, pp. 290–309. DOI: 10.1111/j.1365-2966.2012.20605.x. arXiv: 1109.3147.

Stadel, J. G. (2001). "Cosmological N-body simulations and their analysis". PhD thesis. UNIVERSITY OF WASHINGTON.

Stinson, G. et al. (2006). "Star formation and feedback in smoothed particle hydrodynamic simulations - I. Isolated galaxies". In: MNRAS 373, pp. 1074–1090. DOI: 10.1111/j.1365-2966.2006.11097.x. eprint: astro-ph/0602350.

Stinson, G. S. et al. (2009). "Feedback and the formation of dwarf galaxy stellar haloes". In: MNRAS 395, pp. 1455–1466. DOI: 10.1111/j.1365-2966.2009.14555.x. arXiv: 0902.0775 [astro-ph.CO].

Strickland, D. K. and I. R. Stevens (2000). "Starburst-driven galactic winds - I. Energetics and intrinsic X-ray emission". In: MNRAS 314, pp. 511–545. DOI: 10.1046/j.1365-8711.2000.03391.x. eprint: astro-ph/0001395.

Strömholm, C. et al. (1995). "Absolute cross sections for dissociative recombination of HD^+: Comparison of experiment and theory". In: Phys. Rev. A 52, R4320–R4323. DOI: 10.1103/PhysRevA.52.R4320.

Susa, H. (2013). "The Mass of the First Stars". In: ApJ 773, 185, p. 185. DOI: 10.1088/0004-637X/773/2/185. arXiv: 1304.6794.

Sutherland, R. S. and M. A. Dopita (1993). "Cooling functions for low-density astrophysical plasmas". In: ApJS 88, pp. 253–327. DOI: 10.1086/191823.

Tanaka, M., T. J. Moriya, and N. Yoshida (2013). "Detectability of high-redshift superluminous supernovae with upcoming optical and near-infrared surveys - II. Beyond z = 6". In: MNRAS 435, pp. 2483–2493. DOI: 10.1093/mnras/stt1469. arXiv: 1306.3743.

Tegmark, M. et al. (1997). "How Small Were the First Cosmological Objects?" In: ApJ 474, p. 1. DOI: 10.1086/303434. eprint: astro-ph/9603007.

Telesco, C. M. (1988). "Enhanced star formation and infrared emission in the centers of galaxies". In: ARA&A 26, pp. 343–376. DOI: 10.1146/annurev.aa.26.090188.002015.

Thacker, R. J. and H. M. P. Couchman (2000). "Implementing Feedback in Simulations of Galaxy Formation: A Survey of Methods". In: ApJ 545, pp. 728–752. DOI: 10.1086/317828. eprint: astro-ph/0001276.

Theuns, T. et al. (2002). "Galactic Winds in the Intergalactic Medium". In: ApJ 578, pp. L5–L8. DOI: 10.1086/344521. eprint: astro-ph/0208418.

Thielemann, F.-K., K. Nomoto, and K. Yokoi (1986). "Explosive nucleosynthesis in carbon deflagration models of Type I supernovae". In: A&A 158, pp. 17–33.

Tornatore, L., A. Ferrara, and R. Schneider (2007). "Population III stars: hidden or disappeared?" In: MNRAS 382, pp. 945–950. DOI: 10.1111/j.1365-2966.2007.12215.x. arXiv: 0707.1433.

Trenti, M. and M. Stiavelli (2009). "Formation Rates of Population III Stars and Chemical Enrichment of Halos during the Reionization Era". In: ApJ 694, pp. 879–892. DOI: 10.1088/0004-637X/694/2/879. arXiv: 0901.0711 [astro-ph.CO].

Trevisan, C. S. and J. Tennyson (2002a). "Calculated rates for the electron impact dissociation of molecular hydrogen, deuterium and tritium". In: *Plasma Physics and Controlled Fusion* 44, pp. 1263–1276. DOI: 10.1088/0741-3335/44/7/315.

– (2002b). "Calculated rates for the electron impact dissociation of molecular hydrogen: mixed isotopomers and scaling laws". In: *Plasma Physics and Controlled Fusion* 44, pp. 2217–2230. DOI: 10.1088/0741-3335/44/10/309.

Tseliakhovich, D. and C. Hirata (2010). "Relative velocity of dark matter and baryonic fluids and the formation of the first structures". In: Phys. Rev. D 82.8, 083520, p. 083520. DOI: 10.1103/PhysRevD.82.083520. arXiv: 1005.2416.

Uehara, H. and S.-i. Inutsuka (2000). "Does Deuterium Enable the Formation of Primordial Brown Dwarfs?" In: ApJ 531, pp. L91–L94. DOI: 10.1086/312529.

Vasiliev, E. O. and Y. A. Shchekinov (2005). "Role of HD Molecules in the Cooling of the Primordial Gas". In: *Astrophysics* 48, pp. 491–504. DOI: 10.1007/s10511-005-0048-x. eprint: astro-ph/0507603.

Veilleux, S., G. Cecil, and J. Bland-Hawthorn (2005). "Galactic Winds". In: ARA&A 43, pp. 769–826. DOI: 10.1146/annurev.astro.43.072103.150610. eprint: astro-ph/0504435.

Verner, D. A. and G. J. Ferland (1996). "Atomic Data for Astrophysics. I. Radiative Recombination Rates for H-like, He-like, Li-like, and Na-like Ions over a Broad Range of Temperature". In: ApJS 103, p. 467. DOI: 10.1086/192284. eprint: astro-ph/9509083.

Wada, K. and A. Venkatesan (2003). "Feedback from the First Supernovae in Protogalaxies: The Fate of the Generated Metals". In: ApJ 591, pp. 38–42. DOI: 10.1086/375335. eprint: astro-ph/0303449.

Wadsley, J. W., J. Stadel, and T. Quinn (2004). "Gasoline: a flexible, parallel implementation of TreeSPH". In: New A 9, pp. 137–158. DOI: 10.1016/j.newast.2003.08.004. eprint: astro-ph/0303521.

Wadsley, J. W., G. Veeravalli, and H. M. P. Couchman (2008). "On the treatment of entropy mixing in numerical cosmology". In: MNRAS 387, pp. 427–438. DOI: 10.1111/j.1365-2966.2008.13260.x.

Weidemann, V. (1987). "The initial-final mass relation - Galactic disk and Magellanic Clouds". In: A&A 188, pp. 74–84.

Whalen, D., T. Abel, and M. L. Norman (2004). "Radiation Hydrodynamic Evolution of Primordial H II Regions". In: ApJ 610, pp. 14–22. DOI: 10.1086/421548. eprint: astro-ph/0310283.

Whalen, D. J. et al. (2013). "Seeing the First Supernovae at the Edge of the Universe with JWST". In: ApJ 762, L6, p. L6. DOI: 10.1088/2041-8205/762/1/L6. arXiv: 1209.3457.

White, S. D. M. and M. J. Rees (1978). "Core condensation in heavy halos - A two-stage theory for galaxy formation and clustering". In: MNRAS 183, pp. 341–358. DOI: 10.1093/mnras/183.3.341.

Wiersma, R. P. C., J. Schaye, and B. D. Smith (2009). "The effect of photoionization on the cooling rates of enriched, astrophysical plasmas". In: MNRAS 393, pp. 99–107. DOI: 10.1111/j.1365-2966.2008.14191.x. arXiv: 0807.3748.

Wiersma, R. P. C. et al. (2009). "Chemical enrichment in cosmological, smoothed particle hydrodynamics simulations". In: MNRAS 399, pp. 574–600. DOI: 10.1111/j.1365-2966.2009.15331.x. arXiv: 0902.1535 [astro-ph.CO].

Williams, R. J. R. and J. E. Dyson (2002). "Resolved shocks in clumpy media". In: MNRAS 333, pp. 1–8. DOI: 10.1046/j.1365-8711.2002.05159.x. eprint: astro-ph/0111380.

Wishart, A. W. (1979). "The bound-free photo-detachment cross-section of H-". In: MNRAS 187, 59P–61. DOI: 10.1093/mnras/187.1.59P.

Wolcott-Green, J. and Z. Haiman (2011). "Suppression of HD cooling in protogalactic gas clouds by Lyman-Werner radiation". In: MNRAS 412, pp. 2603–2616. DOI: 10.1111/j.1365-2966.2010.18080.x. arXiv: 1009.1087.

Wolfire, M. G. et al. (2003). "Neutral Atomic Phases of the Interstellar Medium in the Galaxy". In: ApJ 587, pp. 278–311. DOI: 10.1086/368016. eprint: astro-ph/0207098.

Wolfire, M. G. et al. (2008). "Chemical Rates on Small Grains and PAHs: C^+ Recombination and H_2 Formation". In: ApJ 680, 384-397, pp. 384–397. DOI: 10.1086/587688. arXiv: 0803.0138.

Woosley, S. E. and T. A. Weaver (1995). "The Evolution and Explosion of Massive Stars. II. Explosive Hydrodynamics and Nucleosynthesis". In: ApJS 101, p. 181. DOI: 10.1086/192237.

Wrathmall, S. A. and D. R. Flower (2007). "The rovibrational excitation of H_2 induced by H". In: *Journal of Physics B Atomic Molecular Physics* 40, pp. 3221–3230. DOI: 10.1088/0953-4075/40/16/003.

Wrathmall, S. A., A. Gusdorf, and D. R. Flower (2007). "The excitation of molecular hydrogen by atomic hydrogen in astrophysical media". In: MNRAS 382, pp. 133–138. DOI: 10.1111/j.1365-2966.2007.12420.x.

Yoshida, N., K. Omukai, and L. Hernquist (2007). "Formation of Massive Primordial Stars in a Reionized Gas". In: ApJ 667, pp. L117–L120. DOI: 10.1086/522202. arXiv: 0706.3597.
– (2008). "Protostar Formation in the Early Universe". In: *Science* 321, p. 669. DOI: 10.1126/science.1160259. arXiv: 0807.4928.
Yoshida, N. et al. (2003). "Simulations of Early Structure Formation: Primordial Gas Clouds". In: ApJ 592, pp. 645–663. DOI: 10.1086/375810. eprint: astro-ph/0301645.
Yoshida, N. et al. (2006). "Formation of Primordial Stars in a ΛCDM Universe". In: ApJ 652, pp. 6–25. DOI: 10.1086/507978. eprint: astro-ph/0606106.
Yoshida, N. et al. (2007). "Early Cosmological H II/He III Regions and Their Impact on Second-Generation Star Formation". In: ApJ 663, pp. 687–707. DOI: 10.1086/518227. eprint: astro-ph/0610819.